INVESTIGATION OF SOME DIELECTRIC PROPERTIES OF NANOPARTICLES INJECTED OIL-PAPER INSULATION

A Thesis Submitted in Partial Fulfilment

for the Degree of Master of Electrical Engineering

By

SOURAV BISWAS

Examination Roll No.: **M4ELE22017**

Registration No.: **154007 of 2020-2021**

Under the guidance of

Prof. Biswendu Chatterjee

Professor

&

Prof. Sovan Dalai

Professor

Department of Electrical Engineering

Faculty of Engineering and Technology

Jadavpur University

Kolkata, India

JADAVPUR UNIVERSITY

KOLKATA- 700032, INDIA

FACULTY OF ENGINEERING AND TECHNOLOGY

CERTIFICATE OF RECOMMENDATION

*This is to certify that the thesis entitled "**INVESTIGATION OF SOME DIELECTRIC PROPERTIES OF NANOPARTICLES INJECTED OIL-PAPER INSULATION**" is being submitted by **SOURAV BISWAS** (Registration No. 154007 of 2020-2021), in partial fulfilment of the requirement for the degree of "Master of Electrical Engineering" from Jadavpur University has been carried out by him under our guidance and supervision. The project, in our opinion, is worthy of its acceptance.*

BChatterjee
28.06.2022

Prof. Biswendu Chatterjee
Professor,
Dept. of Electrical Engineering,
Faculty of Engineering and Technology,
Jadavpur University

Dr. Biswendu Chatterjee
Professor
Electrical Engineering Department
Jadavpur University
Kolkata-700032

28/06/2022

Prof. Sovan Dalai
Professor,
Dept. of Electrical Engineering,
Faculty of Engineering and Technology,
Jadavpur University

Dr. Sovan Dalai
Professor
Electrical Engineering Department
Jadavpur University
Kolkata-700032

Saswati Mazumdar 28/6/22

Prof. Saswati Mazumdar
Head,
Dept. of Electrical Engineering,
Faculty of Engineering and Technology,
Jadavpur University

Head
Electrical Engineering Department
JADAVPUR UNIVERSITY
Kolkata - 700 032

Mazumdar 28/6/2022

Prof. Chandan Mazumdar
Dean,
Faculty of Engineering and Technology,
Jadavpur University

DEAN
Faculty of Engineering & Technology
JADAVPUR UNIVERSITY
KOLKATA-700 032

JADAVPUR UNIVERSITY
KOLKATA- 700032, INDIA

FACULTY OF ENGINEERING AND TECHNOLOGY

CERTIFICATE OF APPROVAL

The foregoing thesis is hereby approved as a credible study of Master of Electrical Engineering and presented in a manner satisfactory to warrant its acceptance as a pre-requisite to the degree for which it has been submitted. It is understood that by this approval the undersigned do not necessarily endorse or approve any statement made, opinion expressed or conclusion therein but approve this thesis only for the purpose for which it is submitted.

1. _____

_____

2. _____

Signature of the Examiner(s)

Signature of supervisor(s)

*Only in case the recommendation is concurred.

DECLARATION OF ORIGINALITY AND COMPLIANCE OF ACADEMIC ETHICS

I hereby declare that the thesis contains original research work by the undersigned candidate, as part of the Masters of Electrical Engineering studies.
All the information in this document has been obtained and presented in accordance with academic rules and ethical conduct.
I also declare that, as required by these rules and conduct. I have fully cited and referenced all material and results that are not original to this work.

Name : **SOURAV BISWAS**

Class Roll no. : **002010802017**

Examination Roll no. : **M4ELE22017**

Registration no. : **154007 of 2020-2021**

Name of the thesis : **INVESTIGATION OF SOME DIELECTRIC PROPERTIES OF NANOPARTICLES INJECTED OIL-PAPER INSULATION**

Sourav Biswas 28.06.2022

Signature with date

ACKNOWLEDGEMENT

I express my deep sense of gratitude to my supervisors, **Prof. Biswendu Chatterjee**, *Professor*, Department of Electrical Engineering and **Prof. Sovan Dalai**, *Professor*, Department of Electrical Engineering, Jadavpur University for their keen interest, cherished guidance and constant inspiration during the research work. They also worked equally hard to make this work reach its conclusion and beyond. I am obliged and grateful to them for their guidance and for giving me the opportunity to work in the High Voltage Laboratory. Above all, without their moral support and constant guidance, I would not have completed the work.

I express my sincere gratitude to **Dr. Arpan Kumar Pradhan**, *assistant professor*, Department of Electrical Engineering, Jadavpur University, for his encouragement, advice and active support in this work. I also convey special thanks to the High Voltage Laboratory of Jadavpur University, Kolkata, for providing facility and support during this research work.

I am also thankful to **Prof. Saswati Mazumdar**, Head of the Department of Electrical Engineering, Jadavpur University, for providing the necessary facilities for carrying out this research work.

I am taking the opportunity to express my humble indebtedness to **Mr. Biswajit Chakraborty**, research scholar, High Voltage Laboratory, for his invaluable inputs during this work. I am also thankful to the rest of the research scholars of the High Voltage laboratory for their support throughout the tenure of the research work.

I would like to thank my dear friends, EE Department, from whom I received immense support, inexplicable encouragement and assistance. I would like to convey my soulful thankfulness to the rest of the PG scholars of the EE Department for their moral support during this course work. I am extremely grateful to my father for his blessings and all the other contributions to my life. I am also grateful to my mother and my partner for their constant support and motivation, without that I would not have come to this stage. This thesis, a fruit of the combined efforts of my family members, is dedicated to them as a token of love and gratitude.

Above all, it is the wish of the almighty that I have been able to complete this work.

Jaurav Biswas 28.06.2022

Signature with date

CONTENTS

ABSTRACT

Recently, there has been a rising emphasis on bulk power transmission over great distances. Consequently, the operating voltage magnitude for power transmission has increased. Therefore, transformers, circuit breakers, cables, and other power equipment must withstand increased operational stresses. The lifespan of electrical equipment is directly proportional to the lifespan of insulation. For decades, mineral oil impregnated paper has been a popular choice for power equipment insulation. However, in the event of increased operating loads, improving the dielectric and thermal characteristics of mineral oil becomes critical. Due to this nanofluids are being explored as a potential substitute for conventional oils used in transformers. To remark on the applicability of the nano oil-paper insulation in practical applications, the time and frequency domain spectroscopies are usually performed. In this thesis, two liquid dielectrics, mineral oil and vegetable oil (FR3) have been employed to develop nano oil-paper insulation with two nanoparticles, TiO_2 (a semi-conducting nanoparticle) and Al_2O_3 (a non-conducting nanoparticle). In the time domain, the polarisation and depolarization currents as well as the DC conductivity of the samples have been estimated at different temperatures. Then, the degree of non-linearity has been compared. Following that, the activation energy has been estimated using the conductivity values of the samples at various temperatures. Finally, frequency-domain spectroscopy was performed on all the dielectric samples to measure and compare the real and imaginary components of complex relative permittivity as well as the AC conductivity at different temperatures in order to obtain a better knowledge of the dielectric properties of the samples under investigation.

NOMENCLATURE

OPI	Oil-paper insulation
OPS	Oil-paper sample
NOPI	Nano oil-paper insulation
NOPS	Nano oil-paper sample
TIP	Transformer insulation prototype
D	Electric flux density
E	Electric Field
ε_0	Permittivity of vacuum
ε_r	Relative permittivity
ε_r'	Real part of relative permittivity
ε_r''	Imaginary part of relative permittivity
P	Polarization vector
χ	Electrical susceptibility
U_0	Step voltage source
$\delta(t)$	Dirac/delta function
ε_s	Static relative permittivity
ε_∞	High-frequency relative permittivity
χ_s	Static electrical susceptibility
χ_∞	High-frequency susceptibility
J	Displacement current density
σ_0	DC conductivity
C_0	Geometric capacitance

$f(t)$	Polarization function
i_{pol}	Polarization current
i_{depol}	Depolarization current
ω	Frequency of applied voltage
$\hat{\chi}(\omega)$	Complex susceptibility
$\chi'(\omega)$	Real part of complex susceptibility
$\chi''(\omega)$	Imaginary part of complex susceptibility
$\tan\delta$	Dissipation factor
a_i, b_i	Coefficients of fitting parameters
t	Operating temperature in ^oC

Chapter: 1

INTRODUCTION

1.1 INTRODUCTION

Recently, there has been a rising emphasis on bulk power transmission over great distances. Consequently, the operating voltage magnitude for power transmission has increased. Therefore, transformers, circuit breakers, cables, and other power equipment must withstand increased operational stresses. The lifespan of electrical equipment is directly proportional to the lifespan of insulation. For decades, mineral oil and mineral oil impregnated paper have been popular choices for power equipment insulation. However, in the event of increased operating loads, improving the dielectric and thermal characteristics of mineral oil becomes critical. Nanodielectrics could provide a realistic and beneficial solution to this issue.

Nanofluids are fluid suspensions containing uniformly dispersed nanoparticles with diameters less than 100 nm. This term was coined by S. Choi (1995) [1]. He stated that the thermal properties of this novel class of nanotechnology-based heat transfer fluids outperform those of their host fluids. Following that, various studies reported the development of mineral oil-based nanofluids with enhanced breakdown voltage at power frequency and lightning impulse voltage withstand capacity.

There has been increased concern in recent years over the usage of mineral oil because it is prone to fire hazards and accidents. So, vegetable oils are being researched as a potential replacement for mineral oil in power equipment insulation. Vegetable oils also have stronger fire resistance, which assures the safety of employees and the environment. As a consequence, the attention of the researchers has been drawn to vegetable oil-based nanofluids. Due to the aforementioned properties, nanofluids are being explored as a potential substitute for conventional oils used in transformers.

It should be noted that larger breakdown strengths do not ensure improved dielectric liquid performance. To remark on the applicability of the dielectric liquid in practical applications, a full analysis of its dielectric properties is essential. Among the numerous dielectric response approaches, time-domain spectroscopy and frequency-domain spectroscopy have acquired prominence for this purpose. The conductivity of the dielectric medium is estimated using time-domain spectroscopy. The study of conductivity is particularly important since temperature and moisture variations have a large impact on the conductivity of the dielectric medium. The frequency-domain spectroscopy gives information about the dissipation factor, which represents the losses of the dielectric medium.

In this thesis, two liquid dielectrics, mineral oil and vegetable oil (FR3) have been used as the base oil. These two base oils have been employed to develop NOPI with two nanoparticles: a semi-conducting nanoparticle, TiO_2 (Titania), and a non-conducting nanoparticle, Al_2O_3 (Alumina). Various studies have been performed on these two base OPS(s) and four synthesised NOPS(s) (altogether six samples). In the time domain, the polarisation and depolarization currents, and the DC conductivity of the developed samples have been estimated. Then the degree of non-linearity has been compared. Following that, the activation energy has been estimated using the conductivity values of the samples at various temperatures. Finally, frequency-domain spectroscopy has been performed on all the dielectric samples to evaluate and compare the real and imaginary components of complex relative

permittivity as well as the AC conductivity in order to obtain a better knowledge of the dielectric properties of the samples under investigation.

1.2 AIM OF THE THESIS

In this thesis, DIRANA and IDAX, two completely automatic instruments, have been utilised to analyse the dielectric spectroscopy measurements. The DIRANA has been used to measure and investigate polarisation and depolarization currents, while the IDAX has been used to investigate the real and imaginary capacitance (hence, the complex permittivity).

This thesis aims to comprehend the dielectric properties of the synthesised NOPS(s) through the estimation of parameters such as AC & DC conductivity, complex permittivity, and degree of non-linearity.

1.3 WORK DONE AND CONTRIBUTION

- At different operating temperatures, a comparison of the polarization and depolarization currents of the developed NOPS(s) with their respective base OPS(s) has been performed using DIRANA.
- The DC conductivities of all six samples have been estimated utilizing the polarisation and depolarization current measurements using DIRANA.
- The degree of non-linearity for each sample has been tabulated using the plot of conduction current versus applied voltage.
- The activation energies of the samples have been evaluated using conductivity values at different temperatures.
- Comparative investigations have been undertaken on parameters like the real and imaginary component of complex relative permittivity as well as AC conductivity at various temperatures from the measurements recorded using IDAX.

These above-mentioned works are done and thoroughly discussed in this thesis. The results obtained from this work will be helpful for further modelling and analysis of NOPI in future.

1.4 OUTLINE OF THE THESIS

Chapter 1 provides the aim and contribution of the thesis.

Chapter 2 discusses the details of the basic information about the nanofluids.

Chapter 3 explains the brief theory and methodology of dielectric response measurement.

Chapter 4 describes the experimental details involved in the present work which includes sample preparation and experimental procedure.

Chapter 5 demonstrates the results of the experiments and analysis that were done on the basis of those results.

Chapter 6 presents the conclusions and future scope of the present work.

Chapter: 2

STUDY OF NANOFLUIDS

2.1 INTRODUCTION

Nanofluids have been regarded as a hot research topic in recent decades, following their discovery in 1995 by the brilliant researcher Dr. Choi of the Argonne National Laboratory, United States [1]. Several research papers have provided comprehensive and systematic summaries of nanofluid development and state-of-the-art. After a string of failures by scientists attempting to develop microfluids, it is regarded as one of the most promising ideas. Microfluids were ruled out due to their non-dispersibility. An inspiring response to the nanofluids came from the breakthrough when it was established that nanofluids showed exceptional thermal conductivity [20]. As a result, the electrical properties of the new class of colloid were investigated further.

The electrical industry has grown tremendously in recent years, particularly in the high voltage application area. To develop the future of the power industry, The ever-increasing levels of voltage in the electrical industry necessitate an insulating fluid with enhanced electrical and dielectric properties [2]. So far, research has shown that nanofluids have enhanced breakdown strength and excellent dielectric properties [5-11]. However, the prerequisite is indeed the preparation of the nanofluids, which is a difficult task to accomplish on an industrial scale.

Based on rigorous experiments, researchers have successfully developed nanofluids in the laboratory. A comprehensive study on nanoparticle classification has been presented here to help understand the properties of nanofluids. A thorough examination of the electrical, dielectric, thermal, and physical properties of nanofluids have been presented. Following that, a few mechanisms for analysing the stability of nanofluids are discussed. Finally, the benefits and drawbacks of nanofluids have been presented. The scope of the new class of colloid has been discussed here for its future prospects in the dielectrics industry. In addition, the limitations and challenges are addressed and presented [11].

2.2 CLASSIFICATION OF NANOFLUIDS

Nanofluids, a new class of colloid, have demonstrated promising thermal, electrical, and dielectric properties. However, as proper dispersion of nanoparticles is difficult, meticulous preparation needs to be carried out [11]. As a result, the materials used in the preparation of nanofluids play an important role in the development of this magical colloid. At the same time, the material selected should be cost-effective in order to ensure its industrial development. Thereby, classifying different nanomaterials is important for envisioning the applicability of various nanofluids in the dielectrics industry.

The nanofluids are primarily classified based on the type of nanoparticles used in their synthesis. The following types of nanoparticles exist:

- Conducting (e.g., Fe_3O_4, Fe_2O_3, SiC, ZnO)
- Semi-Conducting (e.g., TiO_2, Cu_2O, CuO)
- Insulating (e.g., Al_2O_3, BN, SiO_2)

The types of nanoparticles that have been investigated in the past few decades include pure metals (Cu, Al, Au, Ag and Fe), metal oxides (Fe_3O_4, SiO_2, Al_2O_3, TiO_2, CuO, and ZnO), Carbides (TiC, SiC) and different carbon materials (graphite, diamond, single/multi-wall carbon nanotubes). A lot of these types of nanoparticles have been incorporated into fluids like water, ethylene glycol and oils. Since, the scope of the present work resorts to the goal of improving the electrical characteristics of OPI, a considerable number of nanoparticles have, thus, been examined [5,6,21].

Conductive nanoparticles (especially Fe_3O_4) have already proven to have outstanding insulating and thermal properties [20- 22]. Later, several studies discovered that nonconductive nanoparticles (like Al_2O_3 and TiO_2) can also aid to improve transformer oil insulation strength of transformer oil [6]. The current work has been entirely focused on the development of NOPI based on Al_2O_3 and TiO_2 under the pretext of the aforementioned motivation. In general, nanoparticles have been chosen for nanofluid preparation by investigating their basic features such as conductivity and permittivity [11].

2.3 ELECTRICAL PROPERTIES

As previously mentioned, nanofluids are regarded as prospective substitutes for traditional transformer oils due to their impressive increase in electrical properties such as power frequency breakdown strength, Lightning Impulse Voltage Breakdown strength etc. These electrical properties are elaborately discussed in the following subsections.

2.3.1 POWER FREQUENCY BREAKDOWN STRENGTH

Power frequency breakdown voltage can be referred to as the value of applied AC voltage at which disruptive discharge initiates in the liquid. The most consequential prerequisite for investigating an insulating liquid is determining its power frequency breakdown strength (dielectric strength). According to IS 6792:1992, the conventional test method uses a small amount of insulating fluid that is drained in a beaker containing two electrodes separated by 2.5 mm. The voltage rise rate is 2kV/s. Impurities, such as moisture, tiny particles, and air or gas bubbles, have a major impact on the breakdown test. As a result, the measured breakdown voltage of a dielectric liquid mostly demonstrates oil quality instead of oil attributes. This breakdown strength of nanofluids is influenced by several factors. The elements influencing power frequency breakdown strength have been explored in the next section.

❖ **Factors Affecting Power Frequency Breakdown Strength:**

This part presents experimental investigations on the power frequency breakdown strength of nanofluids based on transformer oil

1. Moisture:

The moisture content of an insulating liquid has a major impact on its breakdown strength. Many studies have been conducted to examine moisture's effect on the breakdown strength of the insulating liquid. Segal *et al*. [21] created conductive mineral oil-based nanofluids from

Fe_3O_4 nanoparticles. They estimated the breakdown voltages of developed samples according to the ASTM D877 standard. They demonstrated that the breakdown strength of both the pure oil and nanofluid reduces as the water content increases, although the ferro nanofluid showed less dependency on moisture than the pure oil. Thereby, it was concluded that this could be due to dissolved water that is bound to the surface of nanoparticles.

Later on, Du *et al*. [26] evaluated the power frequency breakdown strength of mineral oil and nanofluids made of TiO_2 nanoparticles (semiconducting nanoparticles) with respect to humidity. At high relative humidity, this particular nanofluid comprising TiO_2 nanoparticles demonstrated a higher breakdown voltage than the mineral oil. This is because, the semiconducting TiO_2 nanoparticles reduced the distortion field created by moisture content, resulting in higher AC breakdown voltages.

2. Concentration of Nanoparticles:

Du *et al*. [27] investigated the breakdown strength of mineral oil and its respective TiO_2 (average particle diameter < 20 nm) nanofluids with varying nanoparticle concentrations (0.003 to 0.05 g/L). The power frequency breakdown strength was shown to improve with increasing concentration until a specific concentration was reached. When nanoparticle concentration is increased further, the power frequency breakdown voltage begins to deteriorate. It was determined that this decline is caused by agglomeration (clogging) of nanoparticles leading to a reduction in the breakdown voltage of the nanofluid.

The above results indicate that particle aggregation has a negative influence on the power frequency breakdown voltage of transformer oil, however, reverse nanoparticle aggregation produced by an electric field might constitute a favourable impact. This induced aggregation might be more effectual in scavenging the free electrons, resulting in sluggish streamer production and thus improved breakdown voltages [68–71].

3. Modification of the Surface of Nanoparticles:

Du *et al*. [28] evaluated the impact of several surface modifications of TiO_2 nanoparticles (0.006 g/ml), on the power frequency breakdown strength of transformer oil. Three distinct surface modifications were applied to investigate the influence on the breakdown strength. It was deduced that the addition of surfactants alters the trapping and de-trapping process of electrons, thus improving the breakdown strength of transformer oil. As the compatibility of the surfactant with the nanoparticle is a matter of serious introspection and extensive investigation, it finally boils down to the right selection of surfactants.

4. Types of Nanoparticles:

As previously stated in the preceding subsections, the selection of nanoparticles for the development of nanofluids for electrical requirements is based on their electrical conductivity and dielectric permittivity. This influences the relaxation time constant and thus the breakdown properties. Researchers have investigated and analysed a large number of nanoparticles to determine their effect on the breakdown strength of transformer oil and even different vegetable oils.

Lv *et al.* [7] evaluated the influence of three types of nanoparticles with varying dielectric characteristics on the power frequency breakdown strength of transformer oil without surface modification for nanoparticles. The concentrations of those nanoparticles in developed oil samples ranged from 0 to 5% g/L. The enhancement of power frequency breakdown strength was described by using the relaxation time constant of the nanoparticles.

A similar study was carried out by developing a ferrofluid with rapeseed oil as the base fluid. The average breakdown voltage of the aforementioned nanofluid samples was almost 20% higher than that of the base oil samples [29]. This increase could be attributed to the polarised nanoparticles capturing free electrons, preventing further streamer growth [22].

2.3.2 IMPULSE VOLTAGE BREAKDOWN STRENGTH

The impulse voltage breakdown voltage may be characterised as simulating a lightning strike. The IEC 60897 standard specifies a rising time of 1.2 microseconds and a fall duration of 50 microseconds. The impulse breakdown strength of produced nanofluids was studied by a large number of researchers. Many studies have been conducted to determine the impulse voltage breakdown strength of mineral oil-based and vegetable oil-based nanofluids [21,30]. The discussion of Impulse Breakdown Strength is beyond the scope of this paper.

2.3.3 CONDUCTIVITY, PERMITTIVITY AND LOSS FACTOR

Du *et al.* [6] and Ramu *et al.* [31] evaluated the fundamental dielectric parameters like conductivity, permittivity, and loss factor for both mineral oil and its corresponding nanofluids using TiO_2 and Fe_3O_4. The resistivity of nanofluids decreased with respect to the typical values of the transformer oil but it was quite close to that of transformer oil in service.

However, the relative permittivity value was significantly higher than mineral oil, which was reported to be advantageous in establishing a homogeneous electric field in an OPI system. Sartoratto *et al.* [32] investigated the dielectric characteristics of transformer oil-based ferrofluids at various concentrations. The relative permittivity of those samples varied significantly from 8.8 to 2.1. The resistivity was found to be in the $(0.7 – 2.5) \times 1010$ Ω-m range.

Mergos *et al.* [33] investigated the dielectric characteristics of paraffin oil suspended with TiO_2, CuO, Fe_2O_3, Al_2O_3 and Cu_2O nanoparticles, concluding that the dielectric properties of nanofluids are mostly determined by the grain size and chemical composition of the nanoparticles. In fact, it was deduced that the surface polarisation of nanoparticles produced by absorbed water molecules affected the dielectric behaviour of the nanofluids under investigation.

2.4 PHYSICAL AND THERMAL PROPERTIES

It is well known that the oil used in transformers serves two functions: insulation and cooling. Hence, in this context, the physical and thermal properties of the fluid play an important role in the development of nanofluids. Some of the physical and thermal properties have been discussed below.

2.4.1 THERMAL CONDUCTIVITY

Thermal conductivity is referred to as the property of a substance that allows it to conduct heat. The transformer fluids should serve as a heat transfer medium. Hence, thermal conductivity is a crucial criterion for increasing the heat transfer ability of a transformer fluid. As a result, the fluid should have high thermal conductivity, which determines the course for the choice of materials as transformer liquids. As mineral oil has a limited thermal conductivity, there is a greater risk of forming thermal hotspots and triggering breakdowns due to the sudden overloading. As a result, it necessitates the search for strategies to increase the thermal conductivity of transformer oil in order to extend the transformer lifetime and boost the cooling capacity. A transformer fluid should have high thermal conductivity to dissipate heat and low viscosity to allow oil to flow. It is therefore evident to include such nanoparticles in a base oil to dissipate heat by increasing oil thermal conductivity. The suspension of silica nanoparticles [34] and alumina nanoparticles [35] was reported to improve thermal conductivity. However, further investigation is beyond the scope of the thesis.

2.4.2 VISCOSITY

The viscosity of a fluid is an estimation of its resistance to shear flow. The capacity of an insulating fluid to transmit heat through conduction is affected by its viscosity. Cooling by conduction is the primary heat disposal process in transformers and higher viscosity results in the thermal hotspots within the transformer. Researchers discovered that the viscosity of copper oil-based nanofluids declined with rising temperature and increased with the increase in nanoparticle concentration, though it was consistently high when compared to mineral oil. Jin *et al*. [36] examined the viscosity of silica nanofluids with varying concentrations of nanoparticles. The results stated that the viscosity remained the same as that of mineral oil. The elements influencing the viscosity of oil are as follows: temperature, volume percentage of nanoparticles, nanoparticle shape and size, and various dispersion methods.

2.4.3 FLAMMABILITY

There have been reports of transformer explosions. They are quite tough to extinguish. It could even wipe out the surroundings with fire in case the oil leaks out. Hence, the flammability of transformer oil is a dangerous and complex safety problem. Therefore, a few metrics, such as the Flash Point and Fire Point, have been specified in the context of the flammability of transformer oil. The flash point of a volatile fluid is defined as the lowest temperature at which the fluid surface produces enough vapours to generate an ignitable mixture in the air. The temperature at which vapours continue to burn after being ignited is known as the fire point. It is the lowest temperature at which the sample sustains a fire.

The flash point is one of the best quality indicators for identifying the likelihood of fire danger. Beheshti *et al*. [37] estimated the flash point with respect to the nanoparticle concentration. At a specific concentration, the flash point of nanofluid increased by 4.6 per cent, but as concentration increased further, the flash point dropped. The critical parameters of the developed nanofluids were investigated by Karthik *et al*. [38]. The modification in the

nanoparticle volume concentration in transformer oil leads to a significant improvement in the fire point, flash point as well as viscosity.

2.5 STABILITY OF NANOFLUIDS

The primary goal of developing nanofluids was to improve their thermal conductivity. However, because of agglomeration, the nanofluids lose their ability to transfer heat. As a result, study on stability is a vital topic that can have a significant impact on the thermo-physical characteristics of nanofluids for application. Thereby, it is crucial to discuss the parameters influencing the stability of such nanofluids [12].

2.5.1 STABILITY DETERMINING MECHANISMS

The different stability determining mechanisms are discussed as follows:

1. Zeta Potential Analysis:

The potential difference between the dispersion medium and the stationary layer of fluid (attached to the particle) is referred to as the zeta potential. The zeta potential represents the degree of repulsion between adjacent, same charged particles in the dispersion. As a result, nanofluids with high zeta potentials are electrically stable, whereas colloids with low zeta potentials have a tendency to agglomerate. Nanofluids with zeta potentials ranging from (40-60) mV are extremely stable. Kim *et al*. [39] performed a zeta potential study on Au nanofluids and claimed exceptional stability.

2. Sedimentation Method:

The sedimentation method is the simplest way for determining the stability of nanofluids [40]. To initiate the sedimentation of nanoparticles in nanofluids, an external force field is to be introduced. The weight of sediment demonstrates the stability of nanofluids. In this context, nanofluids are called stable if the concentration of supernatant particles remains unchanged with time. Wang *et al*. investigated the sedimentation of an alumina-water nanofluid [41].

3. Centrifugation Method:

The aforementioned procedure requires a significant amount of time to complete the experiment. As a modified method over sedimentation, the centrifugation method is developed for stability assessment. Singh *et al*. [42] adopted this method to assess the stability of a silver nanofluid developed by reducing $AgNO_3$ and selecting polyvinylpyrrolidone (PVP) as a stabiliser. The remarkable stability of silver nanofluids was discovered due to the protective role of PVP, which decelerates particle agglomeration by steric action.

4. Electron Microscopy and Light Scattering Methods:

Two general approaches for visualising particle agglomeration include measuring the particle size distribution with a microscope and using light scattering techniques. To capture the digital image of nanoparticles, high-resolution microscopes such as TEM and SEM are

used. Researchers obtained TEM and SEM images of CuO nanoparticles in order to assess the stability of suspension [43,44]. The light scattering technique can also be utilised to investigate complicated nanocolloids. A long-term study has led to an assessment of the stability of the new class of colloids. As a result, researchers have offered several strategies for improving stability in the future.

2.5.2 STABILITY IMPROVEMENT METHODS

Some of the procedures for improving stability are shown below.

1. Addition of Surfactants:

Surfactants are chemical substances that are added to nanoparticles to reduce the surface tension of liquids and increase particle immersion. According to the literature, adding surfactants to nanoparticles prevents rapid sedimentation. Researchers have discussed many sorts of surfactants that have been utilised in various types of nanofluids. Some important surfactants quoted here are Salt and oleic acid [46], Sodium dodecyl sulphate (SDS) [45], Dodecyltrimethylammonium bromide (DTAB) [47] etc. It is to be kept in mind that this method cannot be implemented for nanofluids in a high-temperature ambience due to probable damage to bonding between surfactant and nanoparticle. Surfactants might also tend to raise the thermal resistance between the nanoparticle and the base oils, which may reduce the enhancement in thermal conductivity [48].

2. Surface Modification Techniques:

This procedure eliminates the need for surfactants. According to a few researchers, injecting functional nanoparticles into base fluids may come up with long-term stability for nanofluids. The stability of carbon nanotubes (CNTs) can be enhanced by adding hydroxyl groups present on their surfaces [49]. Plasma treatment has also been adopted to modify the surface of diamond nanoparticles to improve their dispersion in the water base [50]. Surface modification approaches are described in detail in the reference [48].

3. pH Control of Nanofluids:

The pH of a nanofluid is closely connected to its stability. Simple acid treatment, for example, could improve the stability of Carbon Nanotubes in water [51]. Li *et al*. [52] investigated several pH values for Al_2O_3 nanofluid and showed that adjusting the pH reduced the rate of agglomeration.

4. Ultrasonic Agitation:

Agglomerations were observed to occur over time after the nanofluids were prepared, resulting in quick sedimentation of nanoparticles because of increased downward body force. Manson *et al*. [52] worked on two different nanofluids; carbon black-water and silver-silicon oil. They used high-energy cavitation to break down particle clusters.

2.6 ADVANTAGES AND LIMITATIONS OF NANOFLUIDS

The advantages of nanofluids are discussed as follows:

2.6.1 ADVANTAGES

- Nanofluids have demonstrated superior power frequency and impulse breakdown performance with respect to Carrier oils. Therefore, it is implemented in HV applications.
- The rate of degradation of the nanofluid insulation is less influenced by the moisture ingression into it. Hence, it ensures extended transformer life.
- Nanofluids have proven to be more efficient in terms of thermal conductivity than conventional oil. As a result, it aids in more efficient transformer cooling.
- The anti-ageing properties of nanofluids improve the reliability of high voltage transformers.

The limitations of nanofluids are discussed as follows:

2.6.2 LIMITATIONS

- If the nanoparticle size in nanofluid is less than 100 nm, it is regarded as stable [53]. Although, it is difficult to keep this size down to 100 nm due to the attractive forces that exist between the nanoparticles, which potentially leads to agglomeration.
- Due to their highly reactive nature, nanoparticles are considered to be way more dangerous than micron-sized particles [54]. The nasal cavity can easily be penetrated by the nanosized particles, which could potentially result in major health issues. Iron oxide is regarded as catastrophic for the human lungs [55]. According to studies [56], ZnO nanoparticles are highly toxic, whilst Alumina nanoparticles are moderately toxic and magnetite nanoparticles are barely toxic. Titanium nanoparticles have been proved to be fatal because, when inhaled, they can enter the human brain through the olfactory neurons [57].
- Nanoparticles have occupational health and safety (OHS) risks and concerns are shown regarding them in the international guidelines [58]. During production, transportation, and preparation phases, the nanoparticles can enter the atmosphere, soil and water to cause serious damage to the ecology.
- One of the factors limiting the usage of nanofluids on a commercial and industrial level is their high manufacturing costs. Both one-step and two-step processes use expensive, cutting-edge equipment to prepare nanofluids, making them a fairly expensive alternative to transformer oil.

Chapter: 3

BRIEF DESCRIPTION OF METHODOLOGY

3.1 INTRODUCTION

In recent years, there has been an increase in interest in the condition assessment and monitoring of transformer insulation due to the increasing popularity of transformers in utilities around the world. Transformers are one of the most vital items of equipment in an electric power transmission and distribution system, and they play a significant role in delivering an efficient and reliable electricity supply. The state of transformer oil-paper insulation deteriorates during operation under a combination of electrical, thermal, chemical, mechanical and environmental stresses. The physical and chemical degradation processes caused by these stresses, such as ageing and moisture generation, affect the molecular microstructure of dielectrics and consequently influence the polarization and conduction processes. Conventional diagnostic procedures such as dissolved gas analysis (DGA) and degree of polymerization (DP) are used to monitor the ageing process of transformer insulation. However, the increasing demands for adequate tools to assess power system insulation non-destructively and reliably in the field drive the development of diagnostic tools based on changes in the dielectric characteristics of the insulation. Recovery Voltage Measurement (RVM), Frequency Domain Spectroscopy (FDS), and Polarization and Depolarization Current Measurements (PDC) are some of the newer diagnostic approaches [14,18,19]. These two later became available as user-friendly approaches quite recently and can be used to diagnose, monitor and check new insulating materials, as well as non-destructively qualify insulating systems during/after the production of power equipment.

3.2 TIME-DOMAIN SPECTROSCOPY

The dielectric response of an insulation system can be measured and represented in either the time domain or the frequency domain. In this section, the theory behind the time domain method is being discussed.

When an electric field is applied to a dielectric medium, a relative shift between positive and negative charge occurs, resulting in dielectric polarisation [21]. There are four types of polarisation mechanisms.

1) Electrical Polarization;
2) Ionic Polarization;
3) Orientational Polarization;
4) Interfacial Polarization.

Interfacial and Orientational polarisation mechanisms are sluggish and active at power frequencies or even lower frequencies [21-22]. For transformer oil-paper insulation this interfacial polarization is predominant at the interfacial region of oil and paper.

Let us suppose for a vacuum insulated electrode arrangement, the flux density D is proportional to electric field vector E,

$$D = \varepsilon_0 . E \tag{3.1}$$

If a homogeneous isotropic dielectric medium is employed instead of vacuum, then polarization, P should be taken into account in the relationship as follows,

$$D = \varepsilon_0 . E + P \tag{3.2}$$

Where,

$$P = \chi . \varepsilon_0 . E \tag{3.3}$$

Here, χ represents the electrical susceptibility of the material.

If the electric field is produced by a time-varying voltage, then equation (3.3) may be expressed as follows,

$$P(t) = \chi(t) . \varepsilon_0 . E(t) \tag{3.4}$$

Similarly, the expression for the electric flux density D(t) is

$$D(t) = \varepsilon_0 . E(t) + P(t) = \varepsilon_0 . \left[1 + \chi(t)\right] . E(t) \tag{3.5}$$

The polarization process, P(t) is comprised of the combined effect of all the polarization mechanisms. All the polarization takes a plenty amount of time to settle and finally becomes static $P(t \to \infty) = P_s$. The polarization vector, P(t) maintains a monotonically growing profile when a step voltage V_{dc} is applied to a charge-free dielectric medium. This polarization vector P(t) can be expressed as,

$$P(t) = \left(P_s - P_\infty\right) . g\left(t - t_0\right) + P_\infty . \delta\left(t - t_0\right) \tag{3.6}$$

Where $\delta\left(t - t_0\right)$ is dirac delta function which is considered for the fast polarization processes and $g\left(t - t_0\right)$ represents monotonically increasing function with time and it is considered for the interfacial polarization process.

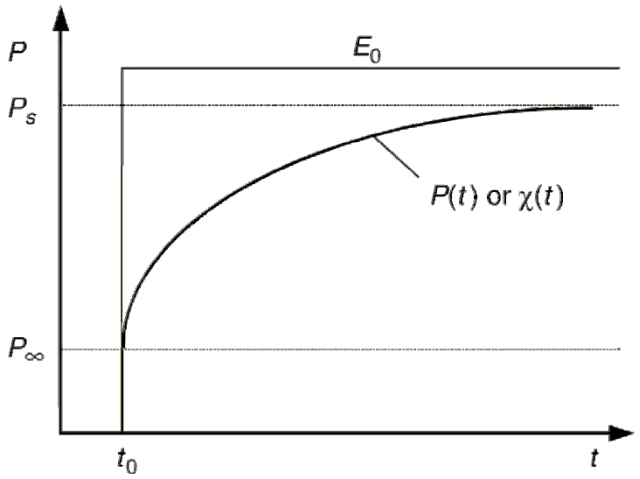

Fig. 3.1. Polarization of a dielectric under a step electric field of magnitude, E_0 at t = t_0.

Where,

$$g\left(t - t_0\right) \geq 0, \ \frac{\mathrm{d}g\left(t - t_0\right)}{\mathrm{d}t} \geq 0 \ for \ all \ t_0 < t < \infty$$
$$g\left(t - t_0\right) = 0 \ for \ all \ t \leq t_0$$
$$g\left(t - t_0\right) = 1 \ when \ t \to \infty \tag{3.7}$$

As per the equation (3.7) the polarization vector, P(t) due to the electric field at any time instant can be expressed as follows,

$$P(t) = \varepsilon_0 \cdot \left[\chi_\infty + \left(\chi_s - \chi_\infty \right) . g\left(t - t_0 \right) \right] . E(t) \tag{3.8}$$

Since susceptibility and the permittivity of the dielectric medium are related, the equation (4.8) can be expressed as,

$$P(t) = \varepsilon_0 \cdot \left[\left(\varepsilon_\infty - 1 \right) + \left(\varepsilon_s - \varepsilon_\infty \right) . g\left(t - t_0 \right) \right] . E(t) \tag{3.9}$$

Generally, a material cannot instantly polarize in response to an applied field. The polarization is a convolution of the electric field at previous times with time-dependent susceptibility. So, this P(t) can be expressed by,

$$P(t) = \varepsilon_0 \cdot \left(\varepsilon_\infty - 1 \right) . E(t) + \varepsilon_0 \cdot \int_{-\infty}^{t} f(t-\tau) . E(\tau) \, \mathrm{d}\tau \tag{3.10}$$

Where f(t) represents the dielectric response function which is a monotonically decreasing function and is expressed as follows,

$$f(t-\tau) = \left(\varepsilon_s - \varepsilon_\infty \right) . \frac{dg(t-\tau)}{dt} \tag{3.11}$$

Thereby, total current density J(t) under an electric field E(t) in the dielectric medium can be expressed as,

$$J(t) = \sigma_0 . E(t) + \varepsilon_0 . \varepsilon_\infty . \frac{\partial E(t)}{\partial t} + \frac{\partial P(t)}{\partial t} \tag{3.12}$$

Where ε_0 represents the permittivity in free space and σ_0 represents the dc conductivity of the dielectric medium.

The total current flowing through the dielectric medium for a homogeneous material can be written as,

$$i(t) = C_0 \cdot \left[\frac{\sigma}{\varepsilon_0} . U(t) + \varepsilon_r . \frac{\mathrm{d}U(t)}{\mathrm{d}t} + \varepsilon_0 \cdot \frac{\mathrm{d}}{\mathrm{d}t} \int_0^t f(t-\tau) . U(\tau) \, \mathrm{d}\tau \right] \tag{3.13}$$

Where C_0 is the geometric capacitance. The conductivity of the test sample is taken into account in the first part of the equation (3.13), and the other term is attributed to the various polarisation processes taking place inside the test sample. This equation is true whether there are one or more dielectric materials arranged in series or parallel.

3.2.1 POLARIZATION AND DEPOLARIZATION CURRENT MEASUREMENT

Polarization and depolarization current methods are the mainstays of time-domain dielectric diagnostics. This approach measures the charging and discharging currents of the insulation. The measurement of polarization and depolarization currents (PDC) following a dc voltage step is one way in the time domain to investigate the slow polarization processes. Before performing a PDC measurement, the dielectric memory of the test object must be erased. In order to accurately record the small polarisation current, the voltage source should be free of ripple and noise.

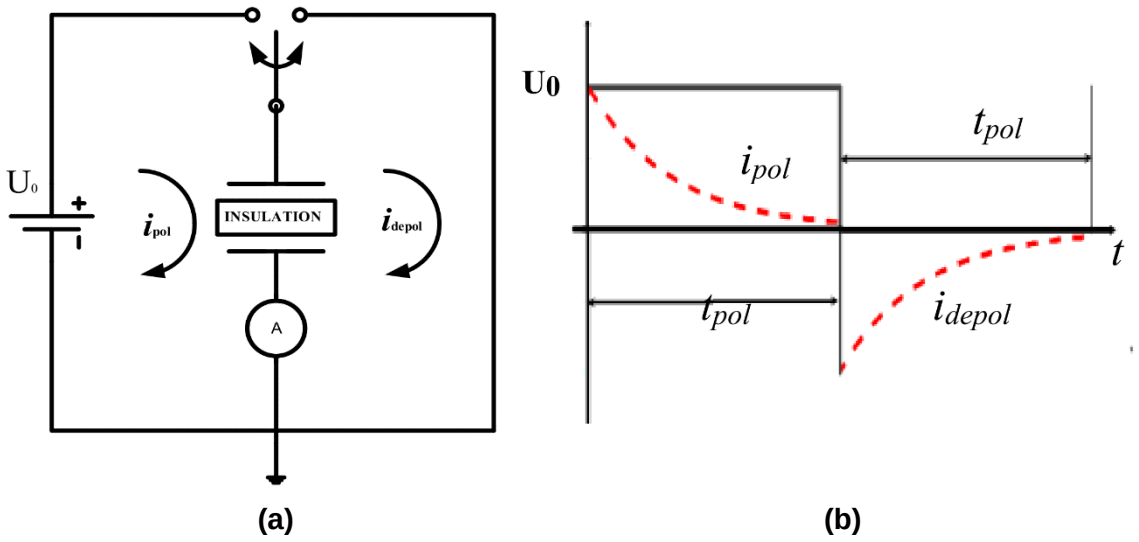

(a) (b)

Fig. 3.2. (a) PDC measuring circuit [14], (b) Principle of polarization and depolarization currents [14].

Fig. 3.2(a) shows the test setup for the PDC measuring methodology. This technique is acquired by applying a dc charging voltage of magnitude U_c (or, U_0, V_{dc}) to the test object for an extended period of time (e.g., 10,000s). During this period, the polarization current through the test object is measured. This current originates from the activation of the polarisation process with different time constants corresponding to different insulation materials and to the conductivity of the object which has been previously discharged carefully.

$$i_{pol}(t) = C_0 . V_{dc} . \left[\frac{\sigma_0}{\varepsilon_0} + \varepsilon_\infty . \delta(t) + f(t) \right] \tag{3.14}$$

After that, the voltage is removed and the dielectric is short-circuited at $t = t_c$ enabling the measurement of the depolarization current (or, discharging current), $i_{depol}(t)$ in the opposite direction, without the contribution of the conductivity. When the polarisation current becomes stable or very low, the measurement is normally terminated. In accordance with the superposition principle, the sudden reduction of the voltage U_c to zero is considered as a negative step voltage at $t = t_c$. If the test object is charged for a long time so that $f(t+t_c) = 0$, the dielectric response function f (t) is proportional to the depolarization current.

$$i_{depol}(t) = -C_0 . V_{dc} . \left[f(t) - f\left(t + t_c\right) \right] \; for \; 0 < t < \infty \tag{3.15}$$

Hence, the value of $f(t+t_c)$ is very low compared to f(t) for a longer charging time and thus can be neglected. Therefore, the depolarization current expression can be rewritten as,

$$i_{depol}(t) = -C_0 . V_{dc} . f(t) \quad for \; 0 < t < \infty \tag{3.16}$$

Fig. 3.2(b) depicts the principles of polarisation and depolarization current. The dc step voltage U_c charges the insulation between the windings. To determine the interfacial polarization and paper condition, a prolonged charging period (10,000 s) is required. The initial time dependence of the polarisation and depolarization currents (100 s) is highly sensitive to

oil conductivity, whereas the moisture content of the press board primarily affects the shape of the current over a much longer time period.

The dc conductivity may now be calculated from the PDC curves by subtracting the depolarization current from the polarisation current at longer time periods. As a result, the dc conductivity, σ_0 can be represented as,

$$\sigma_0 = \frac{\varepsilon_0}{C_0 . V_{dc}} \left[i_{pol}(t) - i_{depol}(t) \right] \tag{3.17}$$

3.2.2 FLOW CHART FOR PDC MEASUREMENT

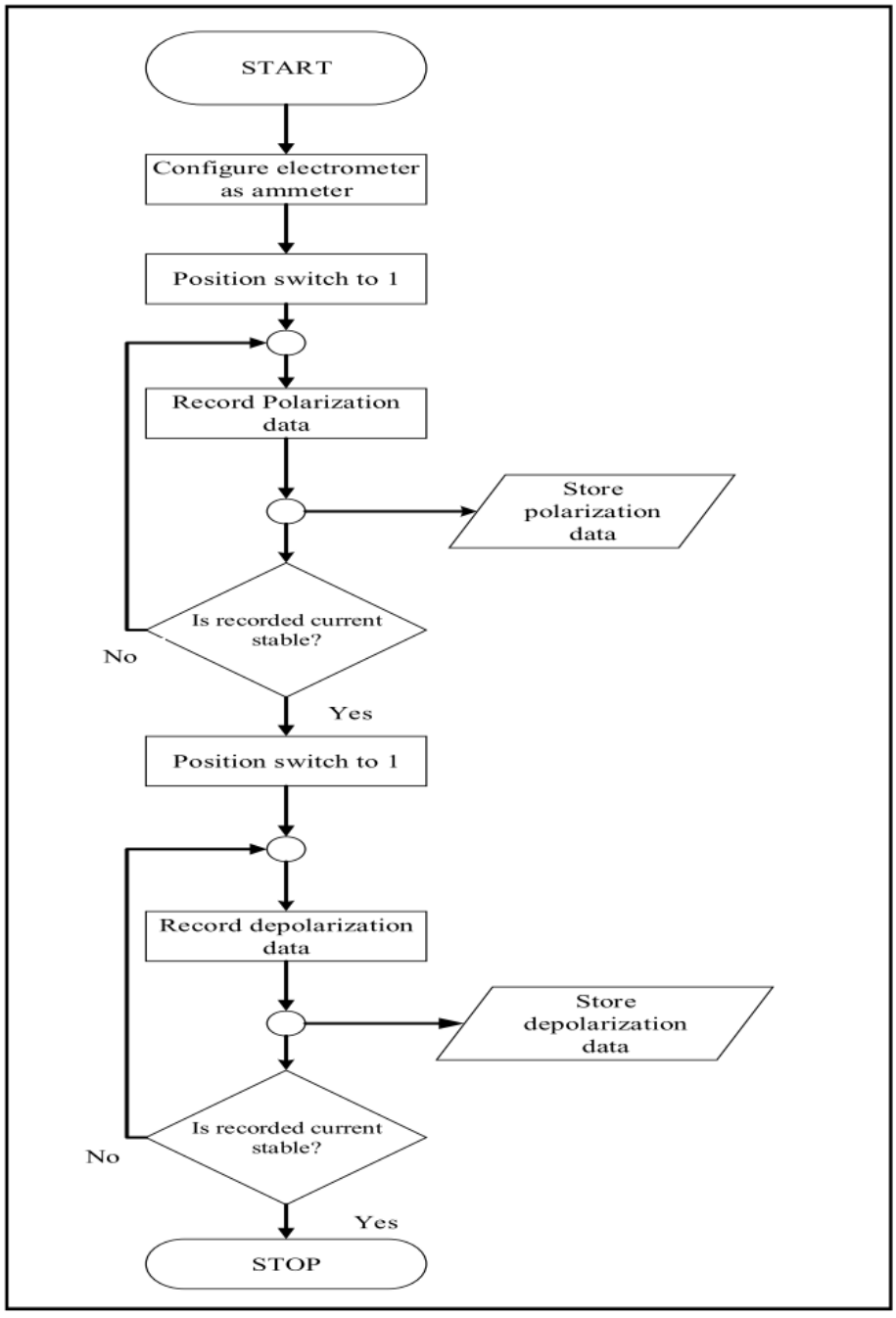

Fig. 3.3. PDC measurement flowchart [14].

The flowchart above illustrates an algorithm for measuring polarization and depolarization currents in order to determine the dielectric response of a specimen. With reference to Fig. 3.2(a), the electrometer detects the polarisation current when the switch is at position 1. Consequently, when the polarization current is found to be stable, the switch position is changed from 1 to 2. At position 2, the electrometer reads the depolarization current through the sample. When the depolarization current is found to be steady, this process is terminated.

❖ **Advantages of PDC Measurement:**

- This non-destructive methodology can determine the moisture content in solid insulation materials as well as the conductivities of oil and paper.
- Other diagnostic parameters, including activation energy and polarisation spectra, can be computed directly from PDC measurements.
- At low frequencies, this method provides a very fast response and it is a reliable method for data acquisition and analysis.

❖ **Limitations of PDC Measurement:**

- As the magnitude of polarisation and depolarization currents are in the range of (nA-pA), measurement can be affected by the external noise.
- Because of the high noise sensitivity, appropriate shielding prior to the experiment is required.
- A high voltage source is required for PDC measurement for better accuracy due to the improvement in signal-to-noise ratio.

3.3 FREQUENCY-DOMAIN SPECTROSCOPY

Another alternative method for exploring polarization phenomena is the dielectric response in the frequency domain. In this AC test, the dissipation factor (tan delta) is calculated as a function of test frequency. FDS typically has a frequency range of 1 mHz to 1 kHz. This entails measuring impedance at various frequencies and possibly voltages as well. The dielectric is

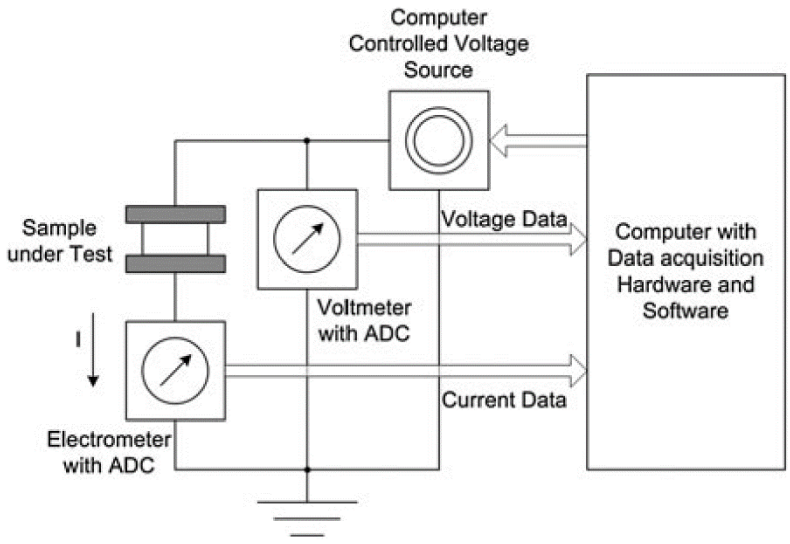

Fig. 3.4. FDS measurement circuit [14].

energised with sinusoidal voltages, and the current measured across it. Measurements in the frequency domain require variable frequency voltage sources and output voltages of these sources are at least a few hundreds of volts for the applications involving HV power equipment. A basic circuit diagram of FDS measurement has been shown in Fig. 3.4.

A pure sinusoidal voltage $U_0(\omega)$ [or, $V(\omega)$, $U_c(\omega)$] is applied to the insulator in the frequency domain analysis. Under the presence of a sinusoidal electric field, the polarization process begins, and the dielectric response current flows through insulation. The relationship between the applied AC voltage $V(\omega)$ and measured current $I_m(\omega)$ can be expressed as follows [14],

$$I_m(\omega) = C_0.U_0.\left[\frac{\sigma_0}{\varepsilon_0} + j\omega\varepsilon_\infty + j\omega F(\omega)\right] \tag{3.18}$$

Where $F(\omega)$ is the Fourier transform of a dielectric function f(t). $F(\omega)$ can be related to the susceptibility of the dielectric sample as,

$$F(\omega) = \int_0^\infty f(t).e^{-j\omega t}dt = \hat{\chi}(\omega) = \chi'(\omega) - j\chi''(\omega) \tag{3.19}$$

Where, $\hat{\chi}(\omega)$ is complex susceptibility of the sample, $\chi'(\omega)$ represents the real component of the complex susceptibility and $\chi''(\omega)$ denotes the imaginary component of the complex susceptibility.

Substituting $F(\omega)$ to equation (3.18),

$$I_m(\omega) = j\omega.C_0.\left[1 + \chi'(\omega) - j\left(\frac{\sigma_0}{\varepsilon_0.\omega} + \chi''(\omega)\right)\right].U_0(\omega) \tag{3.20}$$

$$\text{Or, } I_m(\omega) = j\omega.C_0.\left[\varepsilon'_r(\omega) - j\varepsilon''_r(\omega)\right].U_0(\omega) \tag{3.21}$$

$$\text{Or, } I_m(\omega) = j\omega.\left[C'(\omega) - C''(\omega)\right].U_0(\omega) = j\omega.\widehat{C}(\omega).U_0(\omega) \tag{3.22}$$

Often it is more suitable to use complex permittivity instead of complex susceptibility and it can be expressed as $\varepsilon'_r(\omega) - j\varepsilon''_r(\omega)$.

Complex susceptibility $\hat{\chi}(\omega)$ can be related to the complex permittivity $\hat{\varepsilon}(\omega)$ through the following equation,

$$\varepsilon'_r(\omega) = 1 + \chi'(\omega) \tag{3.23}$$

$$\varepsilon''_r(\omega) = \frac{\sigma_0}{\varepsilon_0.\omega} + \chi''(\omega) \tag{3.24}$$

$\widehat{C}(\omega)$ is the frequency-dependent complex capacitance of the dielectric sample. The real part of complex capacitance $C'(\omega)$ denotes the energy storage capacity of a dielectric during the polarization process. The imaginary part of the complex capacitance, $C''(\omega)$ of an insulating material resembles the lossy nature of the dielectric material. The absorption of electrical energy by the dielectric substance under the application of an alternating electric field is referred to as "dielectric loss." Dielectric losses in a dielectric material under the presence of an alternating electric field are caused primarily by the DC conductivity of the dielectric substance and friction losses between different dipoles. Losses due to the direct current

conductivity is becoming more prevalent in the presence of low-frequency sinusoidal voltage, where the time period of a one-half cycle is long enough to cause long-range charge migration [26]. Frictional losses between dipoles are primarily caused by active polarisation processes within the dielectric material. Dissipation factor (or, $\tan\delta$) is defined as the ratio of heat loss to energy storage in a dielectric medium and can be represented as,

$$\tan\delta(\omega) = \frac{C''(\omega)}{C'(\omega)} = \frac{\frac{\sigma_0}{\varepsilon_0.\omega} + \chi''(\omega)}{\varepsilon'_r(\omega)} \tag{3.25}$$

According to equation (3.25) tanδ is a function of the frequency of applied sinusoidal voltage. Therefore, the measurement of tanδ for assessing the condition of insulation is preferable from a practical point of view because it is independent of the geometry of the test object, and should not depend on the applied voltage [19].

❖ **Advantages of FDS Measurement:**

- FDS provides information on the frequency-dependent heat dissipation factor as well as the real and imaginary components of the complex capacitance.
- It is a non-destructive method for determining the moisture content or migrating water content inside solid insulation.
- FDS has superior noise performance.
- FDS provides an understanding of the attributes of polarizability (χ') and losses (χ'') in a dielectric medium.

Chapter: 4

SAMPLE PREPARATION AND EXPERIMENTAL PROCEDURE

4.1 PREPARATION OF NOPS SAMPLE

Preparation of NOPS comprises two parts, that is,

i. The preparation of nanofluid
ii. The development of transformer insulation prototype.

Firstly, the nanofluid was prepared and then a TI which is already developed is submerged into it. These two processes are discussed thoroughly in the upcoming sections.

4.1.1 PREPARATION OF NANO FLUIDS

Nanodielectric has acquired significant attention due to recent progress in nanotechnology. Previously, researchers have attempted to make stable suspensions with microparticles as well but this did not provide fruitful results. So, they switched to nanoparticles for several number reasons:

- Nanoparticles remarkably boost the electrical properties of the oil like dielectric strength, impulse voltage withstand strength and so on;
- The addition of nanoparticles to transformer oil also significantly increases the thermal conductivity of the oil by improving its cooling capability;
- Clogging can be avoided by the use of nanoparticles instead of microparticles;
- As nanoparticles have wider surface areas, it provides good heat transfer capabilities and that leads to better stability of suspensions.

There are two methods of preparation of nanofluids, namely one-step and two-Step methods. The Two processes are discussed as follows.

❖ **One-Step Process:**

In this method, the development and suspension of nanoparticles in the base liquid are done simultaneously. The process of drying, storage and transportation is avoided to decrease the formation of agglomeration and to enhance the stability of nanoparticle suspension [59, 60]. The implementation of the one-step method is rare due to its high cost and less effectiveness for large-scale production.

❖ **Two-Step Process:**

In this method, the nanoparticles are developed by chemical or physical methods and then it is suspended in the base oil followed by ultrasonication and magnetic stirring. This method constitutes a high probability of agglomeration of nanoparticles. Broadly, this method is employed due to its cost on the lower side [20-22].

4.1.2 PREPARATION OF TIP

Press board and paper are used to make the TIP. The diameter of the pressboard cylinder is 70 mm. A layer of unimpregnated kraft paper B is wrapped around pressboard A, followed by a layer of copper foil C, which resembles the low voltage winding of a real-life transformer. C is covered with another layer of unimpregnated kraft paper D. Over the pressboard strips E,

another layer of unimpregnated kraft paper F is wrapped. The spacing between the pressboard strips is limited to a minimum of 10 mm. The pressboard strips that go between D and F function as oil ducts. Another layer of copper foil G is wrapped around F, which represents the transformer's high voltage winding. To finish the sample preparation, another layer of unimpregnated kraft paper H is placed over G. The laboratory test samples replicate the oil-paper insulation of in-service power transformers. The cross-sectional view is illustrated in Fig. 4.1. While Fig. 4.2(a) and 4.2(b) depict the side and the top view of the transformer insulation sample.

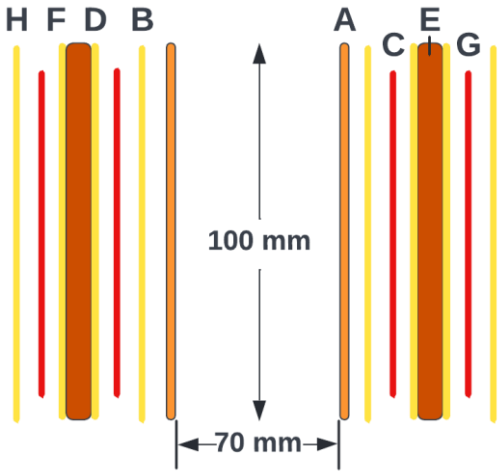

Fig. 4.1. Cross-sectional view of transformer insulation sample.

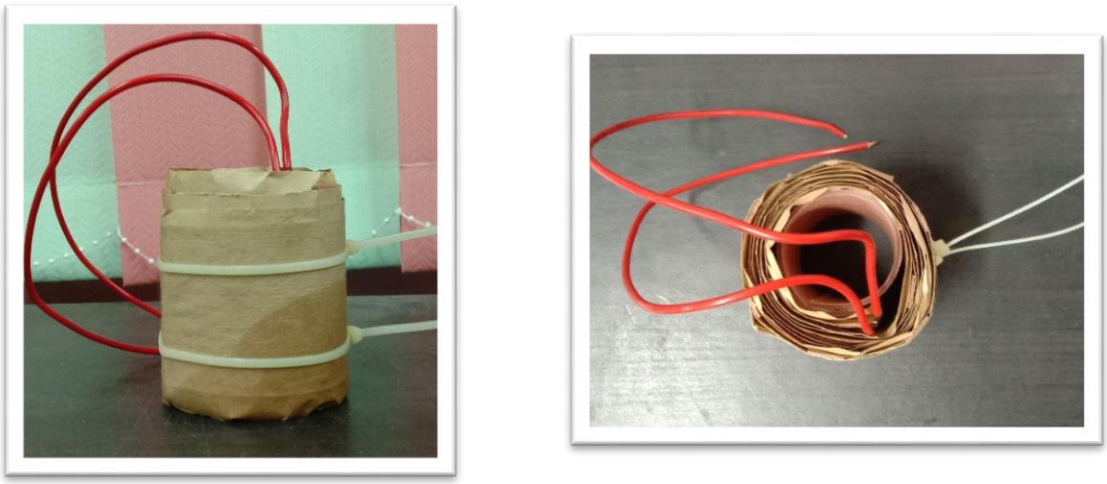

(a) **(b)**

Fig. 4.2. TIP: (a) Side view and (b) Top view.

4.2 MATERIALS USED

In this section, experimental details like the selection of materials, the equipment used, preparation of nano oil-paper insulation sample and different experimental procedures adopted have been presented.

For the preparation of nanofluid two-step process was adopted due to constraints of time and cost. Based on the prerequisite, two particular nanomaterials were purchased from a reputed dealer. A semi-conducting type and a non-conducting type nanomaterial were considered for the development of nanofluids. These were namely:

- Semi-Conducting Nanoparticle: **TiO_2** (Titanium Dioxide/Rutile)
- Non-Conducting Nanoparticle: **Al_2O_3** (Aluminium Oxide/Alpha)

The two nanoparticles are shown in Fig. 4.3(a) and Fig. 4.3(b), respectively. The diameter of TiO_2 and Al_2O_3 nanoparticles were 20 nm and (20-30) nm, dc. Mineral oil and vegetable oils were used as the base oil for both cases. The basic properties of chosen nanoparticles are listed in Table 4.1.

TABLE 4.1

BASIC PROPERTIES OF NANOPARTICLES

PARAMETERS	ALUMINA [Al_2O_3]	TITANIA [TiO_2]
Density (g/cm^3)	3.96	4.2
Electrical Conductivity (S/m)	10E-12	10E-11
Relative Dielectric Constant	9.9	100
Relaxation Time Constant (s)	12.2	77
Thermal Conductivity (W/m/K)	30	7.6

The selection of carrier oils was the next thing to check into. The most obvious alternative was the traditional petroleum-based Mineral oil used in the transformers. Mineral oil is well-known around the world for its great transformer compatibility as well as its electrical and dielectric characteristics. However, in recent years, the issue of environmental conservation has become a top priority for utilities.

As the oil is non-biodegradable, it will be difficult to dispose of it. As a result, the power industry will eventually seek out a variety of naturally acquired and synthetically obtained oils. Because of their biodegradable nature and various other increased qualities relevant to the purpose of transformer insulation, they are envisaged to serve as potential alternatives to conventional mineral oil. FR3 (a natural ester) is one of these alternate biodegradable oils. Some carrier oil properties that were important in choosing the base oil are listed in Table 4.2.

(a) **(b)**

Fig. 4.3. (a) TiO_2 nanoparticle and (b) Al_2O_3 nanoparticle.

TABLE 4.2

COMPARISON OF PROPERTIES OF CARRIER OILS

PROPERTIES	MINERAL OIL	VEGETABLE OIL [FR3]
Flash Point (℃)	140	>275
Fire Point (℃)	170	>300
Pour Point (℃)	-6	<-10
Dissipation Factor at 90℃	<0.005	<0.2
Biodegradability	NO	YES
Viscosity (mm^2/sec) at 100℃	2.6	<15
Relative Density at 20℃ (g/cm^3)	0.88	0.96
Dielectric Breakdown (kVrms) at 2.5mm gap	43	65
Price	₹78.25-₹156.51/litre	₹313.01-₹391.26/litre

4.3 EQUIPMENT USED

Several pieces of equipment were used in the development of the nanofluid samples, as well as in the subsequent experiments. The Jadavpur University High Tension Laboratory houses a variety of equipment and instruments for the development and investigation of NOPS(S). Hence, the major equipment used in the preparation of the sample has been illustrated with their specifications in the subsequent subsections.

1. THE MAGNETIC STIRRER:

As shown in Fig. 4.4, a magnetic stirrer or magnetic mixer is a laboratory instrument that uses a rotating magnetic field to cause a stir bar immersed in a liquid to spin very quickly. A rotating magnet or a series of stationary electromagnets could be used to create the revolving field beneath the liquid-filled vessel. The stir bar was spun at 1200 rpm in this experiment. Before performing sonication, it was used to mix the nanoparticles with the base liquid. The main difference between a magnetic stirrer and an ultrasonic bath is that the latter employs ultrasonic waves to agitate the particles in the liquid medium, resulting in uniform dispersion, whilst the former only stirs the mixture mechanically.

Fig. 4.4. Magnetic stirrer.

2. THE ULTRASONIC BATH:

The ultrasonic bath is a device that generates ultrasonic waves of high frequencies. Inside this, high-frequency electrical energy is converted into ultrasound waves by means of ultrasonic transducers. The device is shown in Fig. 4.5. The mixture obtained from magnetic stirring, when exposed to these ultrasonic waves results in the formation of bonds between the nanoparticle and the base oil through dispersion. A stable and homogeneous suspension of nanoparticles (TiO_2 and Al_2O_3 in our case) was created in the base oils (Mineral oil and FR3 in our case) through this ultrasonication process. The major functions of the ultrasonic bath were:

- Dispersing;
- Deagglomerating;
- Particle size reduction by disintegration.

Fig. 4.5. Ultrasonic bath.

3. THE HEATING OVEN:

The heating oven, as shown in Fig. 4.6, uses a thermostat to maintain a constant temperature in an isolated chamber. The NOPS(s), just after the preparation contain a large number of gas bubbles which are to be eliminated for purpose of dielectric insulation. This was successfully achieved using the heating oven. Different experiments were carried out at various

temperatures (25°C, 40°C, 50°C, and 70°C). The heating oven ensured the controlled temperatures needed to conduct the experiment.

Fig. 4.6. Heating oven.

4. THE VACUUM CHAMBER:

Degasification is the process of removing dissolved gases from liquids, in this context nanofluids. This procedure was performed in a specialized vacuum chamber. The Vacuum Chamber, depicted in Fig. 4.7, maintained extremely low pressures close to the vacuum. Henry's Law, which states that the amount of dissolved gas in a liquid is proportionate to its partial pressure, is being followed. As a result, putting a solution under low pressure makes the dissolved gas less soluble. As a result, the degasser eliminates the dissolved gases from the nanofluid that would otherwise form bubbles. To improve the degassing process, the liquid obtained after sonication was heated to around 50°C before being placed in the vacuum chamber. Therefore, dissolved gases were removed more effectively and quickly.

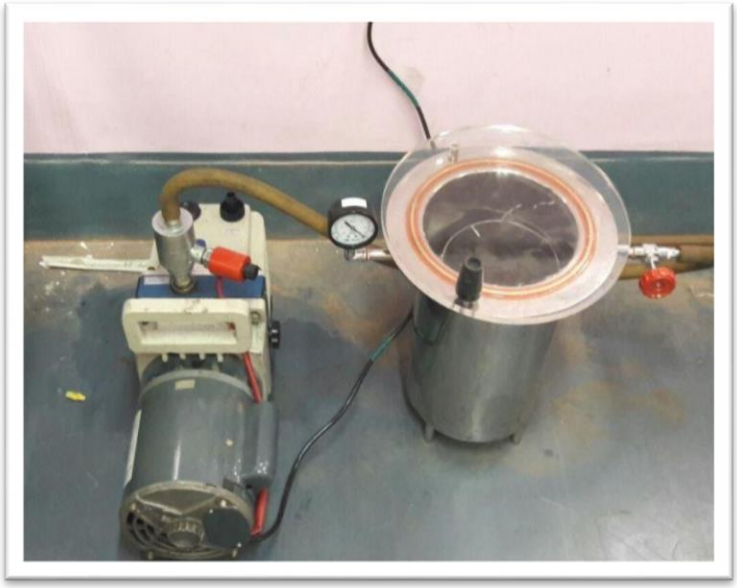

Fig. 4.7. Vacuum chamber.

5. PRECISION BALANCE:

Usually, for precision weighing purposes, precision balance is used. In our experiment, it was used for weighing nanoparticles (Titania and Alumina in our case). The high-tension laboratory hosts SAFFRON laboratory balance, as shown in Fig. 4.8.

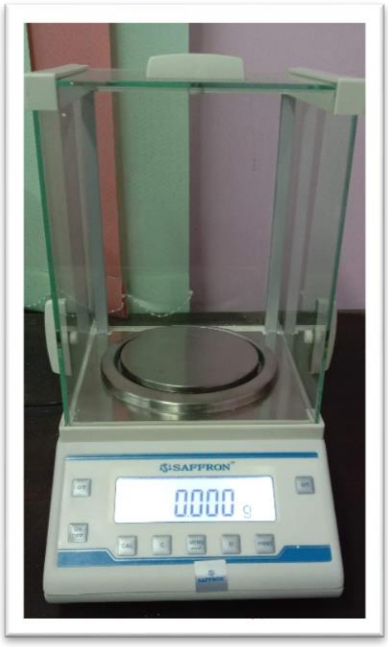

Fig. 4.8. Laboratory balance.

6. THE DIRANA:

The acronym DIRANA stands for Dielectric Response Analyzer, as shown in Fig. 4.9. The model number of the one in the High-Tension Laboratory is VEHP0072. With dielectric response analysis, it can detect the status of high voltage insulation systems such as power transformers, cables, bushings, and generators. It was employed in the current study to detect polarization and depolarization current (PDC) in order to investigate oil conductivity.

Fig. 4.9. DIRANA.

7. THE IDAX:

Insulation Diagnostic Analyzer, abbreviated as IDAX is a DFR (Dielectric Frequency Response) insulation diagnostic tool, sometimes known as FDS (Frequency Domain Spectroscopy), as shown in Fig. 4.10. DFR technology is a well-established laboratory test process that Megger has adapted for field use in the IDAX series of instruments through an inventive effort. In a nutshell, DFR is the measurement of capacitance and losses (tan delta or power factor) over a wide range of frequencies. Dissipation Factor Range is in the range of 0 - 10 (with retained accuracy of capacitance; otherwise higher). The measured DFR curve is affected by the shape of the insulation, moisture, oil conductivity, and temperature. The model number of the one in the High-Tension Laboratory is IDAX-300.

Fig. 4.10. IDAX.

❖ SAMPLE PREPARATION

Section 4.1 discussed the fundamental preparatory processes. The step-by-step approach for preparing nanofluids using the two-step method is detailed in this section. The procedure is stated below:

1. In a Glass beaker, 80 mg of nanoparticles were added to 400ml of base fluid (Mineral Oil/FR3) to reach a nanofluid concentration of 0.2g/litre. The magnetic bead was inserted in the beaker holding the suspension described above. The beaker was then put on the magnetic stirrer. For mechanically mixing the nanoparticle with the fluid, the stirrer was set at 1200 rpm. This procedure took approximately 30-45 minutes to complete.
2. After mechanical agitation with the magnetic stirrer, the nanoparticle-carrier oil combination was placed in the ultrasonic bath. The ultrasonic therapy was scheduled to last 6-6.30 hours. The sample was allowed to relax for 30 minutes every 2 hours during the sonication process.
3. Following the sonication procedure, the produced suspension and one paper transformer insulation prototype were placed in the heating oven and heated to a controlled temperature of around 50°C. This took an additional 30-45 minutes. This was done to expedite the removal of microbubbles from the suspension generated during the ultrasonic dispersion procedure and to remove moisture from the transformer insulation prototype.
4. Now, the developed sample was placed in the vacuum chamber. It was then treated for around 2 hours under low pressure in the vacuum chamber at less than 1kPa to eliminate the remaining moisture content from the sample.
5. After eliminating all bubbles from the sample, the transformer insulation prototype is submerged in it and the beaker was sealed with aluminium foil.

6. Then, it was allowed to settle for 2 hours to accomplish complete dispersion of the nanoparticle in the base fluid. If this was not done, the experimental results obtained differed significantly from those described in the literature. This completes the preparation of the NOPS, which will be employed in subsequent studies.

The complete nano oil-paper preparation process took about 11 hours. For the preparation of the pure mineral oil and vegetable (FR3) oil-based OPS steps, 1 and 2 were skipped. In our experiment, four NOPS(s) were prepared (two from mineral oil-based TiO_2 & Al_2O_3 nanofluids and two from vegetable oil (FR3) based TiO_2 & Al_2O_3 nanofluids). The procedure of experiments is explained in the next section.

4.4 EXPERIMENTAL PROCEDURE

The four effectively manufactured NOPS(s), along with the two pure base OPS(s) (mineral oil and vegetable oil [FR3]), were exposed to various experiments to obtain the dielectric response in order to analyse their behaviour under various physical situations. All of the samples were subjected to dielectric response tests such as time-domain spectroscopy (TDS) and frequency domain spectroscopy (FDS).

Under time-domain spectroscopy, Polarization & depolarization current (PDC) measurements were performed by connecting the leads coming out from the transformer insulation prototype immersed in a beaker holding the samples, to DIRANA, as shown in Fig. 4.11 and 4.13, in the same manner, the frequency domain spectroscopy was performed using IDAX-300, as illustrated in Fig. 4.12 and 4.13.

Fig. 4.11. DIRANA and laptop interfacing.

Fig. 4.12. IDAX and nano sample connection.

For both of the aforementioned tests, the samples were degassed at less than 1kPa in the vacuum chamber after being heated at around 50°C to remove excess moisture that accumulates during the ultrasonication process. Before conducting any tests, the samples were left idle for approximately 24 hours after treatment to achieve stability. To conduct those studies at higher temperatures, the beakers were placed in the controlled heating oven and then connected using external leads. The overall set-up is illustrated in Fig. 4.13.

Fig. 4.13. Overall experimental setup.

Chapter: 5

RESULT AND DISCUSSION

5.1 INTRODUCTION

In the previous chapter, the different techniques and step-by-step procedures to prepare NOPS have been presented. This chapter discusses experiments on two already prepared pure OPS(s) and four NOPS(s), namely:

- Mineral Oil-Based NOPS;
- Mineral Oil-Based TiO_2 NOPS;
- Mineral Oil-Based Al_2O_3 NOPS;
- Vegetable (FR3) Oil-Based NOPS;
- Vegetable (FR3) Oil-Based TiO_2 NOPS;
- Vegetable (FR3) Oil-Based Al_2O_3 NOPS.

Dielectric spectroscopy measurements were performed in these six samples in both the time and frequency domains. As discussed in chapter 3, in time-domain spectroscopy, a DC electric field was applied to a dielectric sample for a fixed time interval and during this interval, the charging or Polarization Current had been recorded. Then the dc field was removed and the insulation was short-circuited. During this time discharging or Depolarization Current had been recorded. The PDC measurements were executed on aforementioned samples at four different voltage levels (50V, 100V, 150V, 200V) and at five different temperatures (25^{o}C, 40^{o}C, 50^{o}C, 60^{o}C, 80^{o}C). From these data, DC Conductivity and Activation Energy of the NOPS have been calculated. In addition, the Nonlinear Nature of the Conduction Current for each sample under the influence of the DC field has been studied.

As explained in chapter 3, In frequency-domain spectroscopy, AC electric field was applied to the specimens at 140 Vrms in a frequency range of 1mHz to 40000 Hz at five different temperatures (25^{o}C, 40^{o}C, 50^{o}C, 60^{o}C, 80^{o}C). From the FDS, parameters like Dissipation Factor, Real and Imaginary Components of Complex Capacitance were found. With the help of these data, the Real and Imaginary Components of Complex Relative Permittivity for each sample have been calculated and presented in the graph. Furthermore, the AC Conductivity of the NOPS has been measured.

5.2 VALUE OF GEOMETRIC CAPACITANCE

The geometric capacitance is defined as the vacuum capacitance of the arrangement between which the dielectric is sandwiched. It is denoted by the symbol, C_o. One method to calculate the geometric capacitance is that the dimensions of the sample (TIP) are measured from which capacitance is calculated manually by using the formula,

$$C = \varepsilon_0 \cdot \frac{A}{d} \tag{5.1}$$

Where ε_0 is the permittivity of free space, "A'' is the area of the conductive plate and "d" is the distance between the plates.

Here, in our experiment calculated value of C_o is 133.40027E-12F.

5.3 COMPARATIVE STUDY OF PDC MEASUREMENT

In this section, the effect of temperature on polarization and depolarization current of each base OPS and NOPS has been studied. Furthermore, a comparative analysis has been performed for different NOPS(s) with their base OPS(s).

5.3.1 EFFECT OF TEMPERATURE ON POLARIZATION CURRENT FOR DIFFERENT NOPS(S)

In this section, the polarization current has been plotted against time for different temperature variations (25°C, 40°C, 60°C, 80°C) for a specific sample. The DC voltage applied across each OPS was 200V. In Fig. 5.1, Fig. 5.2, and Fig. 5.3 the effect of temperature on pure mineral OPS, mineral oil-based Alumina and Titania NOPS(s) are shown, respectively. In Fig. 5.4, Fig. 5.5, and Fig. 5.6 the effect of temperature on pure vegetable (FR3) OPS, vegetable (FR3) oil-based Alumina and Titania NOPS(s) are shown, respectively.

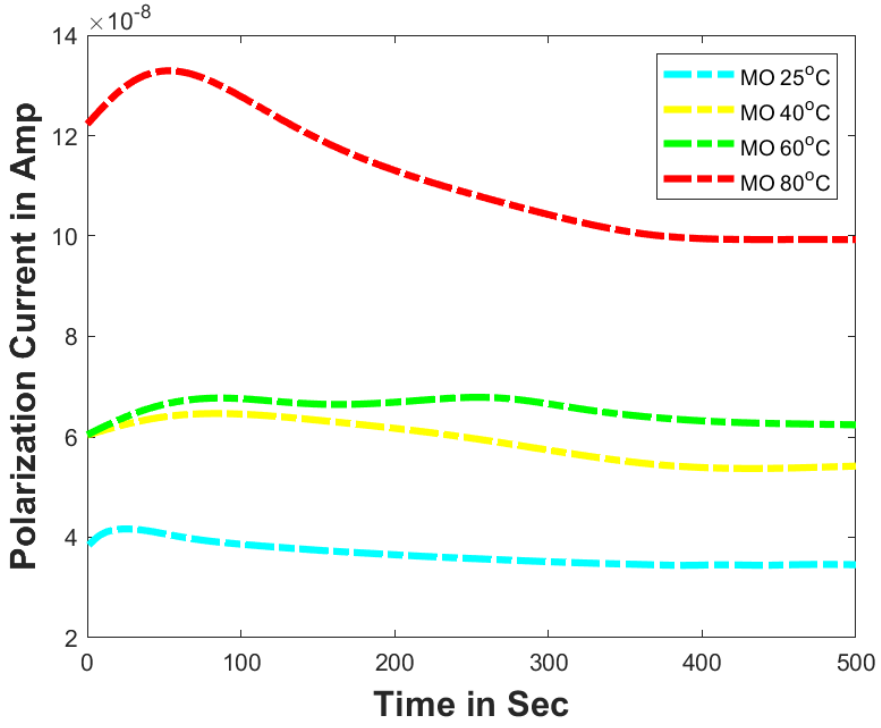

Fig. 5.1: Variation of polarization current of mineral OPS for different temperatures at 200V.

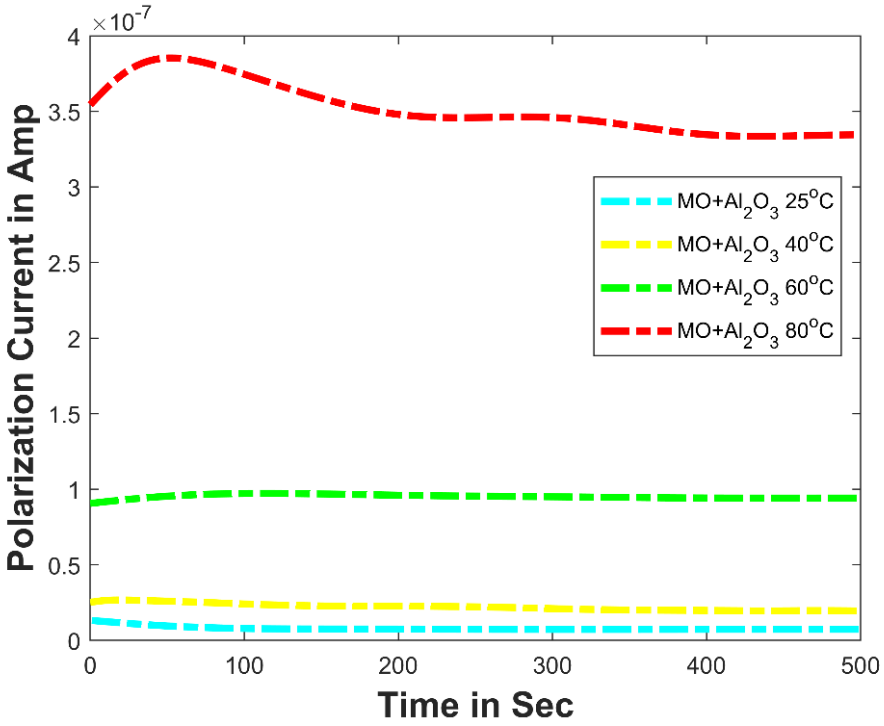

Fig. 5.2: Variation of polarization current of mineral OPS with Alumina for different temperatures at 200V.

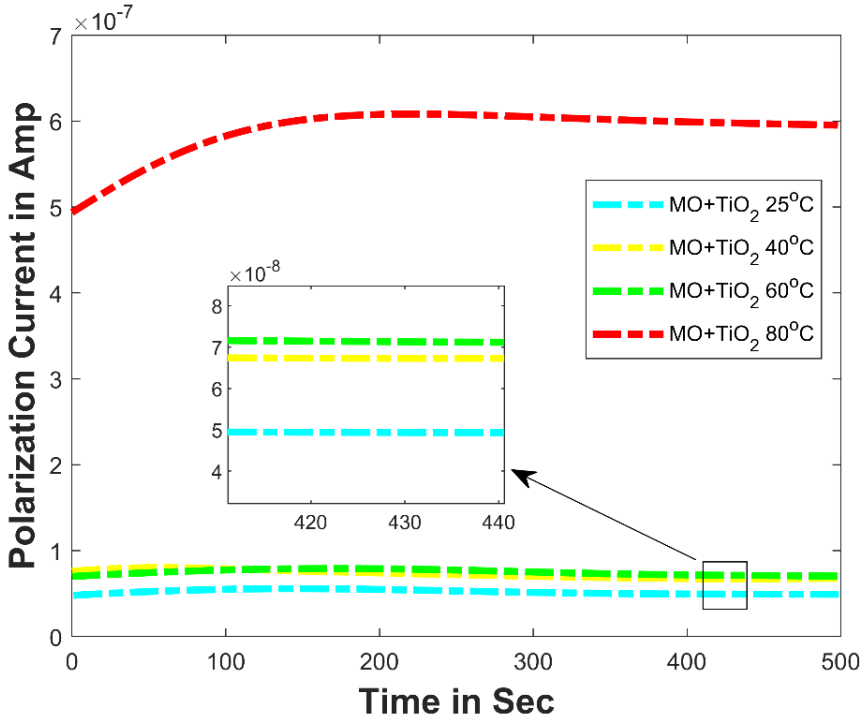

Fig. 5.3: Variation of polarization current of mineral OPS with Titania for different temperatures at 200V.

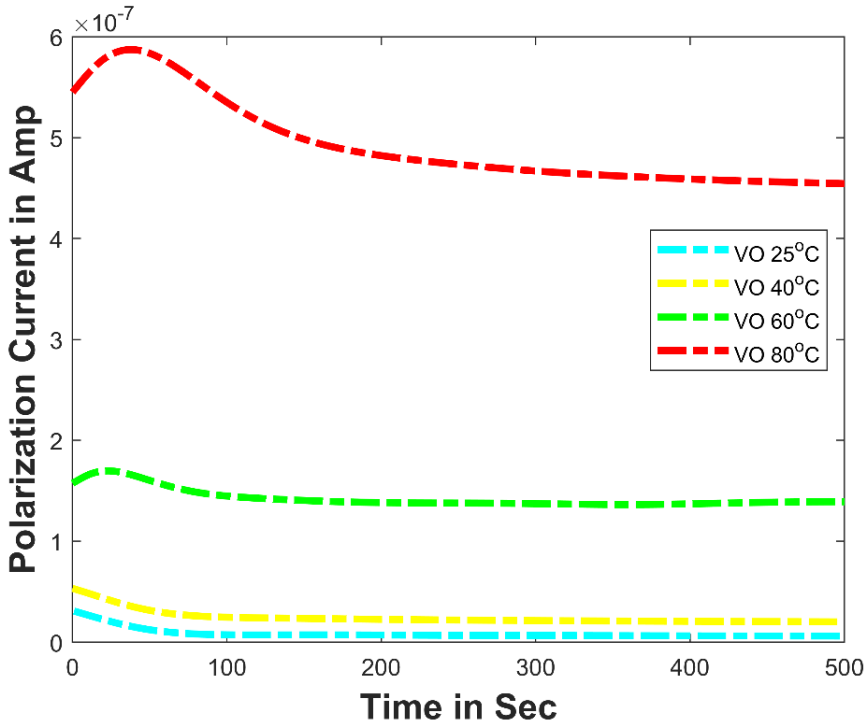

Fig. 5.4: Variation of polarization current of the pure vegetable (FR3) OPS for different temperatures at 200V.

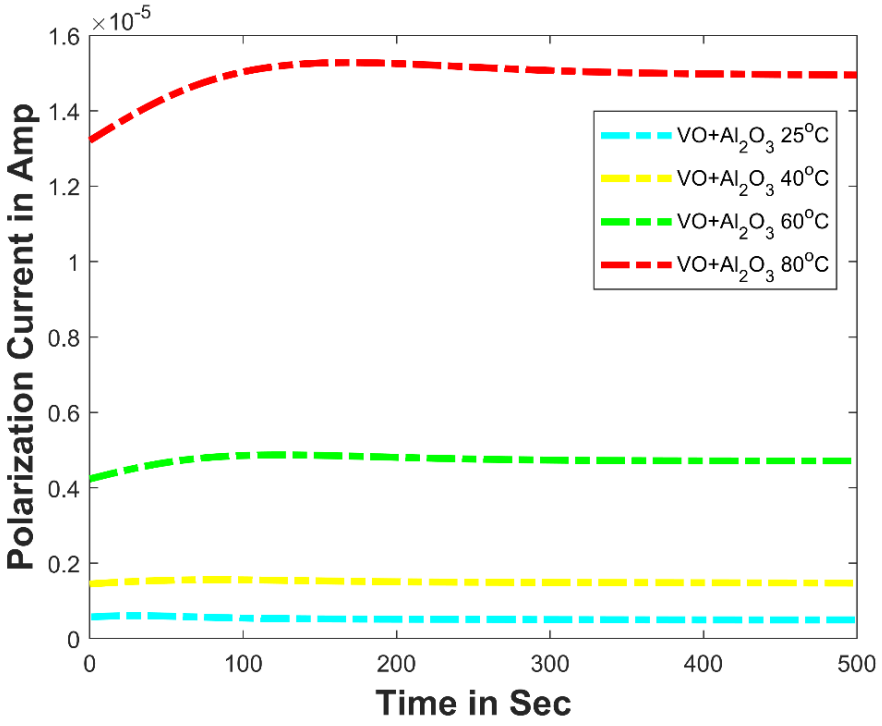

Fig. 5.5: Variation of polarization current of vegetable (FR3) OPS with Alumina for different temperatures at 200V.

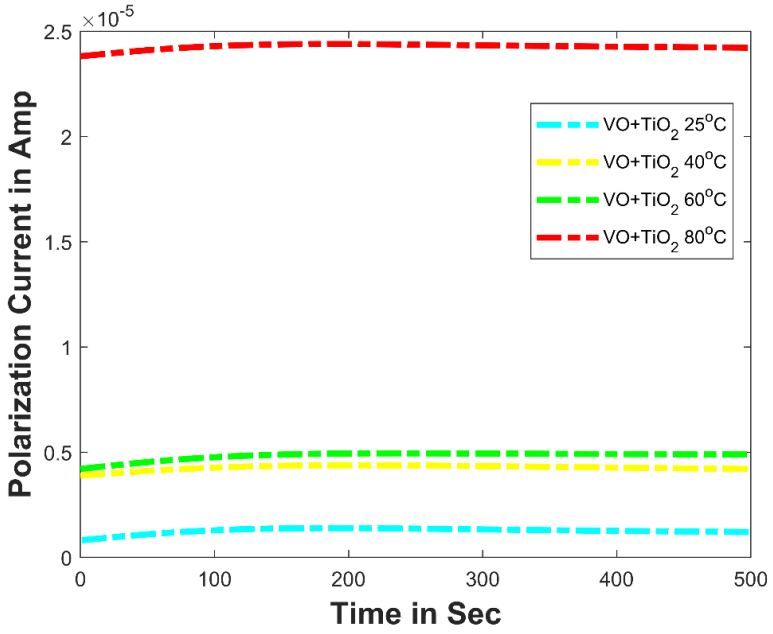

Fig. 5.6. Variation of polarization current of vegetable (FR3) OPS with Titania for different temperatures at 200V.

5.3.2 EFFECT OF TEMPERATURE ON DEPOLARIZATION CURRENT FOR DIFFERENT NOPS(S)

In this section, the depolarization current has been plotted against time for different temperature variations (25ºC, 40ºC, 60ºC, 80ºC) for a specific sample. In Fig. 5.7, Fig. 5.8, and Fig. 5.9 the effect of temperature on pure mineral OPS, mineral oil-based Alumina and Titania NOPS(s) are shown, respectively. In Fig. 5.10, Fig. 5.11, and Fig. 5.12 the effect of temperature on pure vegetable (FR3) OPS, vegetable (FR3) oil-based Alumina and Titania NOPS(s) are shown, respectively.

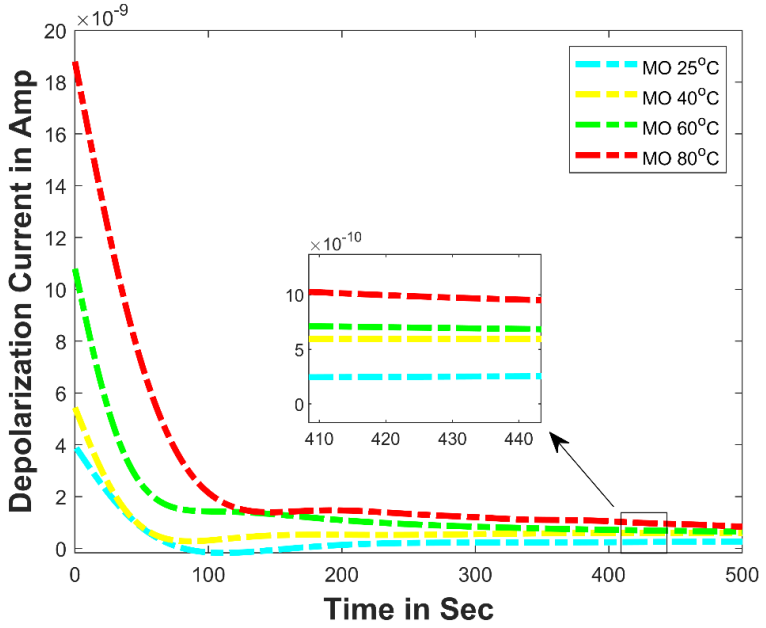

Fig. 5.7: Variation of depolarization current of mineral OPS for different temperatures at 200V.

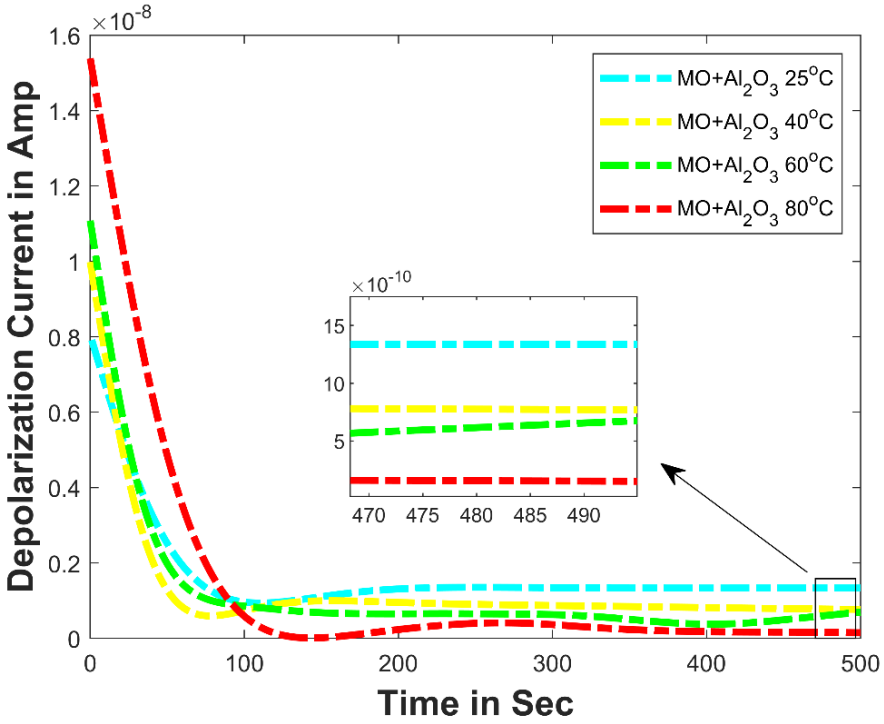

Fig. 5.8: Variation of depolarization current of mineral OPS with Alumina for different temperatures at 200V.

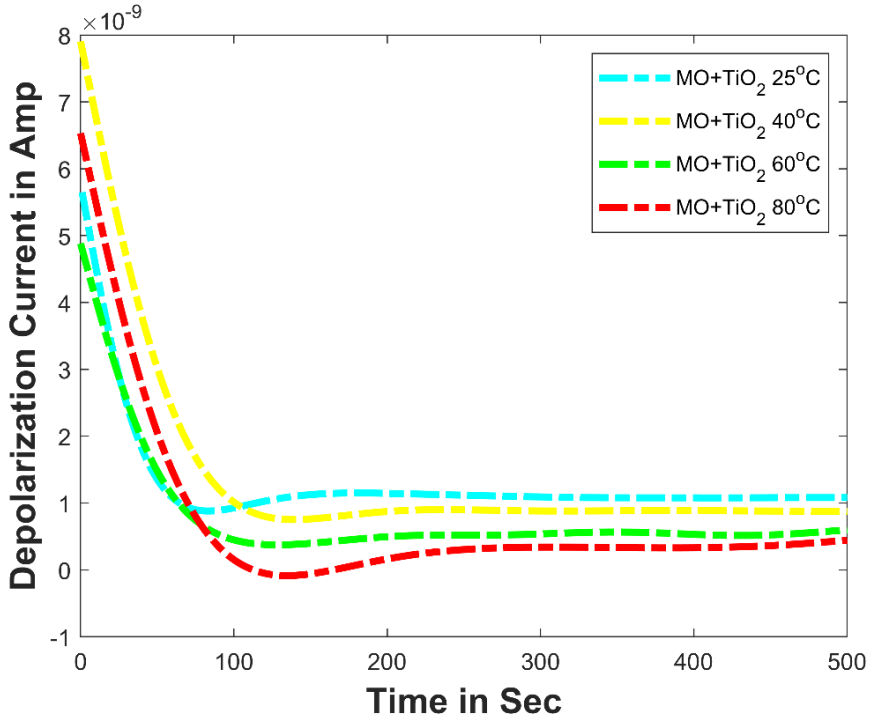

Fig. 5.9: Variation of depolarization current of mineral OPS with Titania for different temperatures at 200V.

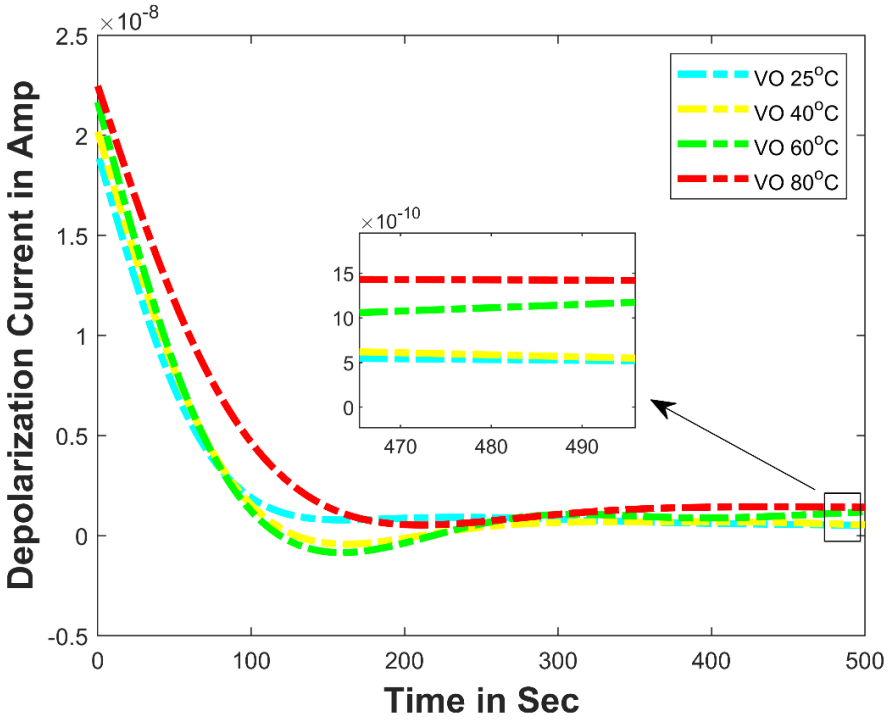

Fig. 5.10: Variation of depolarization current of vegetable (FR3) OPS for different temperatures at 200V.

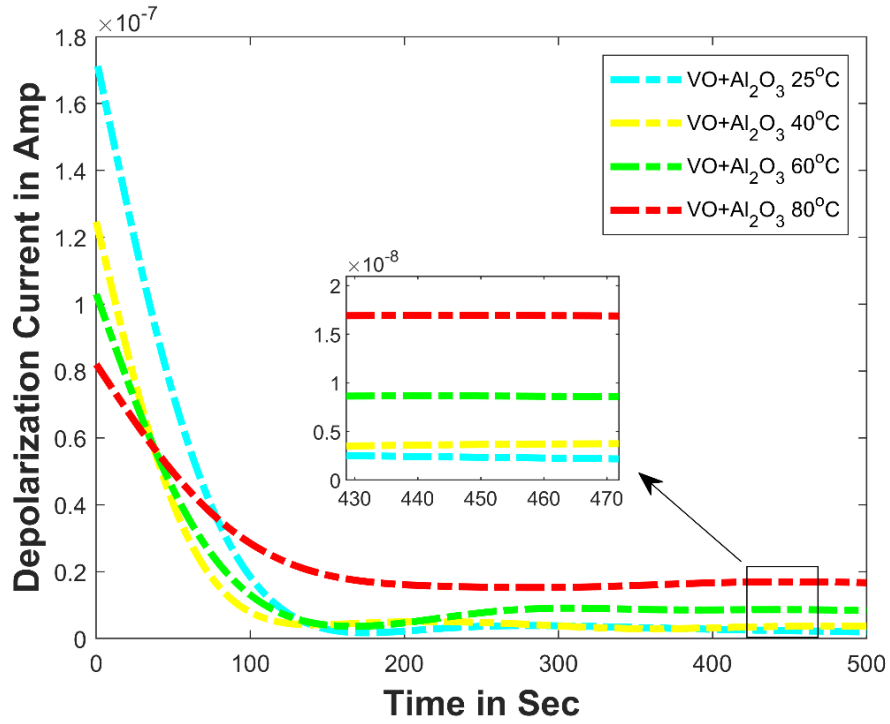

Fig. 5.11. Variation of depolarization current of vegetable (FR3) OPS with Alumina for different temperatures at 200V.

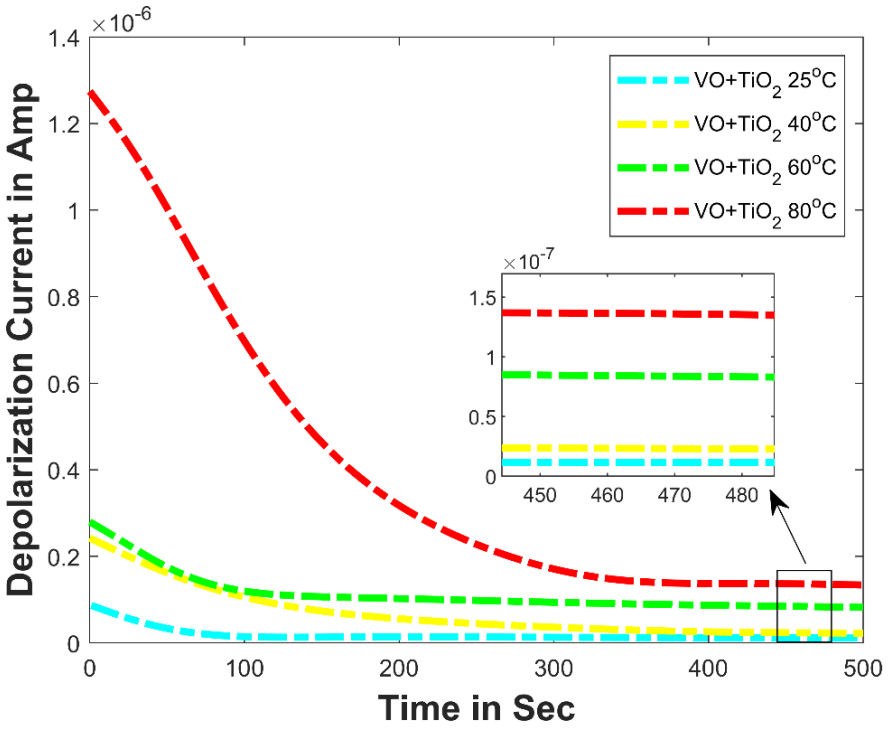

Fig. 5.12. Variation of depolarization current of vegetable (FR3) OPS with Titania for different temperatures at 200V.

5.3.3 COMPARATIVE ANALYSIS FOR POLARIZATION CURRENT FOR DIFFERENT NOPS(S) WITH THEIR BASE OPS(S) AT DIFFERENT TEMPERATURES

In this section, a comparative study of polarization currents has been carried out between pure OPS and its corresponding NOPS at different temperatures. In Fig. 5.13, the charging currents of pure mineral OPS, mineral oil-based Alumina and Titania NOPS(s) at 25ºC have been shown. In Fig. 5.14, the charging currents of the pure vegetable (FR3) OPS, vegetable (FR3) oil-based Alumina and Titania NOPS(s) at 25ºC have been shown, respectively.

In Fig. 5.15, the charging currents of the pure mineral OPS, mineral oil-based Alumina and Titania NOPS(s) at 50ºC have been shown. In Fig. 5.16, the charging currents of the pure vegetable (FR3) OPS, vegetable (FR_3) oil-based Alumina and Titania NOPS(s) at 50ºC have been shown.

In Fig. 5.17, the charging currents of pure mineral OPS, mineral oil-based Alumina and Titania NOPS(s) at 80ºC have been shown. In Fig. 5.18, the charging currents of pure vegetable (FR3) OPS, vegetable (FR3) oil-based Alumina and Titania NOPS(s) at 80ºC have been shown.

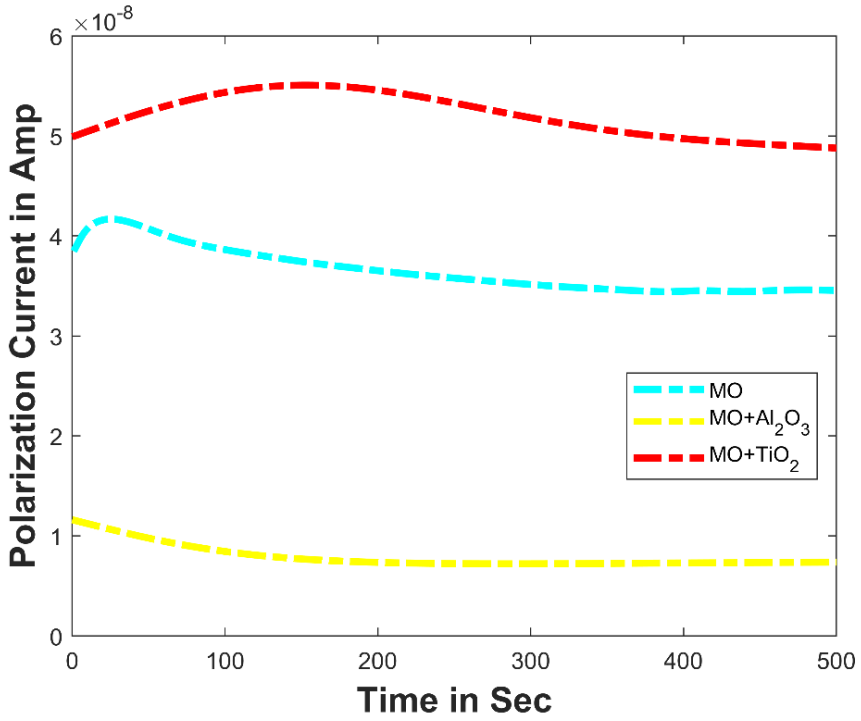

Fig. 5.13. Variation of polarization current of pure mineral OPS and its NOPS(s) at 25°C (at 200V).

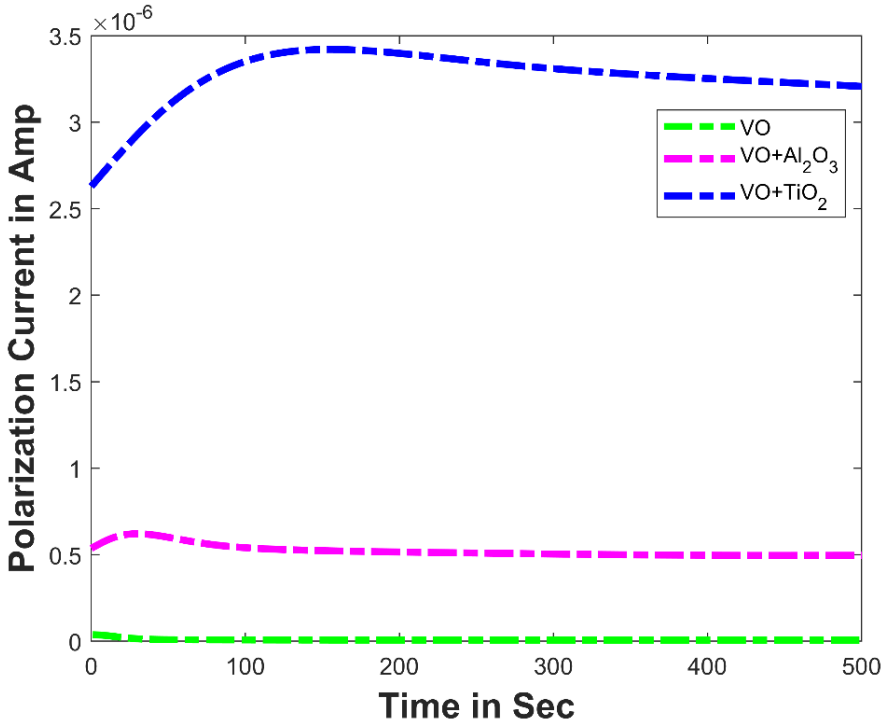

Fig. 5.14. Variation of polarization current of the pure vegetable (FR3) OPS and its NOPS(s) at 25°C (at 200V).

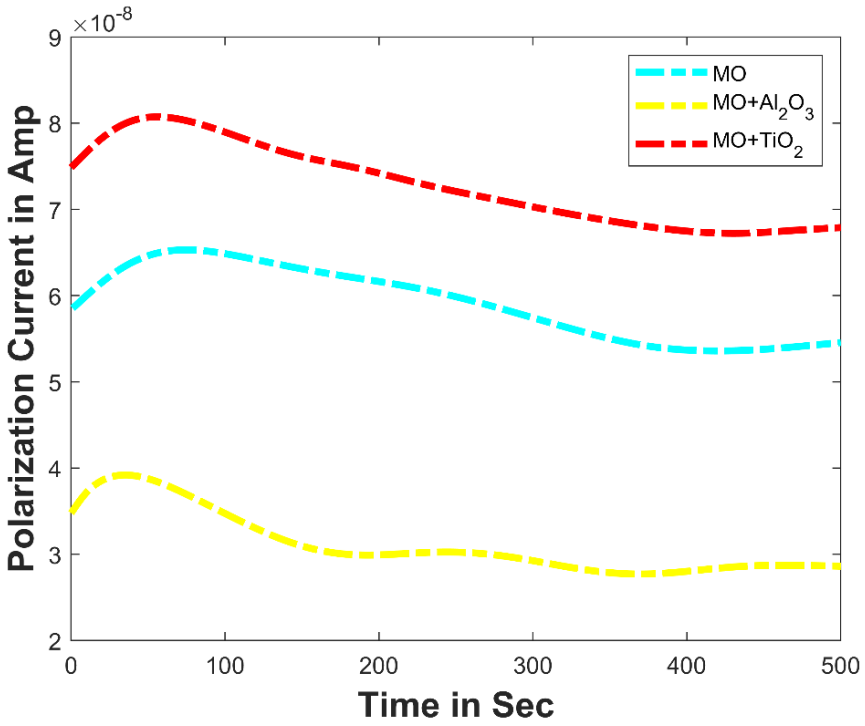

Fig. 5.15. Variation of polarization current of the pure mineral OPS and its NOPS(s) at 50°C (at 200V).

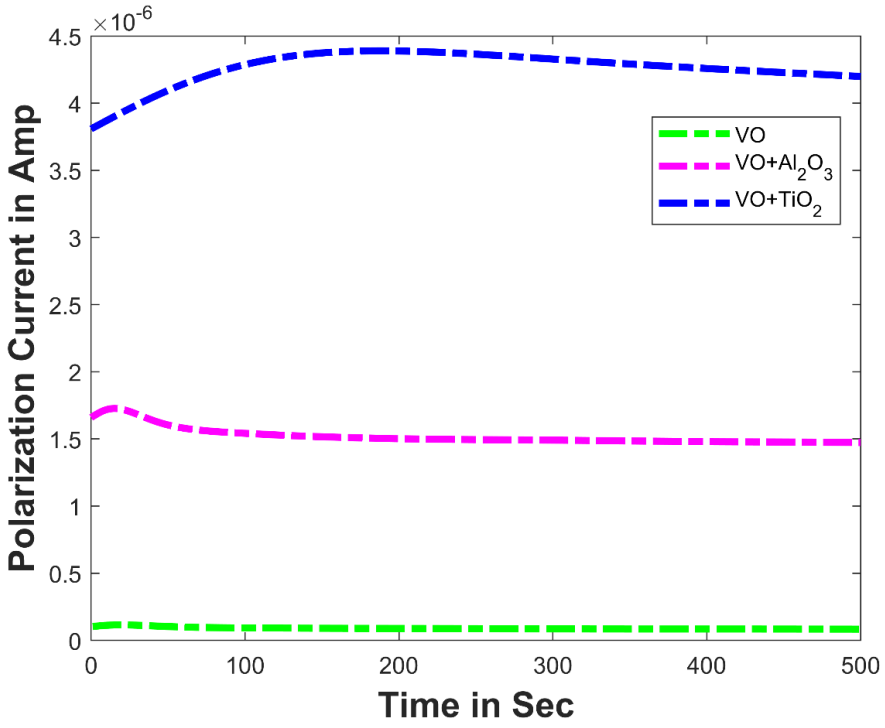

Fig. 5.16. Variation of polarization current of pure vegetable (FR3) OPS and its NOPS(s) at 50°C (at 200V).

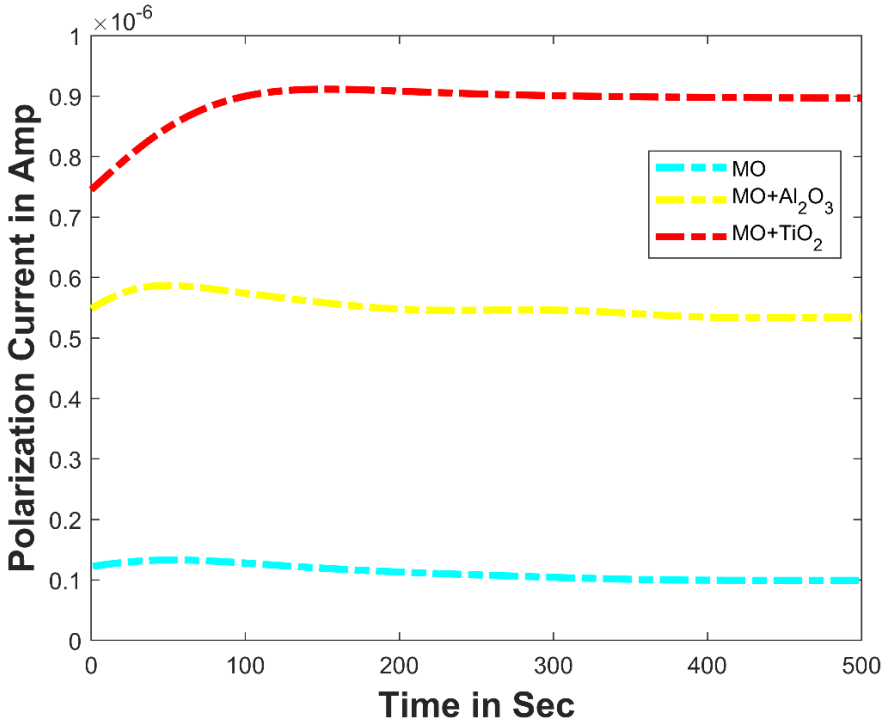

Fig. 5.17. Variation of polarization current of pure mineral OPS and its NOPS(s) at 80°C (at 200V).

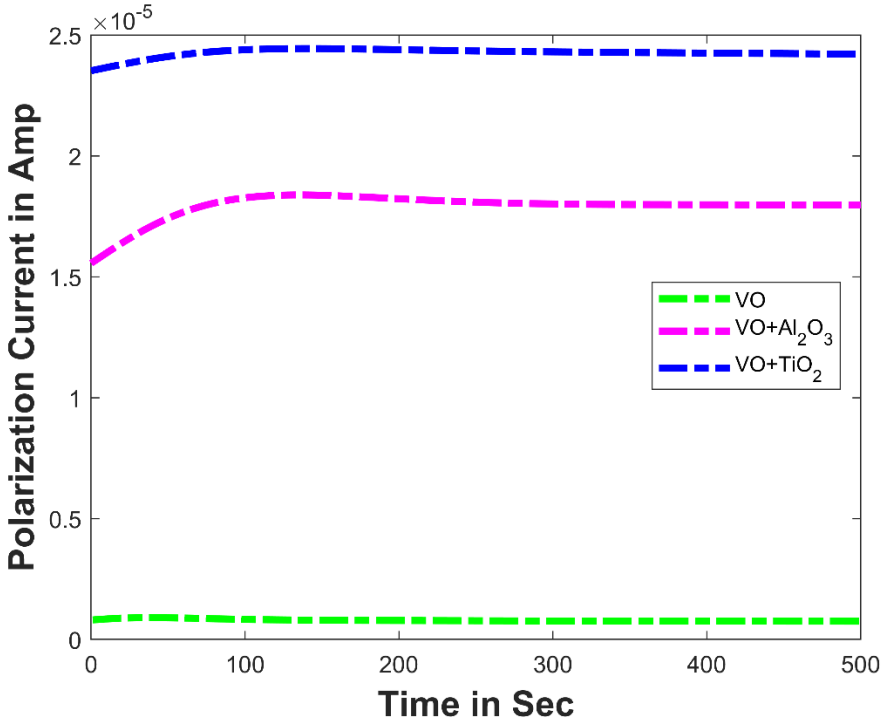

Fig. 5.18. Variation of polarization current of pure vegetable (FR3) OPS and its NOPS(s) at 80°C (at 200V).

5.3.4 COMPARATIVE ANALYSIS FOR DEPOLARIZATION CURRENT FOR DIFFERENT NOPS(S) WITH THEIR BASE OPS(S) AT DIFFERENT TEMPERATURES

In this section, a comparative study of depolarization currents has been carried out between pure OPS(s) and its NOPS(s) at different temperatures. In Fig. 5.19, the discharging currents of pure mineral oil-paper, mineral oil-based Alumina and Titania NOPS(s) at 25^{o}C have been shown. In Fig. 5.20, the discharging currents of pure vegetable (FR3) OPS, vegetable (FR3) oil-based Alumina and Titania NOPS(s) at 25^{o}C have been shown.

In Fig. 5.21, the depolarization currents of the pure mineral oil-paper, mineral oil-based Alumina and Titania NOPS(s) at 50^{o}C have been shown. In Fig. 5.22, the depolarization currents of the pure vegetable (FR3) OPS, vegetable (FR3) oil-based Alumina and Titania NOPS(s) at 50^{o}C have been shown.

In Fig. 5.23, the discharging currents of pure mineral oil-paper, mineral oil-based Alumina and Titania NOPS(s) at 80^{o}C have been shown. In Fig. 5.24, the discharging currents of the pure vegetable (FR3) OPS, vegetable (FR3) oil-based Alumina and Titania NOPS(s) at 80^{o}C have been shown.

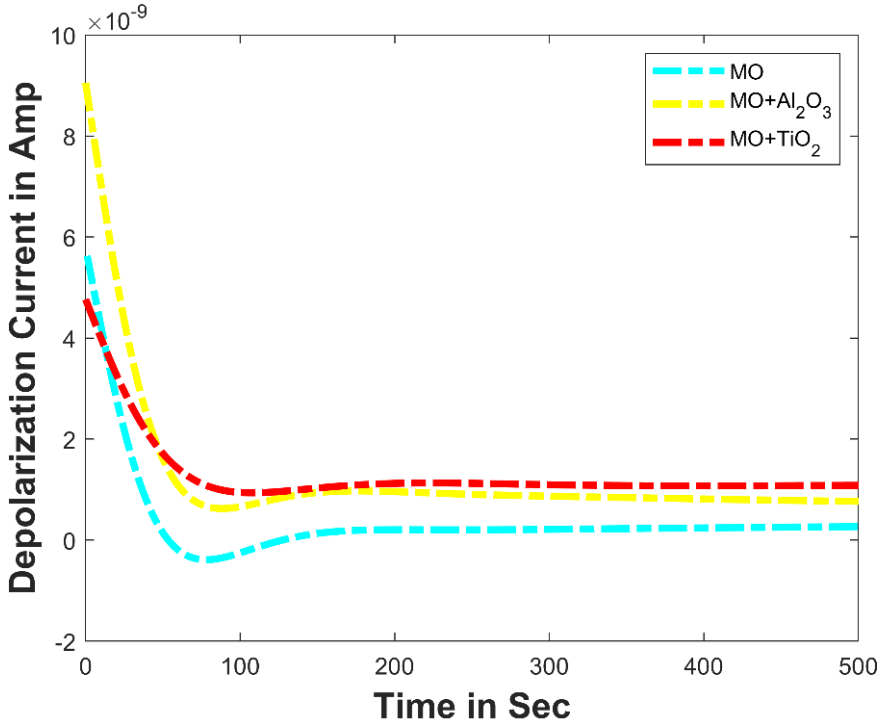

Fig. 5.19. Variation of depolarization current of pure mineral OPS and its NOPS(s) at 25^{o}C (at 200V).

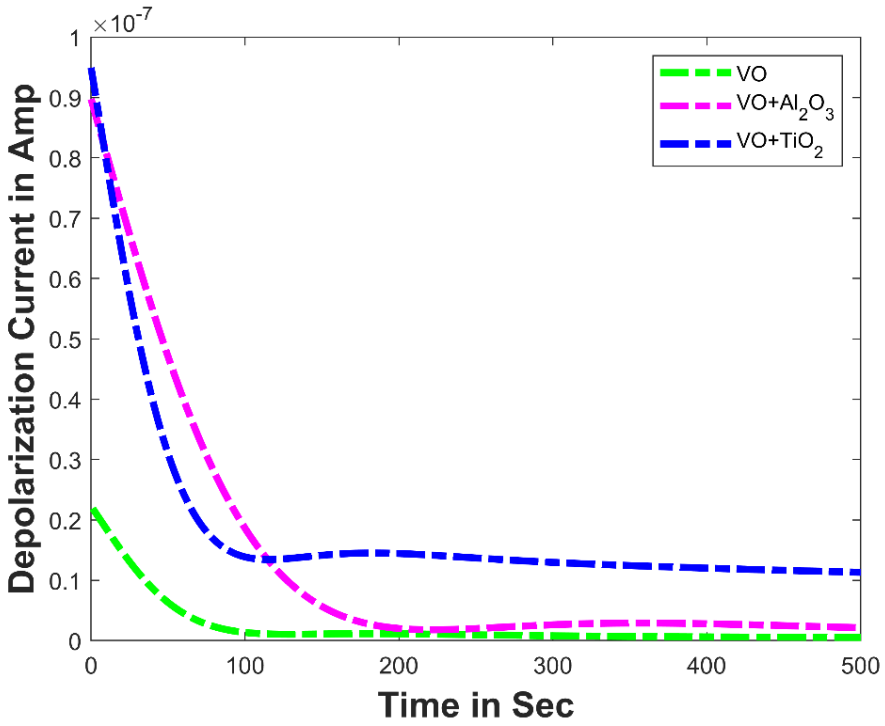

Fig. 5.20. Variation of depolarization current of pure vegetable (FR3) OPS and its NOPS(s) at 25°C (at 200V).

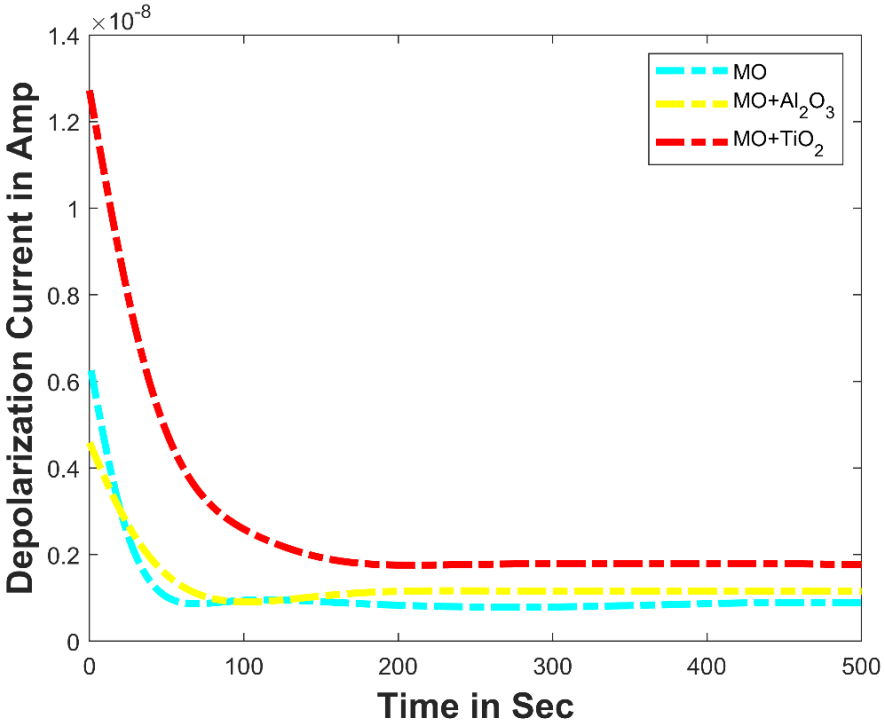

Fig. 5.21. Variation of depolarization current of pure mineral OPS and its NOPS(s) at 50°C (at 200V).

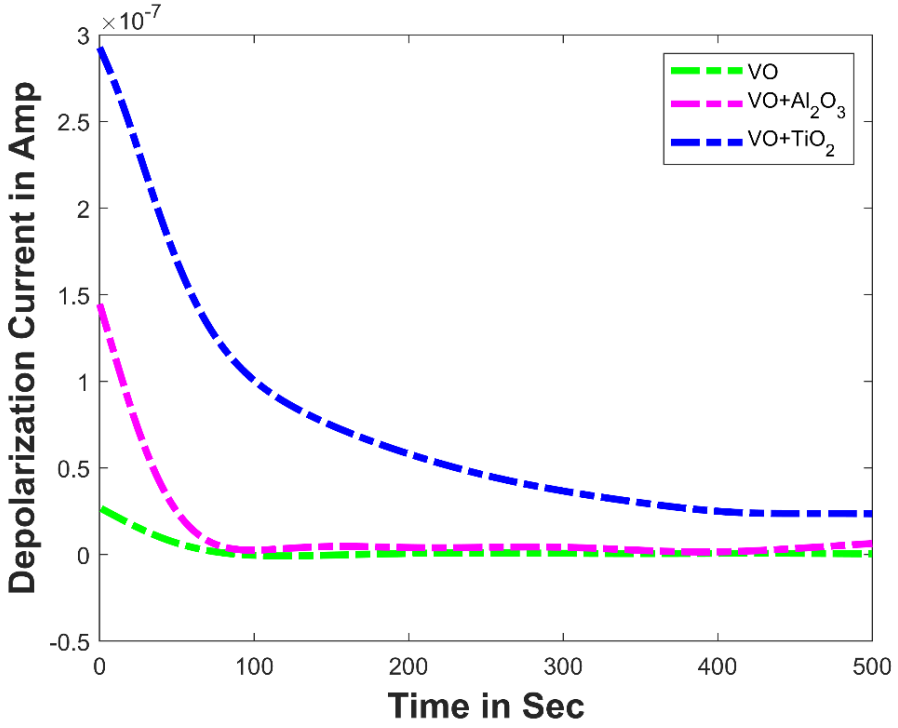

Fig. 5.22. Variation of depolarization current of pure vegetable (FR3) OPS and its NOPS(s) at 50°C (at 200V).

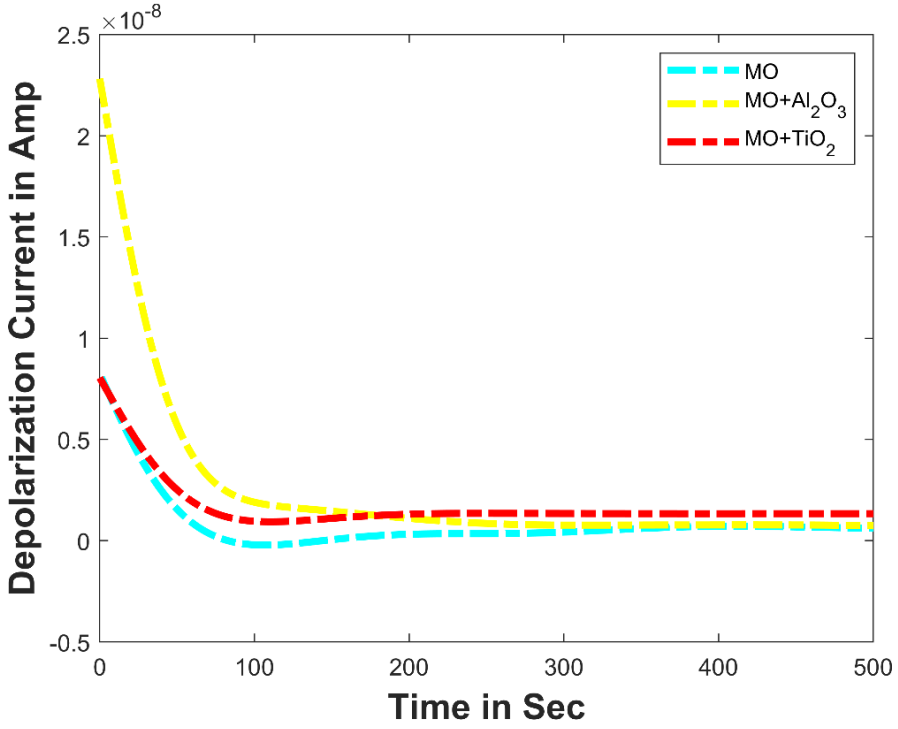

Fig. 5.23. Variation of depolarization current of pure mineral OPS and its NOPS(s) at 80°C (at 200V).

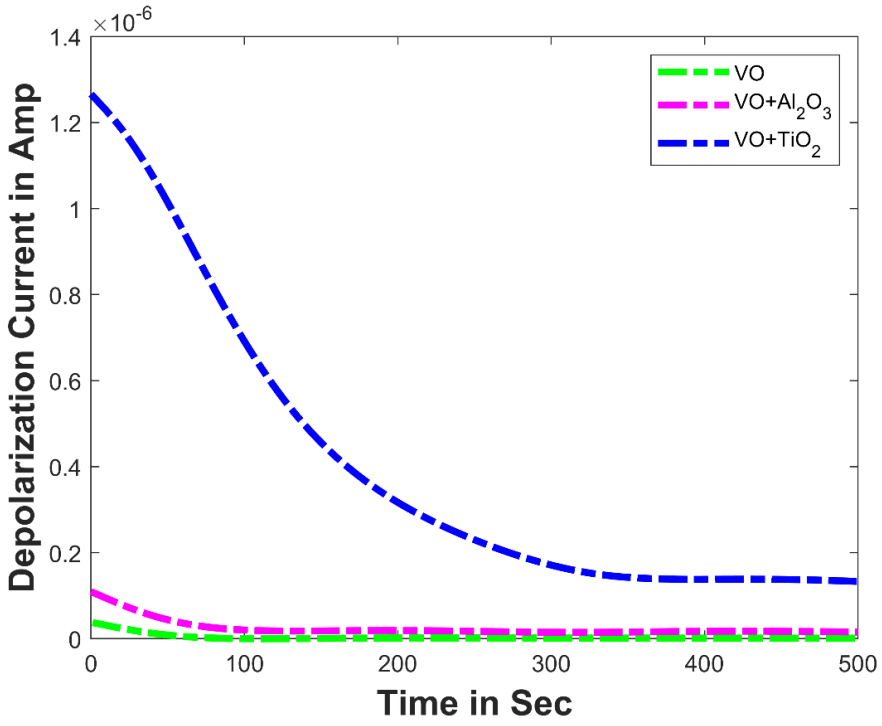

Fig. 5.24. Variation of depolarization current of pure vegetable (FR3) OPS and its NOPS(s) at 80°C (at 200V).

5.4 STUDY OF DC CONDUCTIVITY

In this section, the DC conductivity of the six NOPS(s) has been discussed. The charging and discharging currents from PDC data have been used to find the DC Conductivity. As per section 3.2, the conduction current can be derived by subtracting the depolarization current from the polarization current. Firstly, the conduction currents for each sample at different voltage levels and different temperatures have been recorded. Then, with the help of conduction currents, vacuum permittivity, geometric capacitance and applied DC voltages, the DC conductivity for each OPS has been derived by using the equation below:

$$\sigma_0 = \frac{\varepsilon_o}{C_o V_{dc}} \left[i_{pol}(t) - i_{depol}(t) \right] \qquad (5.2)$$

5.4.1 VARIATION OF DC CONDUCTIVITY WITH VOLTAGE:

The DC Conductivity for each sample is calculated at four voltage levels (50V, 100V, 150V and 200V). The values (in Siemens per meter) are derived at 25°C and listed in Table 5.1.

TABLE 5.1

VARIATION OF CONDUCTIVITY (IN SIEMENS PER METER) OF DIFFERENT OPS(S) WITH DIFFERENT APPLIED VOLTAGE AT 25°C

APPLIED VOLTAGE (V)	MO	MO+ Al_2O_3	MO+ TiO_2	VO	VO+ Al_2O_3	VO+ TiO_2
50	2.80E-12	4.57E-13	8.12E-13	4.99E-13	1.67E-11	4.74E-10
100	4.37E-12	1.05E-12	2.95E-13	1.02E-12	2.83E-11	6.04E-10
150	5.79E-12	1.48E-12	2.23E-12	1.48E-12	3.64E-11	9.38E-10
200	9.32E-12	2.14E-12	1.59E-11	1.89E-12	1.11E-10	1.72E-09

5.4.1 VARIATION OF DC CONDUCTIVITY WITH TEMPERATURE:

The DC Conductivity for each sample is calculated at four temperatures (25°C, 40°C, 60°C and 80°C). The values (in Siemens per meter) are derived at 200V and listed in Table 5.2.

TABLE 5.2

VARIATION OF CONDUCTIVITY (IN SIEMENS PER METER) OF DIFFERENT OPS(S) WITH DIFFERENT TEMPERATURE AT 200V

TEMPER-ATURE	MO	MO+ Al_2O_3	MO+ TiO_2	VO	VO+ Al_2O_3	VO+ TiO_2
25°C	1.32E-11	2.14E-12	1.59E-11	1.89E-12	1.10E-10	2.65E-10
40°C	1.65E-11	5.59E-12	1.86E-11	6.55E-12	1.62E-10	3.72E-10
60°C	2.83E-11	9.38E-12	2.23E-11	4.58E-11	4.88E-10	8.15E-10
80°C	3.04E-10	3.12E-11	3.87E-11	2.49E-10	5.95E-09	6.15E-09

5.5 ANALYSIS OF ACTIVATION ENERGY

An estimation of activation energy of a dielectric sample denotes the barrier potential that the trapped charges would need to acquire in order to carry conduction in the dielectric material. The polarization process in the insulating material is influenced by a variety of external conditions, the most important of which is temperature [59]. This is because temperature affects charge mobility. The values of the time constant of the dipoles change when the thermal energy content of the insulation changes, resulting in variations in conductivity [15]. The activation energy (E_g) of the material is connected to the variation of conductivity value with temperature and it is represented by the equation:

$$\sigma = Ae^{\left[-\frac{E_g}{kT}\right]} \tag{5.3}$$

Where 'E_g' represents activation energy, 'k' denotes the Boltzmann constant, the value of 'k' is $1.38064852 \times 10^{-23}$ m^2 kg s^{-2} K^{-1} And 'A' is constant.

Here in this section, for all the samples, the activation energy is graphically calculated using the Arrhenius equation. The equation above may be simplified as equation (5.4).

$$\ln(\sigma) = \ln(A) - \frac{E_g}{kT} \tag{5.4}$$

This equation is similar to the equation of a straight line, i.e.:

$$y = mx + c \tag{5.5}$$

As per the obtained data of DC conductivity at four different temperatures i.e., 25°C, 40°C, 60°C and 80°C from Table 5.2., The graphs are plotted for the logarithm of DC conductivity vs the inverse absolute temperature. On the obtained curve, the MATLAB curve fitting technique was used according to equation (5.5). The product of the slope of the curve-fit linear equation and the negative of the Boltzmann constant, 'k' as in the equation, yields the value of activation energy, E_g as in equation (5.6).

$$E_g = -k \times slope \tag{5.6}$$

In Fig. 5.25, the natural logarithm of DC conductivity vs the inverse of absolute temperature is plotted for pure mineral OPS, mineral oil-based Alumina and Titania NOPS(s). In Fig. 5.26, the natural logarithm of DC conductivity vs the inverse of absolute temperature is plotted for the pure vegetable (FR3) OPS, vegetable (FR3) oil-based Alumina and Titania NOPS(s).

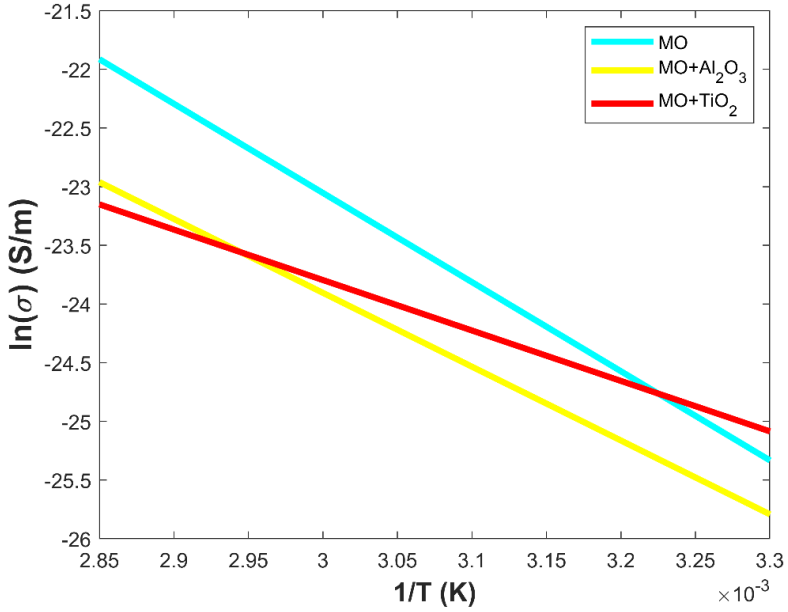

Fig. 5.25. Graph for calculating the activation energy for mineral OPS and its NOPS(s).

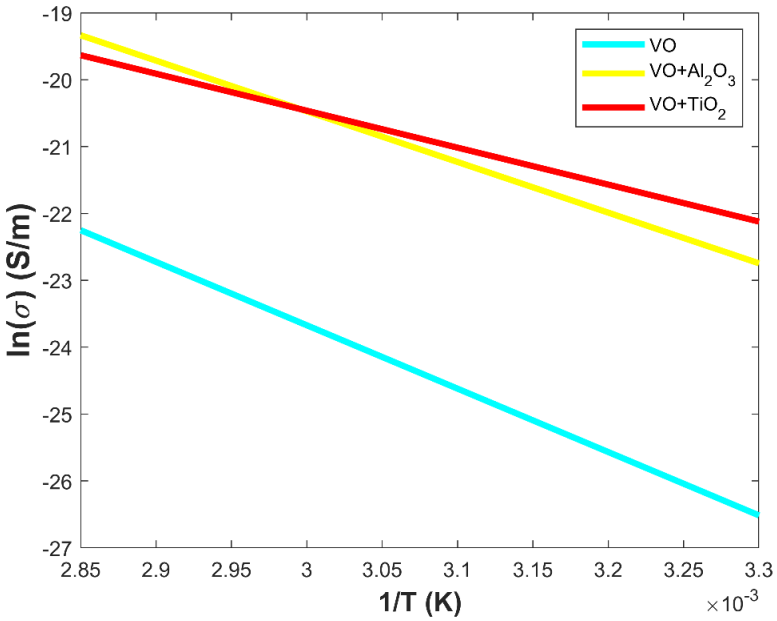

Fig. 5.26. Graph for calculating the activation energy for vegetable (FR3) OPS and its NOPS(s).

From equation (5.6), It is clear that the highest negative slope corresponds to the highest value of activation energy and vice versa. The values of activation energy for each sample are listed below in Table 5.3.

TABLE 5.3

ACTIVATION ENERGY OF DIFFERENT SAMPLES

SAMPLES	ACTIVATION ENERGY	SAMPLES	ACTIVATION ENERGY
MO	0.655 eV	**VO**	0.817 eV
MO+ Al_2O_3	0.543 eV	**VO+ Al_2O_3**	0.654 eV
MO+ TiO_2	0.302 eV	**VO+ TiO_2**	0.477 eV

5.6 INVESTIGATION OF NONLINEARITY OF CONDUCTION CURRENT IN DIFFERENT NOPS(S)

The study of non-linearity in the dielectric conduction phenomenon is essential for real-world applications. At all electric fields and temperatures, the conduction behaviour of dielectric may not follow Ohm's law. As a result, the non-linear features of all OPS(s) in the conduction process have been examined in this section.

The relation between the conduction current, **i** of an ohmic element and applied voltage V is as follows:

$$i = GV \tag{5.7}$$

Where 'G' represents the conductivity of the ohmic element.

In the case of dielectric material, the conduction current, $\mathbf{i_c}$ can be modelled as:

$$i_c = aV^b \tag{5.8}$$

Where "a" and "b" are coefficients that are governed by material properties.

The value of "b" for ohmic elements is 1. If the studied dielectric does not follow ohmic conduction, the value of "b" should be significantly different from unity.

The goal is to investigate how the degree of non-linearity, or parameter 'b', varies for NOPS(s) prepared with various base oils. From the polarization measurements, the conduction current for each pure OPS and NOPS was measured at 25°C at four different voltage levels (50V, 100V, 150V, and 200V). The conduction current was then plotted at each voltage level. The curve-fitting technique was then applied to the generated curve using equation (5.8) for each of the six samples under consideration. A comparison of the non-linear conduction current properties of mineral oil and vegetable (FR3) oil-based NOPS(s) are shown in Fig. 5.27 and 5.28.

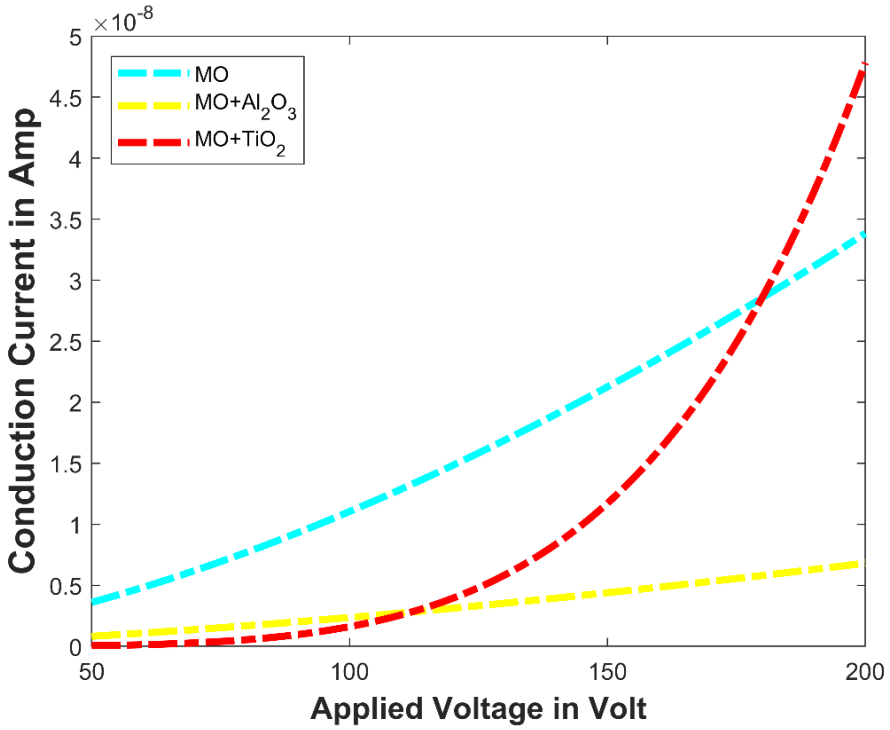

Fig. 5.27. Variation of conduction current with applied voltage of the pure mineral OPS and its NOPS(s).

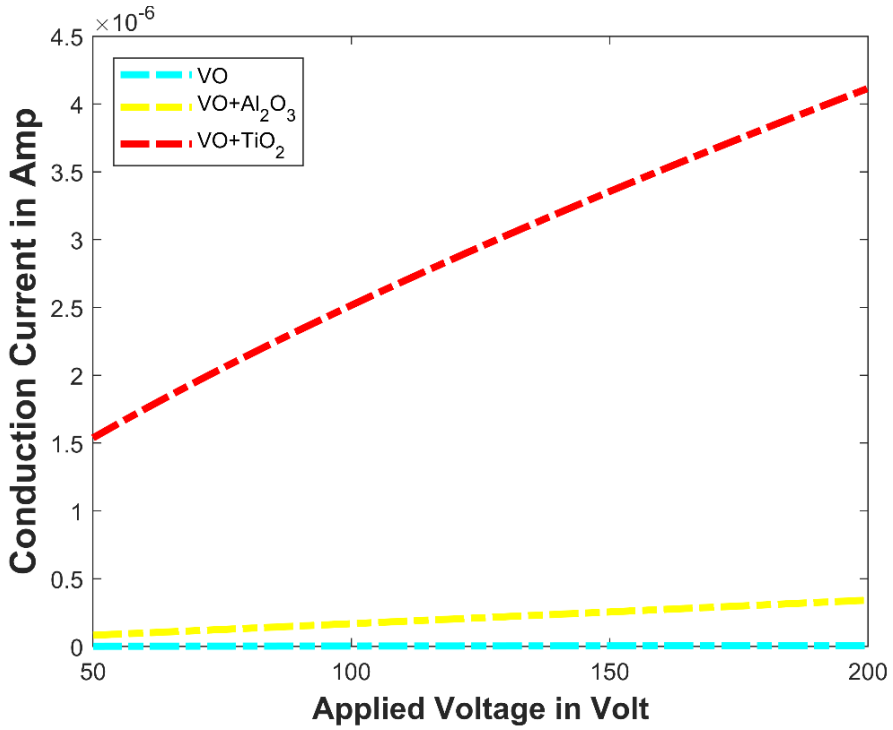

Fig. 5.28. Variation of conduction current with applied voltage of the pure vegetable (FR3) OPS and its NOPS(s).

TABLE 5.4

NON-LINEARITY PARAMETERS FOR DIFFERENT NOPS(S)

MO	MO+Al_2O_3	MO+TiO_2	VO	VO+ Al_2O_3	VO+ TiO_2
a = 6.496E-12	a = 2.088E-12	a = 2.733E-19	a = 6.445E-11	a = 1.539E-09	a = 9.564E-08
b = 1.615	**b = 1.527**	**b = 2.886**	**b = 0.865**	**b = 1.020**	**b = 0.710**

5.7 COMPARATIVE STUDY OF THE REAL & IMAGINARY COMPONENTS OF COMPLEX RELATIVE PERMITTIVITY

From frequency-domain spectroscopy of base OPS(s) and their associated NOPS(s), data (real and imaginary components of complex capacitance) were recorded for various samples. From this dataset, complex relative permittivity has been derived. The real component of the complex permittivity represents the ability to store electrical energy, whereas the imaginary component denotes the dielectric losses that occur in a dielectric when an alternating current field is applied. Conduction and friction between dipoles during alignment are responsible for these losses. 1% moisture is assumed to be existing in all the samples. In this section, the effect of temperature on the real and imaginary components of complex relative permittivity of each base OPS and NOPS has been studied. Furthermore, a comparative analysis has been performed for different NOPSs with their base OPS at different temperatures. Temperature impacts on the samples have been studied in Fig. 5.29 to 5.40, a comparative examination of the same for different nanofluids with the same base oil at different temperatures has been

demonstrated in Fig. 5.41 to 5.52 and an overall comparative study of the same for different nanofluids with the different base oil at different temperatures has been presented in Fig. 5.53 to 5.58.

5.7.1 EFFECT OF TEMPERATURE ON THE REAL COMPONENT OF COMPLEX RELATIVE PERMITTIVITY FOR DIFFERENT BASE OPS(S) AND THEIR CORRESPONDING NOPS(S)

Here in this subsection, the real component of complex relative permittivity has been plotted against frequency for different temperature variations (25°C, 40°C, 60°C, 80°C) for a specific sample. The AC voltage applied across each OPS is 140V (rms). In Fig. 5.29, 5.30, and 5.31, the effect of temperature on pure mineral OPS, mineral oil-based Alumina, and Titania NOPS(s) are shown, respectively. In Fig. 5.32, 5.33, and 5.34, the effect of temperature on pure vegetable (FR3) OPS, vegetable oil-based Alumina and Titania NOPS(s) are shown, respectively.

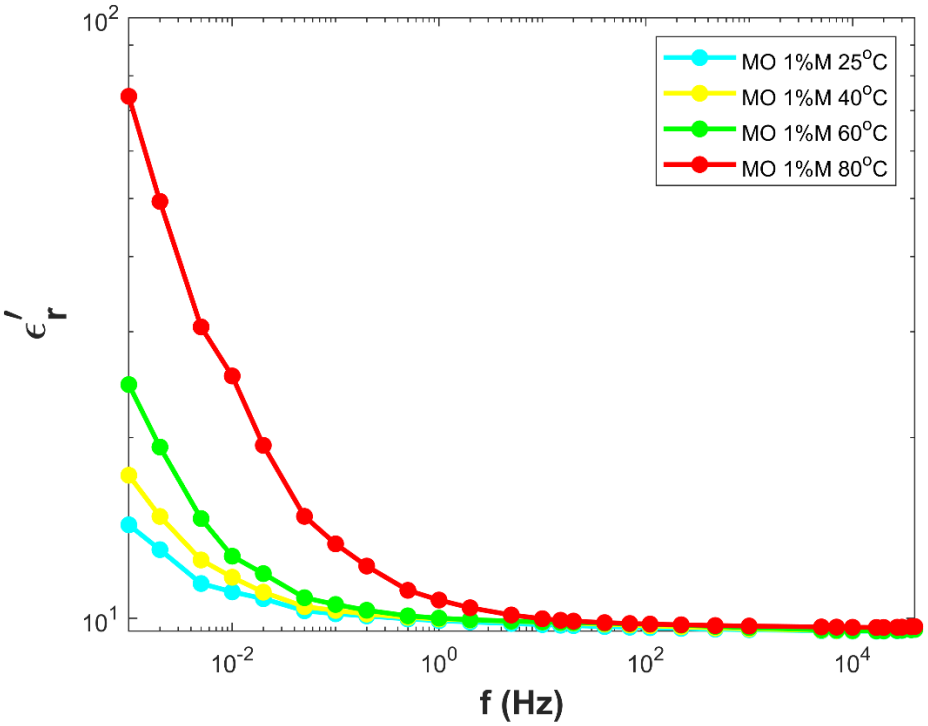

Fig. 5.29. Variation of the real component of complex relative permittivity of the pure mineral OPS for different temperatures at 140V (rms).

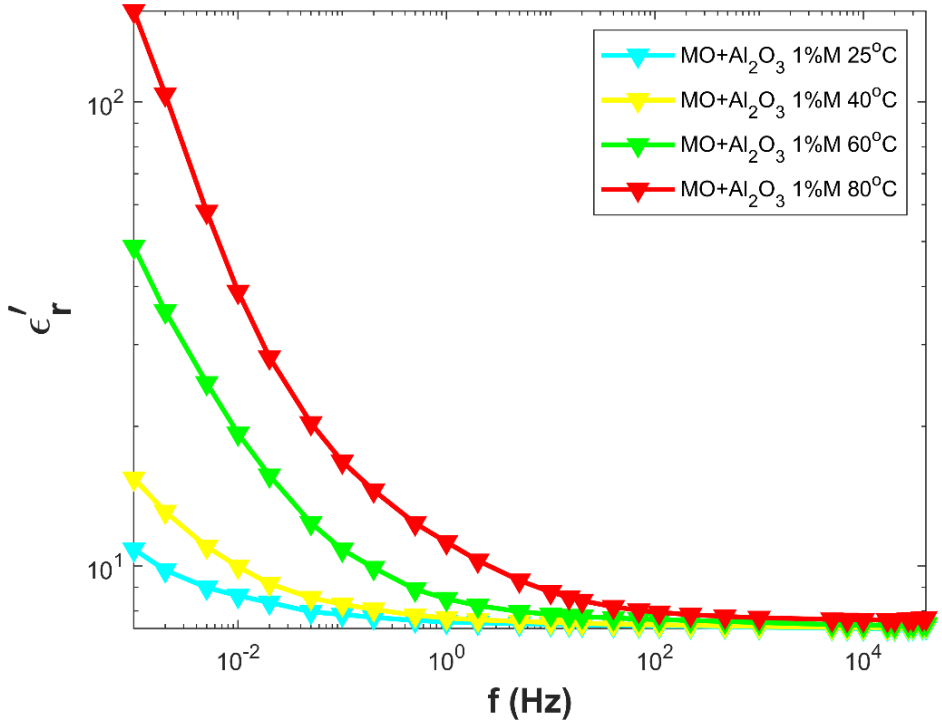

Fig. 5.30. Variation of the real component of complex relative permittivity of mineral oil-based Alumina NOPS for different temperatures at 140V (rms).

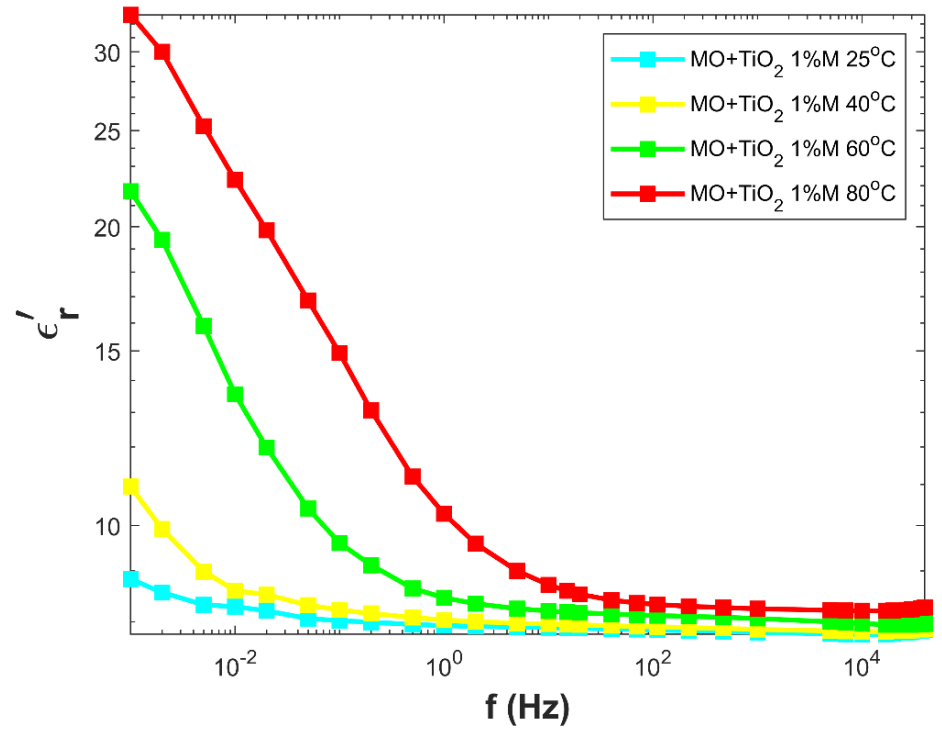

Fig. 5.31. Variation of the real component of complex relative permittivity of mineral oil-based Titania NOPS for different temperatures at 140V (rms).

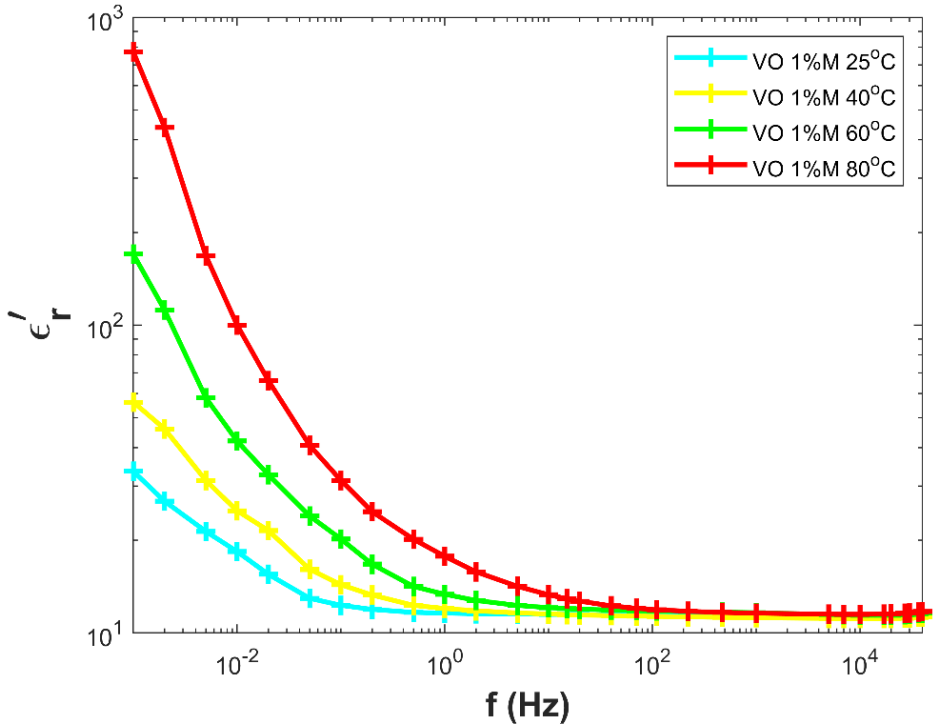

Fig. 5.32. Variation of the real component of complex relative permittivity of the pure vegetable OPS for different temperatures at 140V (rms).

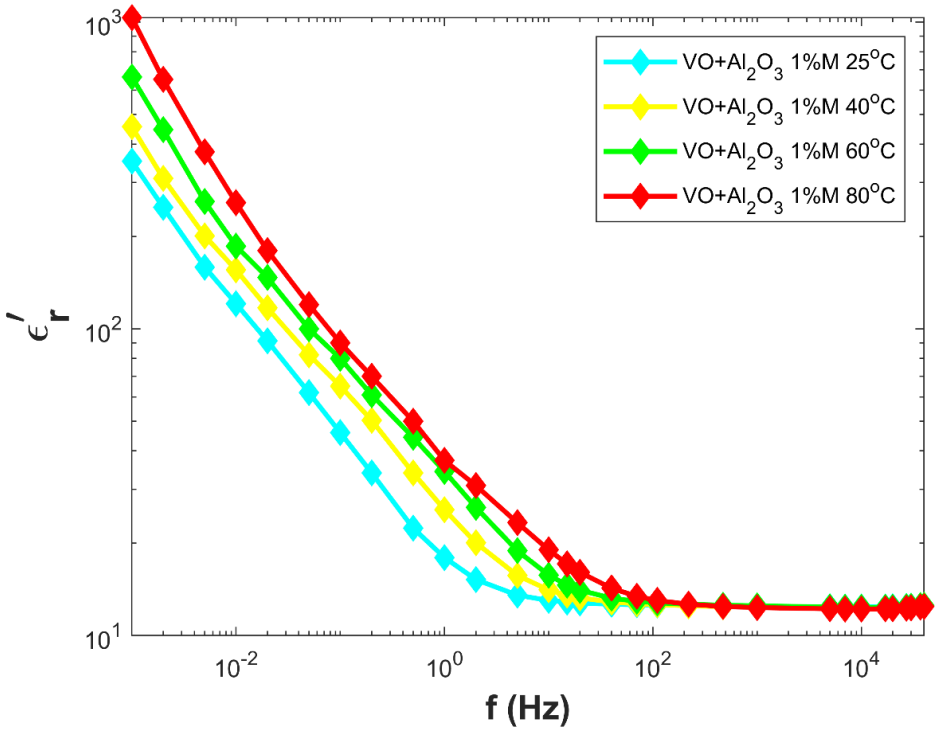

Fig. 5.33. Variation of the real component of complex relative permittivity of vegetable oil-based Alumina NOPS for different temperatures at 140V (rms).

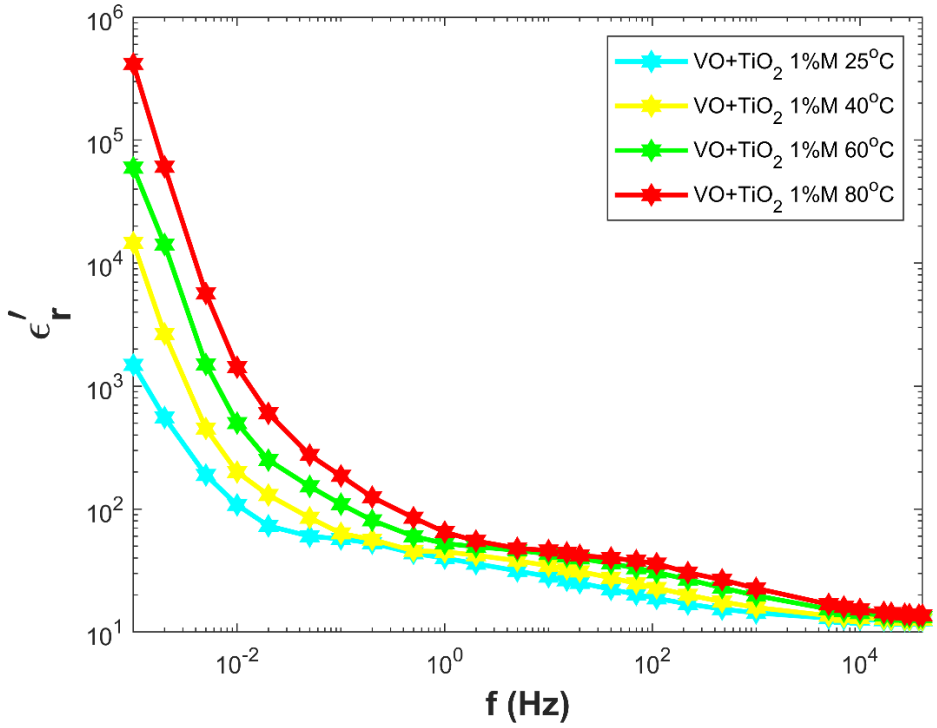

Fig. 5.34. Variation of the real component of complex relative permittivity of vegetable oil-based Titania NOPS for different temperatures at 140V (rms).

5.7.2 EFFECT OF TEMPERATURE ON THE IMAGINARY COMPONENT OF COMPLEX RELATIVE PERMITTIVITY FOR DIFFERENT BASE OPS(S) AND THEIR CORRESPONDING NOPS(S)

In this subsection, the imaginary component of complex relative permittivity has been plotted against frequency for different temperature variations (25ºC, 40ºC, 60ºC, 80ºC) for a specific sample. The AC voltage applied across each OPS is 140V (rms). In Fig. 5.35, 5.36, and 5.37, the effect of temperature on pure mineral OPS, mineral oil-based Alumina, and Titania NOPS(s) are shown, respectively. In Fig. 5.38, 5.39, and 5.40, the effect of temperature on pure vegetable (FR3) OPS, vegetable oil-based Alumina and Titania NOPS(s) are shown, respectively.

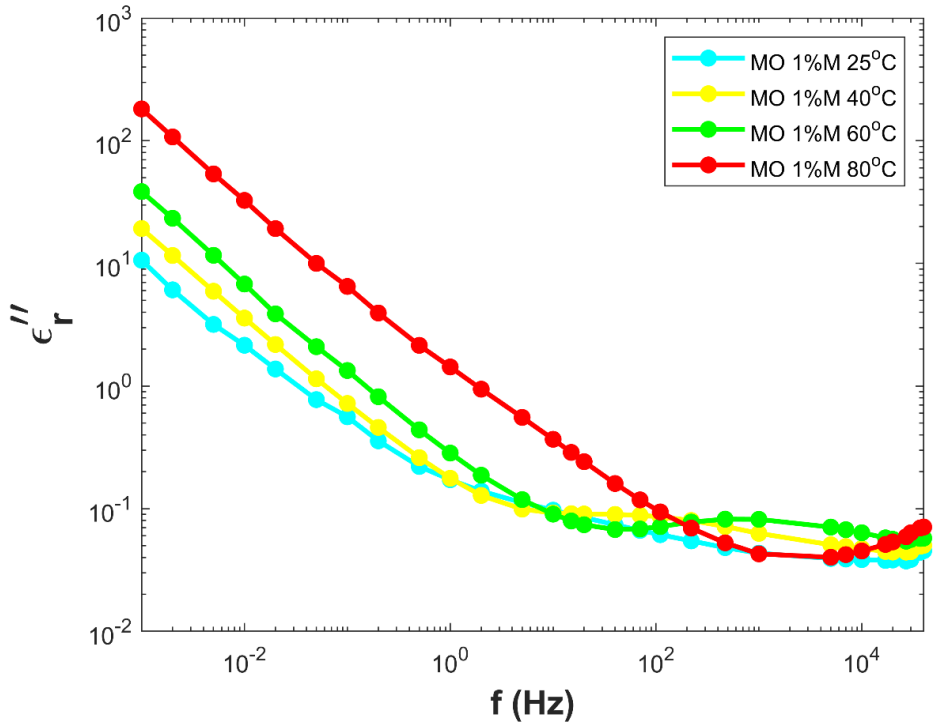

Fig. 5.35. Variation of the imaginary component of complex relative permittivity of the pure mineral OPS for different temperatures at 140V (rms).

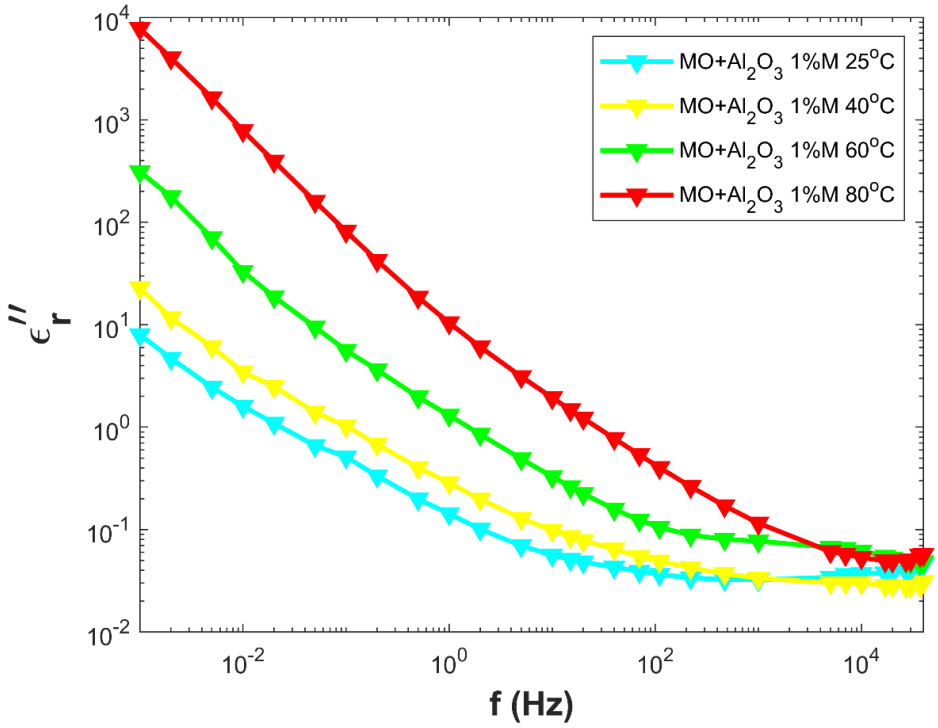

Fig. 5.36. Variation of the imaginary component of complex relative permittivity of mineral oil-based Alumina NOPS for different temperatures at 140V (rms).

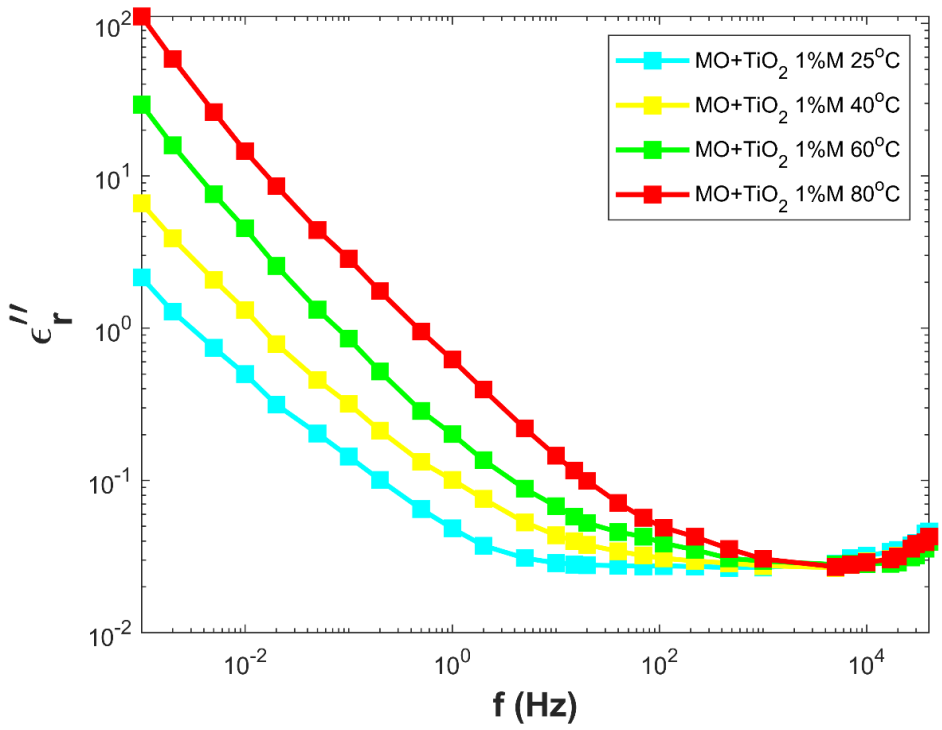

Fig. 5.37. Variation of the imaginary component of complex relative permittivity of mineral oil-based Titania NOPS for different temperatures at 140V (rms).

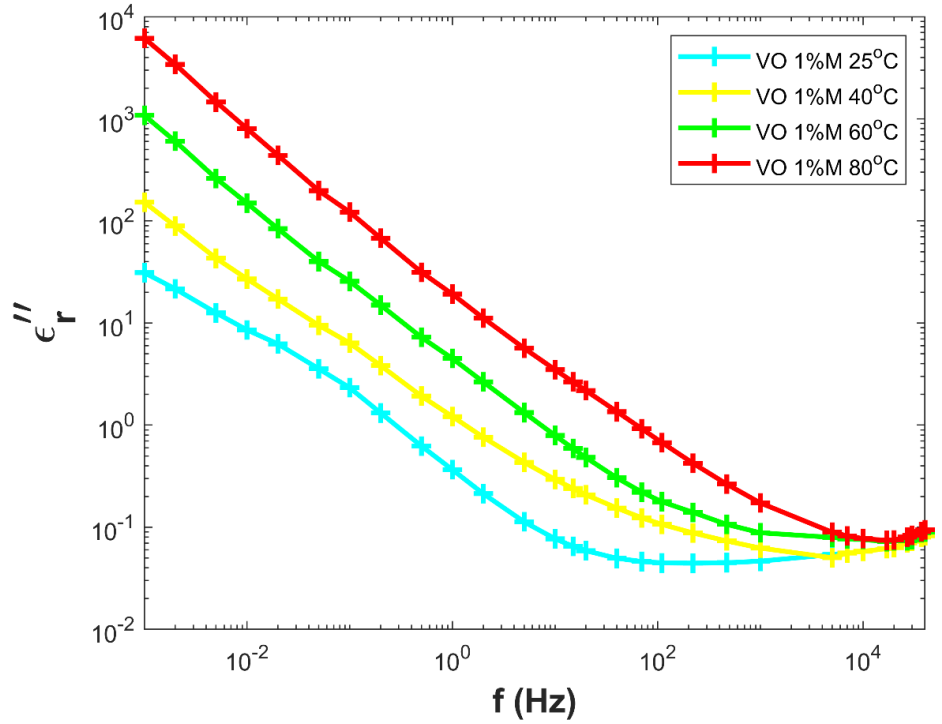

Fig. 5.38. Variation of the imaginary component of complex relative permittivity of pure vegetable OPS for different temperatures at 140V (rms).

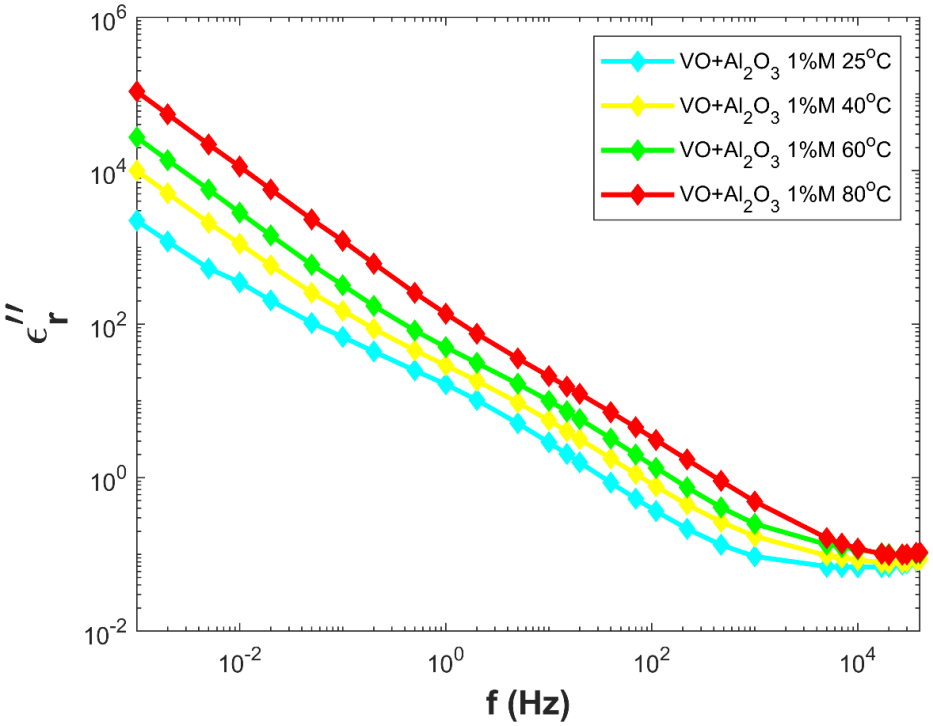

Fig. 5.39. Variation of the imaginary component of complex relative permittivity of vegetable oil-based Alumina NOPS for different temperatures at 140V (rms).

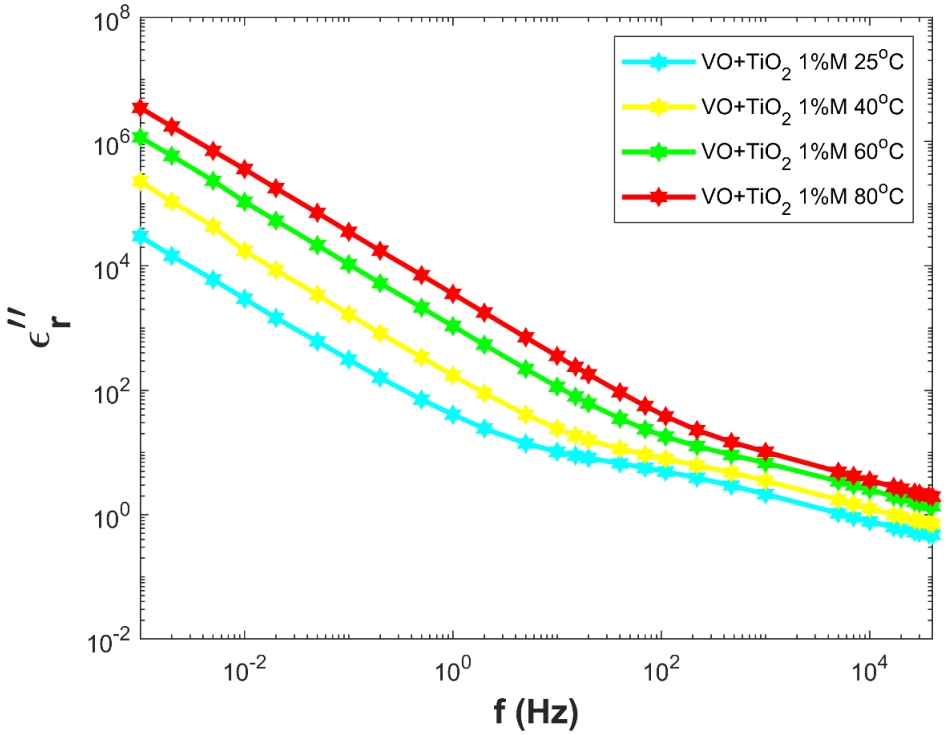

Fig. 5.40. Variation of the imaginary component of complex relative permittivity of vegetable oil-based Titania NOPS for different temperatures at 140V (rms).

5.7.3 COMPARATIVE ANALYSIS FOR THE REAL COMPONENT OF COMPLEX RELATIVE PERMITTIVITY FOR DIFFERENT NOPS(S) WITH THEIR BASE OPS(S) AT DIFFERENT TEMPERATURES

In this section, a comparative study of the real component of the complex relative permittivity has been carried out between pure OPS and its NOPS(s) at different temperatures. In Fig. 5.41, 5.42 and 5.43, the value of the real component of complex relative permittivity of pure mineral OPS, mineral oil-based Alumina and Titania NOPS(s) have been shown at 25°C, 50°C and 80°C, respectively.

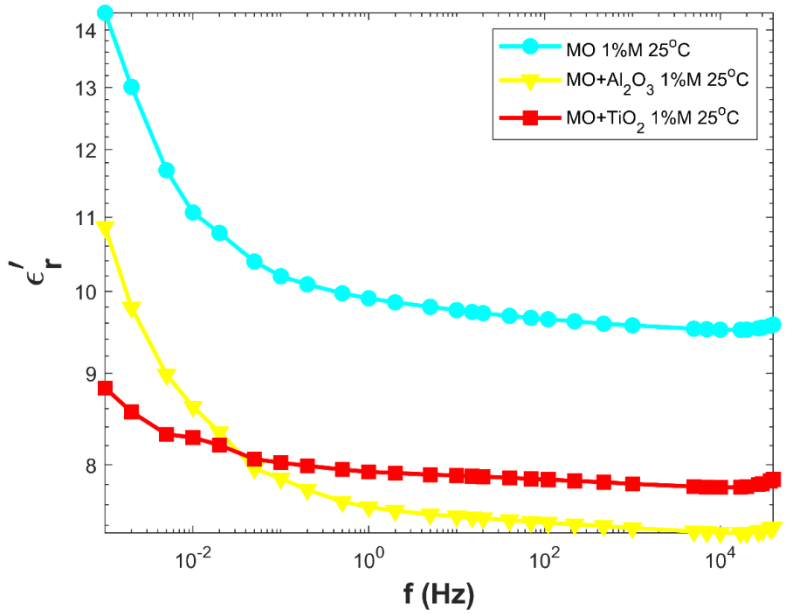

Fig. 5.41. Comparison of the real component of complex relative permittivity of the pure mineral OPS with its NOPS(s) at 25°C [140V (rms)].

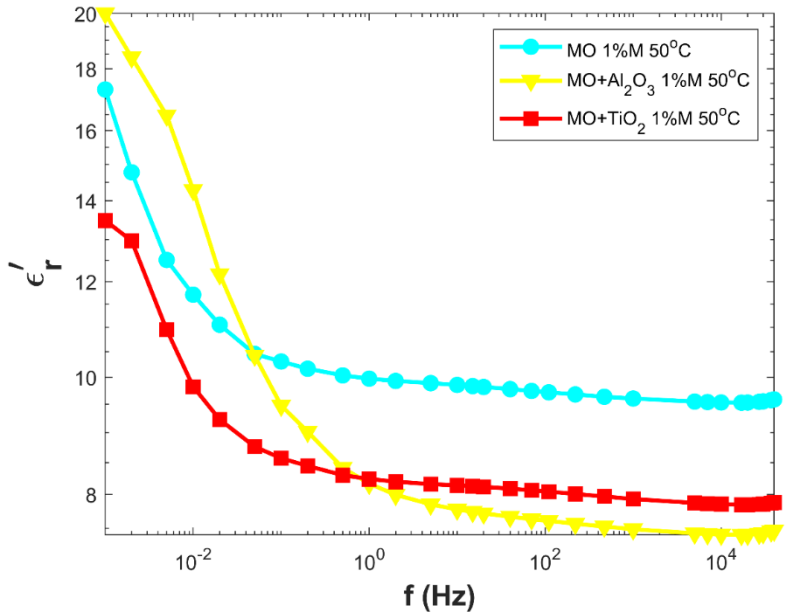

Fig. 5.42. Comparison of the real component of complex relative permittivity of the pure mineral OPS with its NOPS(s) at 50°C [140V (rms)].

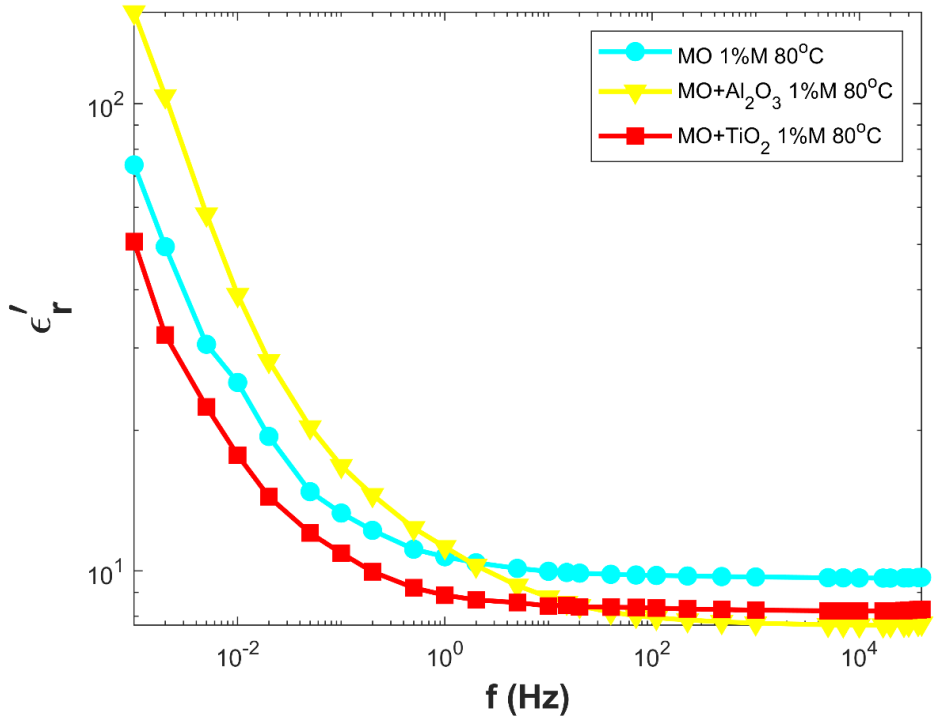

Fig. 5.43. Comparison of the real component of complex relative permittivity of the pure mineral OPS with its NOPS(s) at 80°C [140V (rms)].

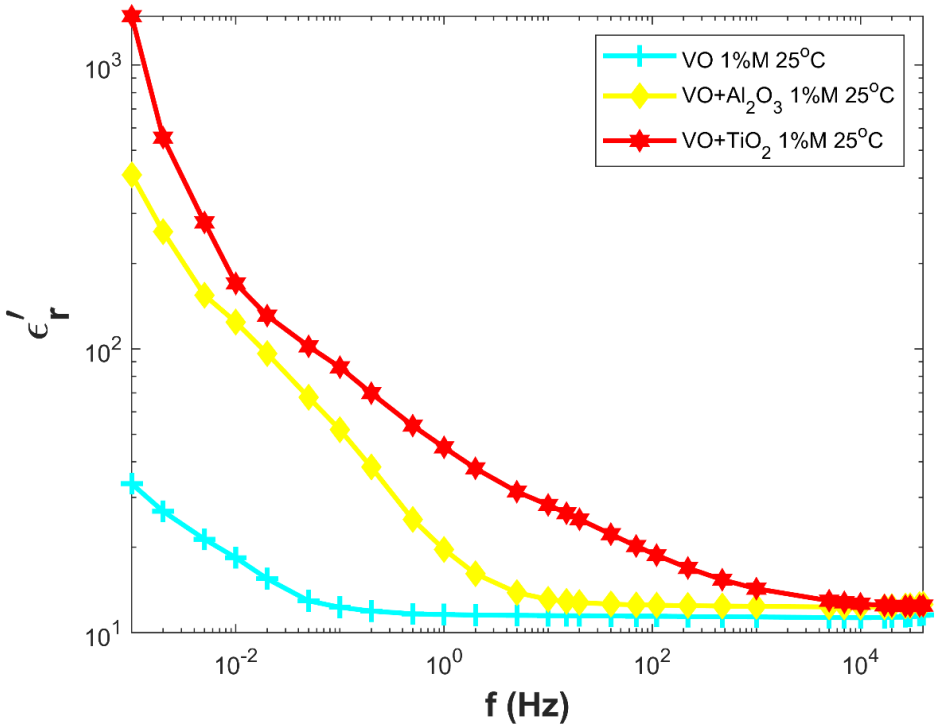

Fig. 5.44. Comparison of the real component of complex relative permittivity of the pure vegetable OPS with its NOPS(s) at 25°C [140V (rms)].

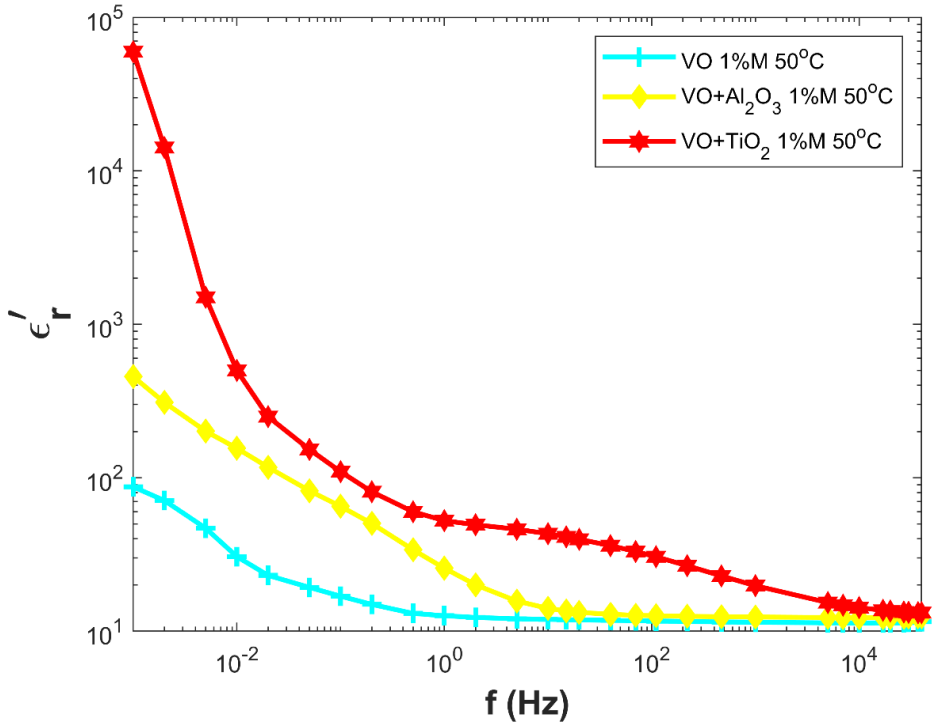

Fig. 5.45. Comparison of the real component of complex relative permittivity of the pure vegetable OPS with its NOPS(s) at 50°C [140V (rms)].

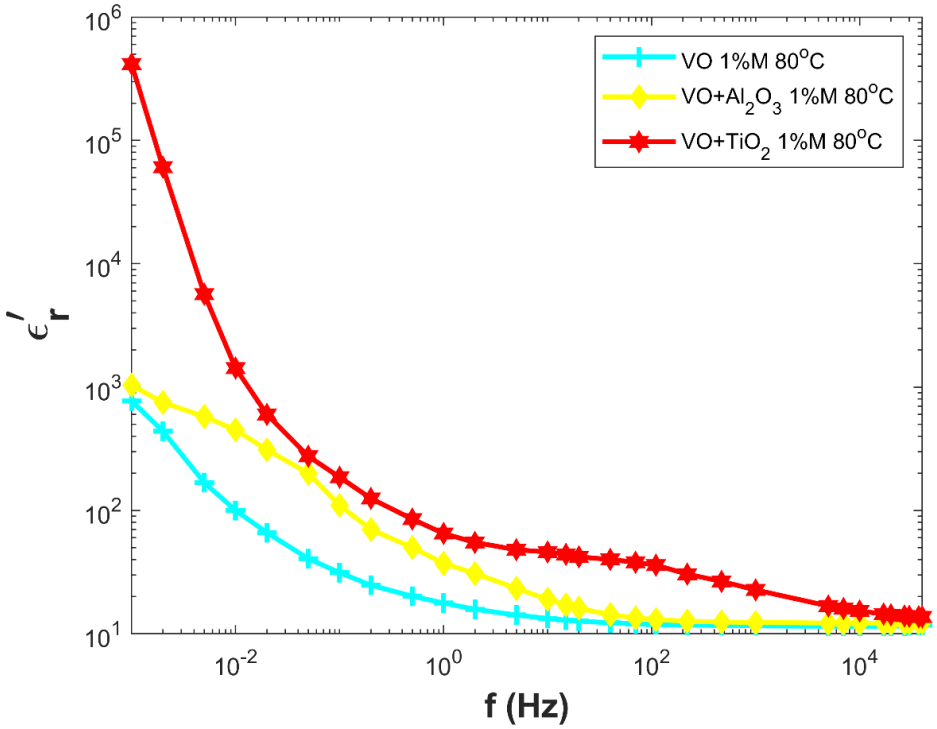

Fig. 5.46. Comparison of the real component of complex relative permittivity of the pure vegetable OPS with its NOPS(s) at 80°C [140V (rms)].

5.7.4 COMPARATIVE ANALYSIS FOR THE IMAGINARY COMPONENT OF COMPLEX RELATIVE PERMITTIVITY FOR DIFFERENT NOPS(S) WITH THEIR BASE OPS(S) AT DIFFERENT TEMPERATURES

Here, in this subsection, a comparative study of the imaginary component of the complex relative permittivity has been carried out between pure OPS and its NOPS(s) at different temperatures. In Fig. 5.47, 5.48 and 5.49, the value of the imaginary component of complex relative permittivity of pure mineral OPS, mineral oil-based Alumina and Titania NOPS(s) have been shown at 25ºC, 50ºC and 80ºC, respectively.

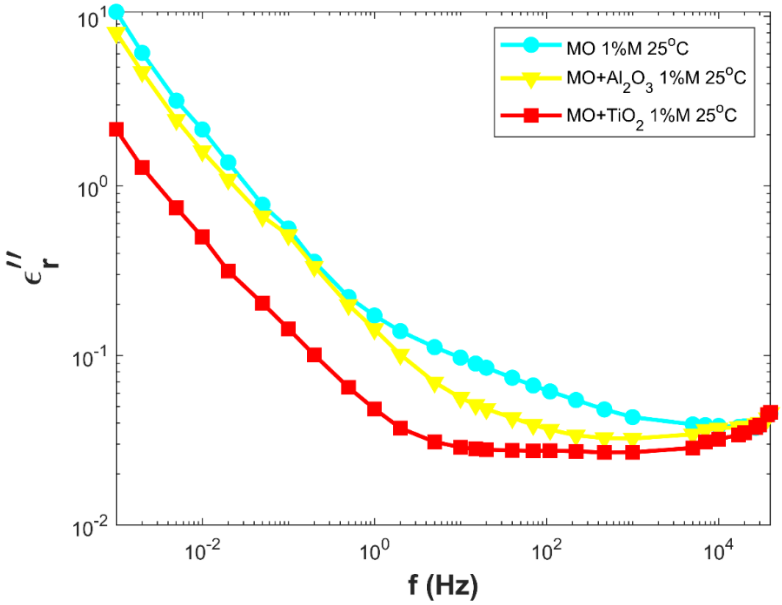

Fig. 5.47. Comparison of the imaginary component of complex relative permittivity of the pure mineral OPS with its NOPS(s) at 25°C [140V (rms)].

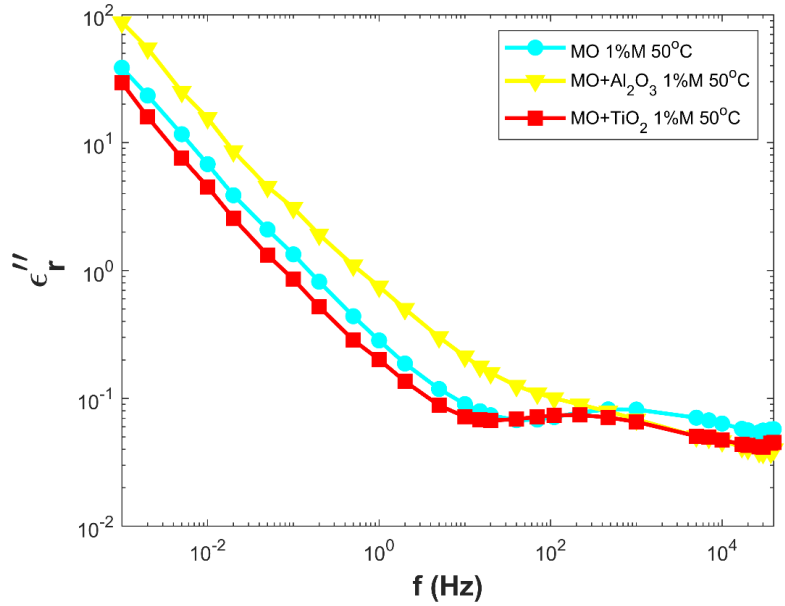

Fig. 5.48. Comparison of the imaginary component of complex relative permittivity of the pure mineral OPS with its NOPS(s) at 50°C [140V (rms)].

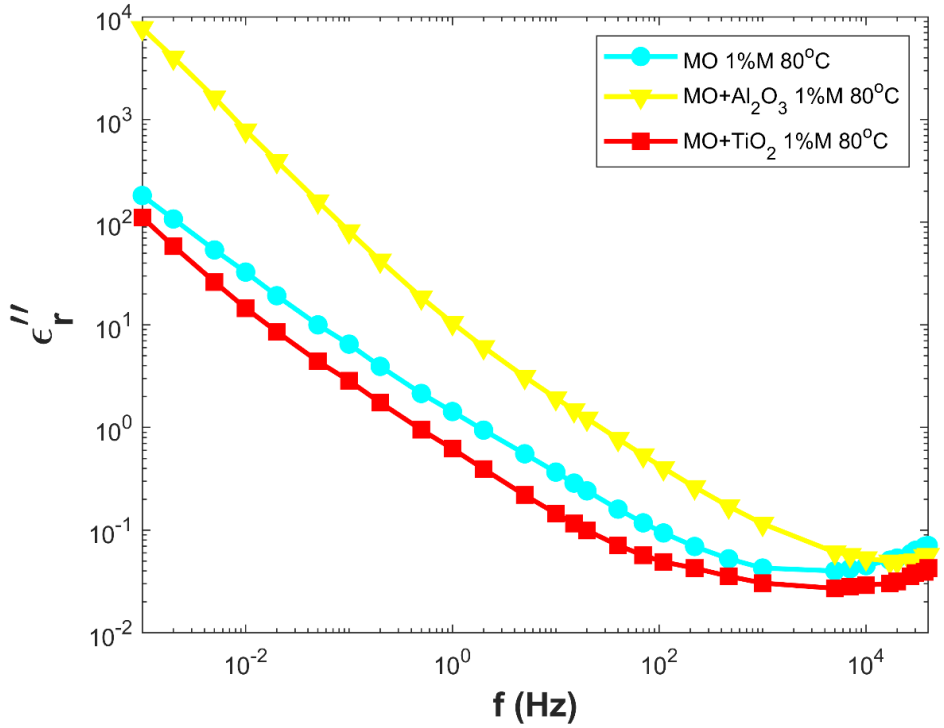

Fig. 5.49. Comparison of the imaginary component of complex relative permittivity of the pure mineral OPS with its NOPS(s) at 80°C [140V (rms)].

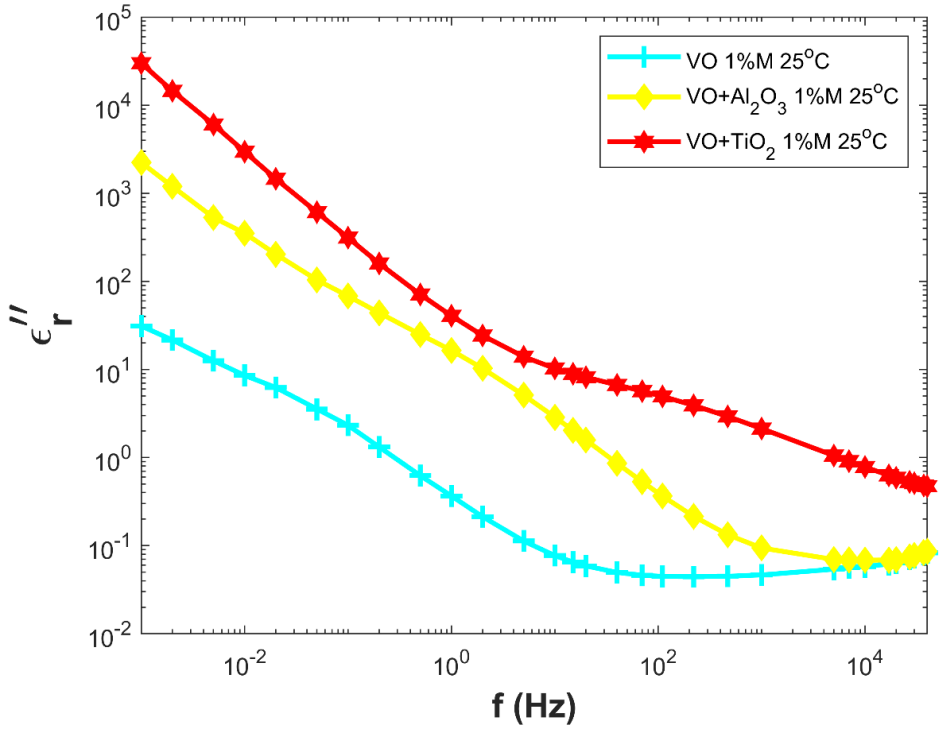

Fig. 5.50. Comparison of the imaginary component of complex relative permittivity of the pure vegetable OPS with its NOPS(s) at 25°C [140V (rms)].

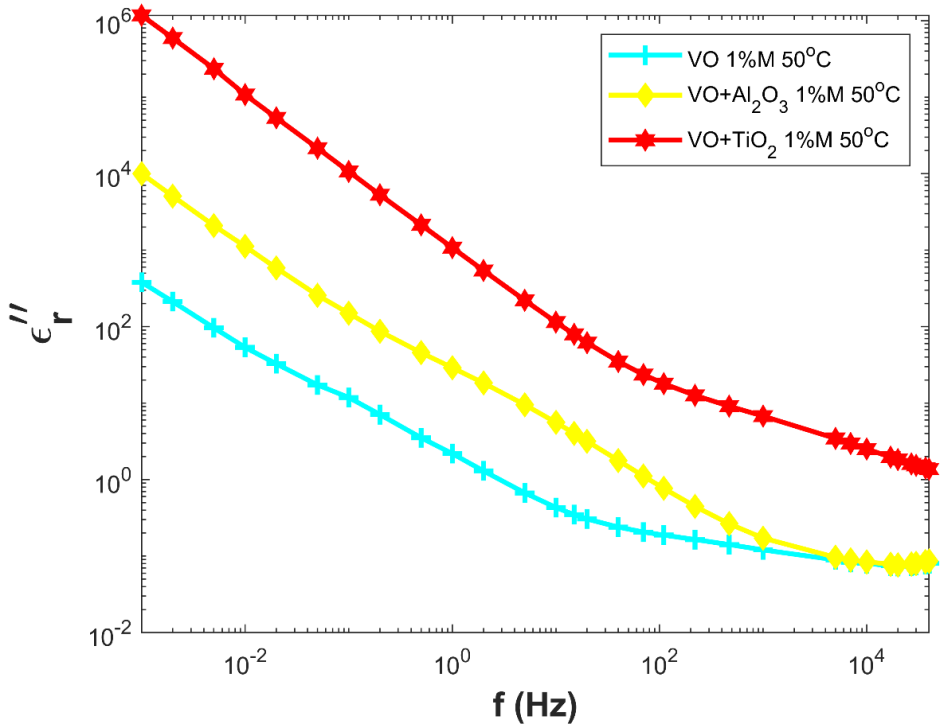

Fig. 5.51. Comparison of the imaginary component of complex relative permittivity of the pure vegetable OPS with its NOPS(s) at 50°C [140V (rms)].

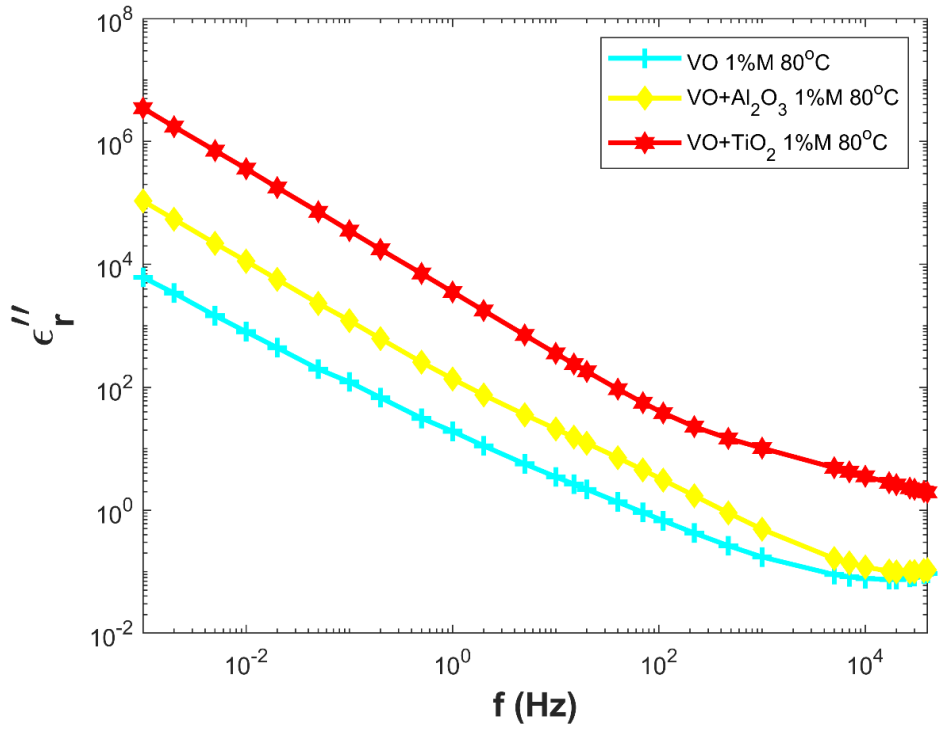

Fig. 5.52. Comparison of the imaginary component of complex relative permittivity of the pure vegetable OPS with its NOPS(s) at 80°C [140V (rms)].

5.7.5 OVERALL COMPARATIVE ANALYSIS FOR THE REAL COMPONENT OF COMPLEX RELATIVE PERMITTIVITY FOR MINERAL OIL-BASED NOPS(S) WITH VEGETABLE OIL-BASED NOPS(S) AT DIFFERENT TEMPERATURES

In this subsection, a comparative study of the real component of the complex relative permittivity has been carried out between mineral oil-based NOPS(s) and vegetable oil-based NOPS(s) at different temperatures. In Fig. 5.53, 5.54 and 5.55, the value of the real component of complex relative permittivity of the pure mineral OPS, pure vegetable OPS, mineral oil-based Alumina and Titania NOPS(s), vegetable oil-based Alumina and Titania NOPS(s) have been shown at 25°C, 50°C and 80°C, respectively.

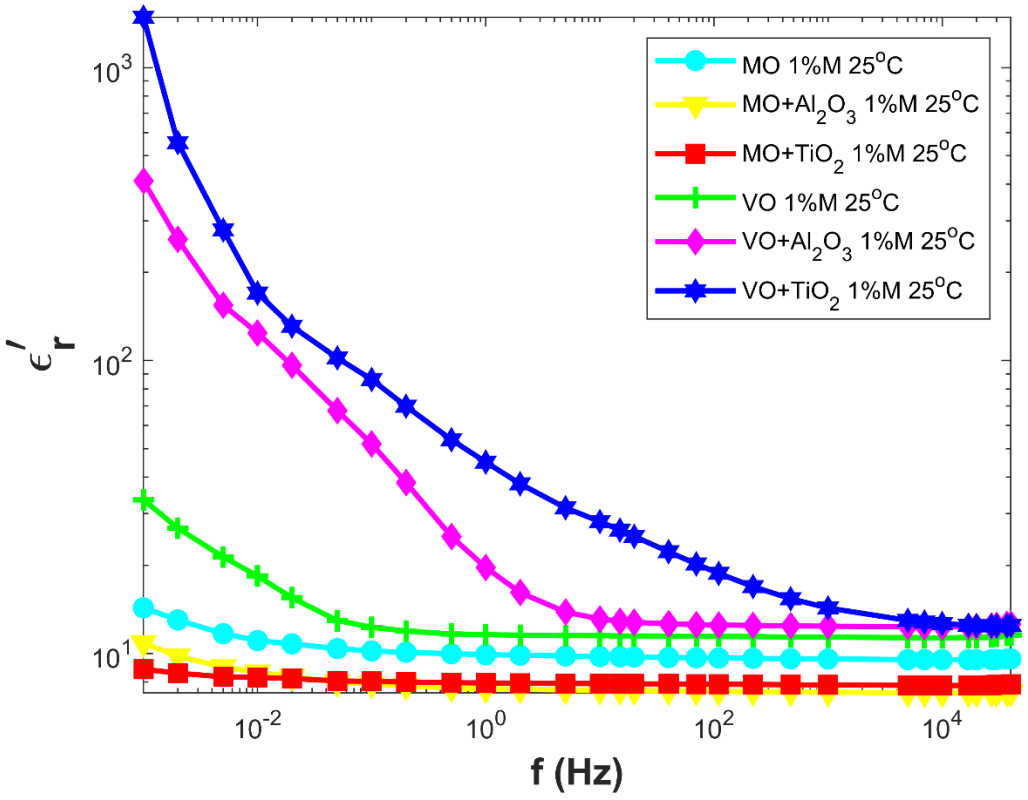

Fig. 5.53. Comparison of the real component of complex relative permittivity of mineral oil-based NOPS(s) with vegetable oil-based NOPS(s) at 25°C [140V (rms)].

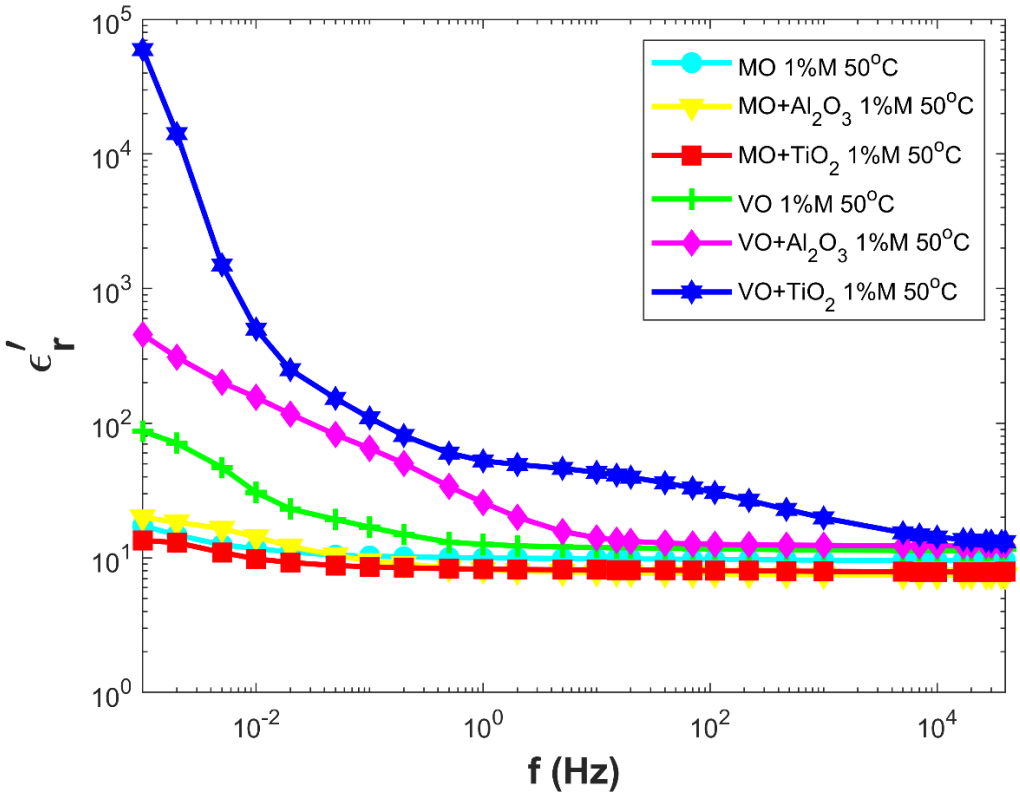

Fig. 5.54. Comparison of the real component of complex relative permittivity of mineral oil-based NOPS(s) with vegetable oil-based NOPS(s) at 50°C [140V (rms)].

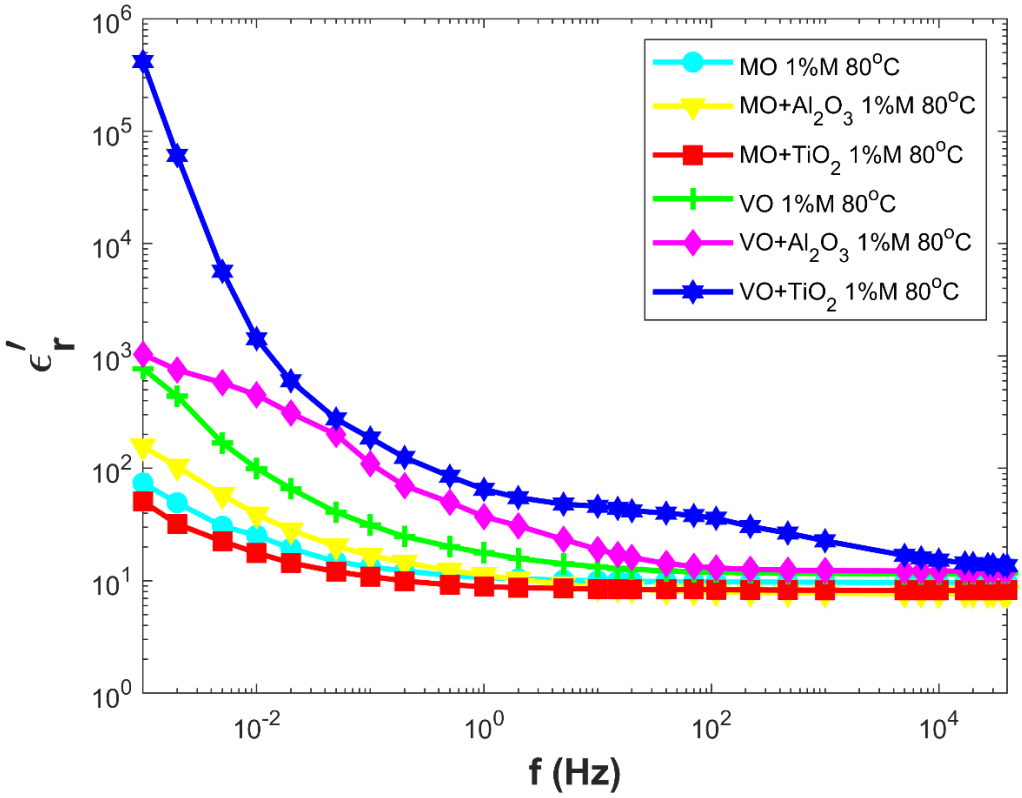

Fig. 5.55. Comparison of the real component of complex relative permittivity of mineral oil-based NOPS(s) with vegetable oil-based NOPS(s) at 80°C [140V (rms)].

5.7.6 OVERALL COMPARATIVE ANALYSIS FOR THE IMAGINARY COMPONENT OF COMPLEX RELATIVE PERMITTIVITY FOR MINERAL OIL-BASED NOPS(S) WITH VEGETABLE OIL-BASED NOPS(S) AT DIFFERENT TEMPERATURES

In this subsection, a comparative study of the imaginary component of the complex relative permittivity has been carried out between mineral oil-based NOPS(s) and vegetable oil-based NOPS(s) at different temperatures. In Fig. 5.56, 5.57 and 5.58, the value of the real component of complex relative permittivity of the pure mineral OPS, pure vegetable OPS, mineral oil-based Alumina and Titania NOPS(s), vegetable oil-based Alumina and Titania NOPS(s) have been shown at 25°C, 50°C and 80°C, respectively.

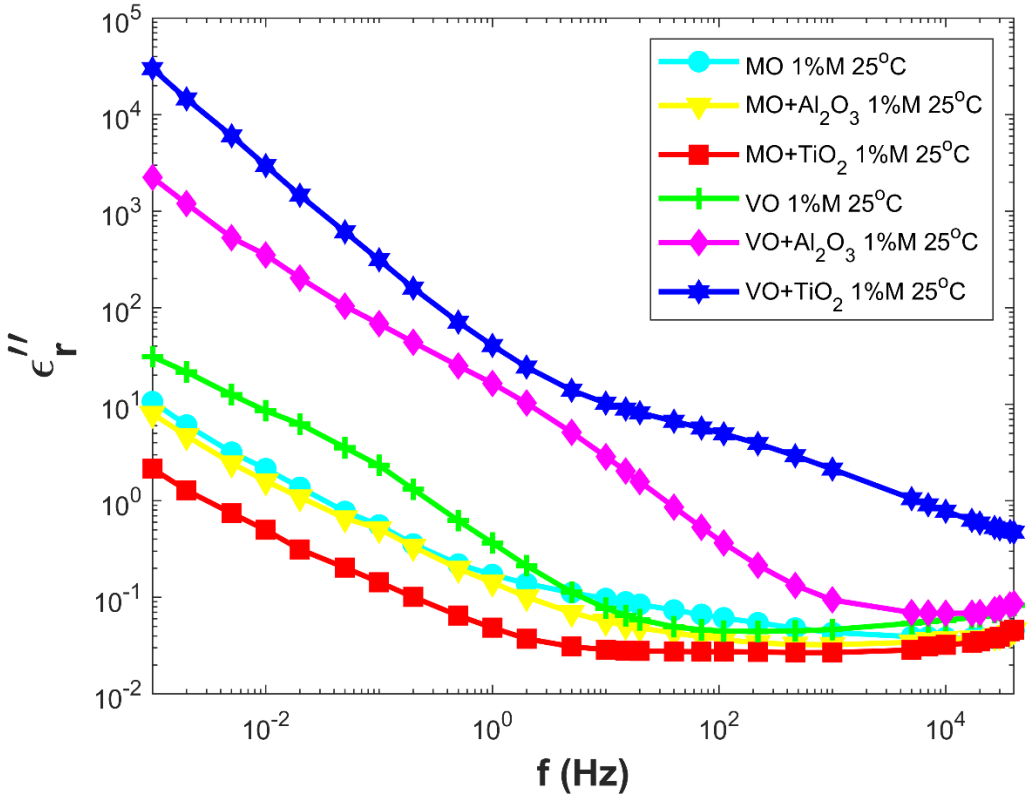

Fig. 5.56. Comparison of the imaginary component of complex relative permittivity of mineral oil-based NOPS(s) with vegetable oil-based NOPS(s) at 25°C [140V (rms)].

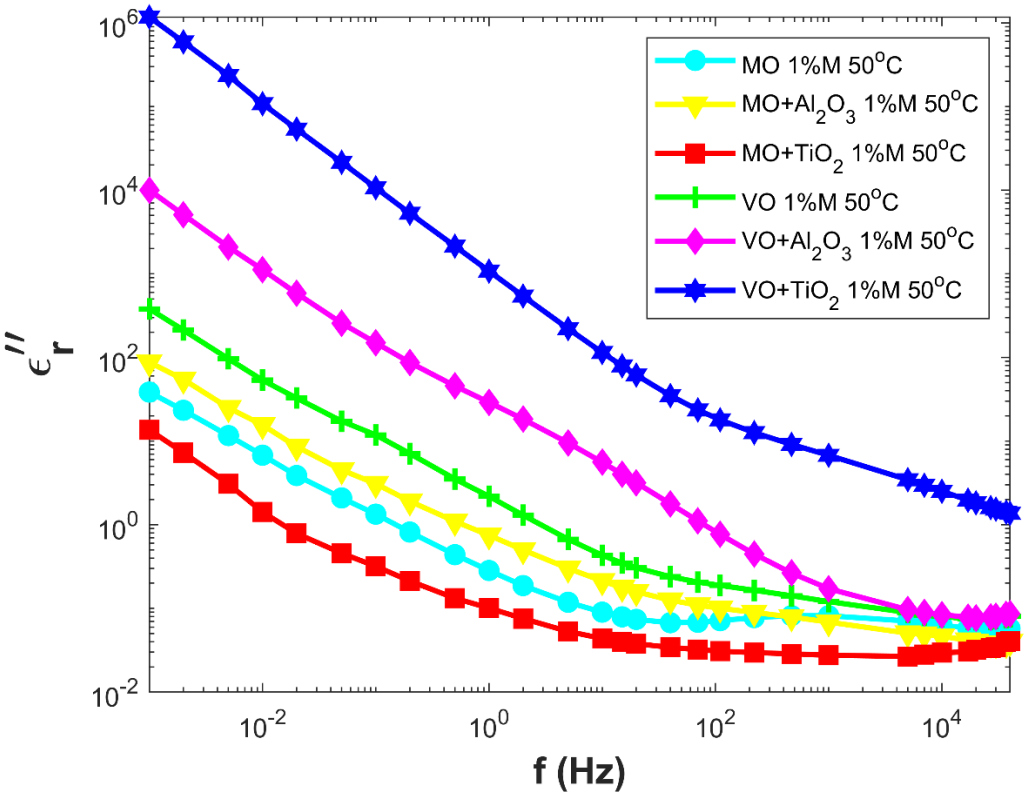

Fig. 5.57. Comparison of the imaginary component of complex relative permittivity of mineral oil-based NOPS(s) with vegetable oil-based NOPS(s) at 50°C [140V (rms)].

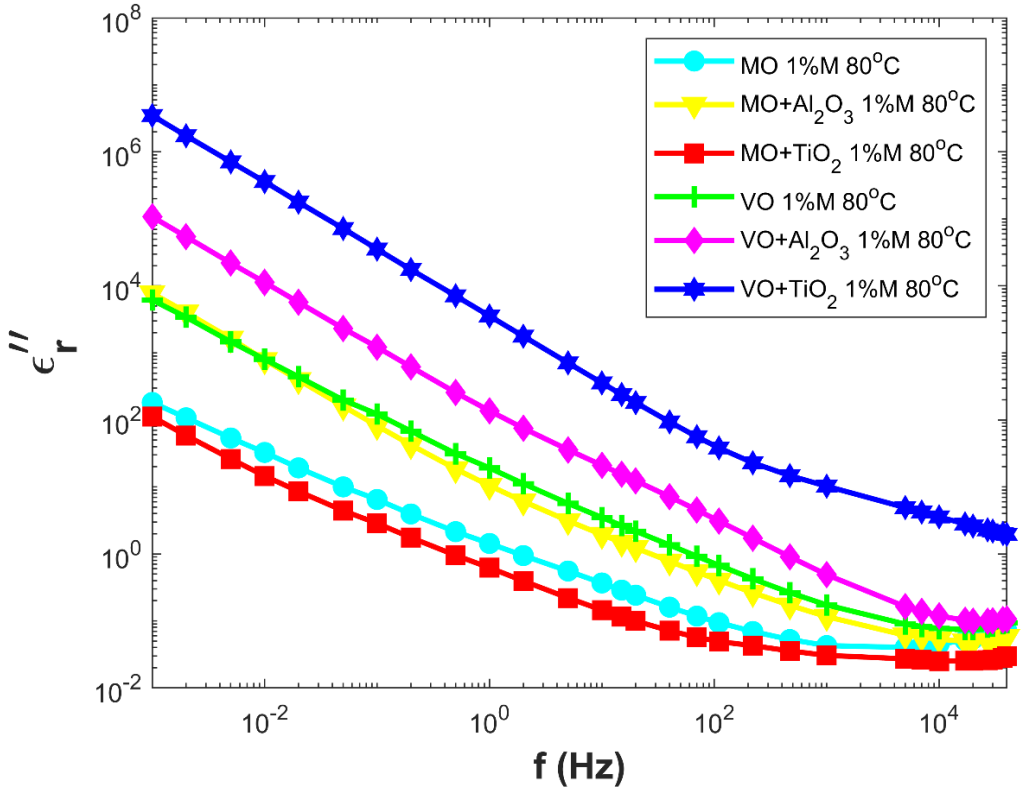

Fig. 5.58. Comparison of the imaginary component of complex relative permittivity of mineral oil-based NOPS(s) with vegetable oil-based NOPS(s) at 80°C [140V (rms)].

5.8 STUDY OF AC CONDUCTIVITY

The imaginary component of complex capacitance which is recorded while performing frequency-domain spectroscopy has been used to calculate the AC conductivity of base OPS(s) and their corresponding NOPS(s) at different frequencies. The AC conductivity has been evaluated as follows:

$$\sigma' = \frac{C'' \times \varepsilon_0 \omega}{C_0} \tag{5.9}$$

Where σ' is the AC conductivity, C″ is imaginary capacitance, ε_0 is the permittivity of free space (8.854E-12 F/m) and C_0 is the geometrical capacitance of the samples.

In all the samples, 1% moisture has been assumed to be existing. In this section, the effect of temperature on the AC conductivity of each base OPS and NOPS has been studied. Furthermore, a comparative analysis has been performed for different NOPS(s) with their base OPS(s) at different temperatures. Temperature impacts on the samples have been studied in Fig. 5.59 to 5.64, a comparative examination of the same for different nanofluids with the same base oil at different temperatures has been demonstrated in Fig. 5.65 to 5.70 and an overall comparative study of the same for different nanofluids with the different base OPS(S) at different temperatures has been presented in Fig. 5.71 to 5.73.

5.8.1 EFFECT OF TEMPERATURE ON THE AC CONDUCTIVITY FOR DIFFERENT BASE OPS(S) AND THEIR CORRESPONDING NOPS(S)

Here in this section, the AC conductivity has been plotted against frequency for different temperature variations (25°C, 40°C, 60°C, 80°C) for a specific sample. The AC voltage applied across each oil-paper insulation sample is 140V (rms). In Fig. 5.59, 5.60 and 5.61, the effect of temperature on pure mineral oil-paper, mineral oil-based Alumina and Titania NOPSs are shown, respectively. In Fig. 5.62, 5.63 and 5.64, the effect of temperature on pure vegetable (FR_3) oil-paper, vegetable oil-based Alumina and Titania NOPS(s) are shown, respectively.

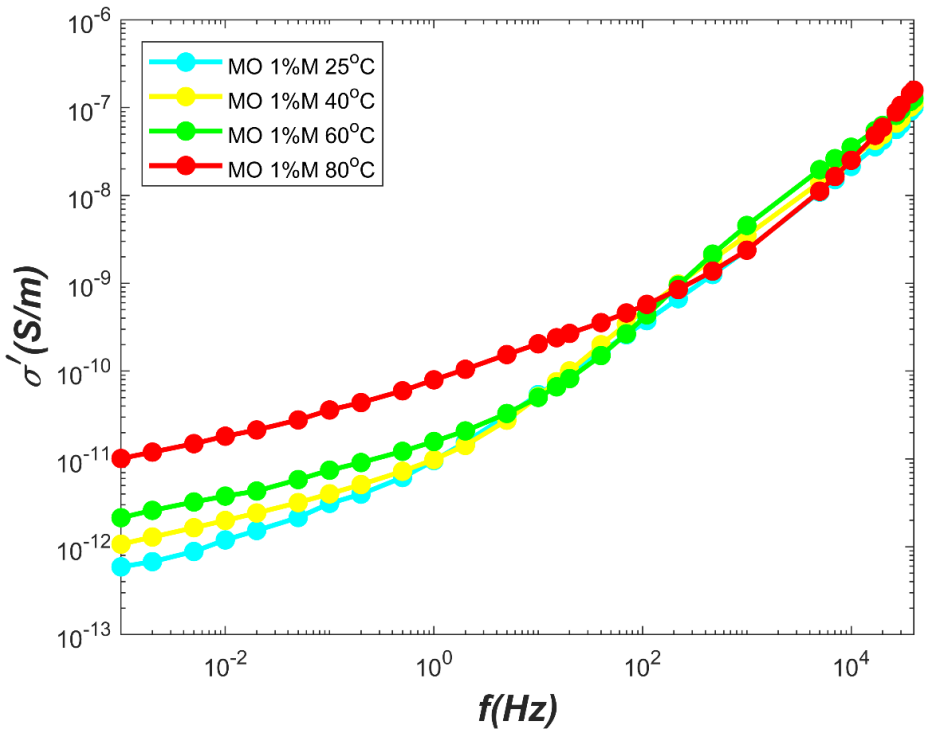

Fig. 5.59. Variation of the AC conductivity of the pure mineral OPS for different temperatures at 140V (rms).

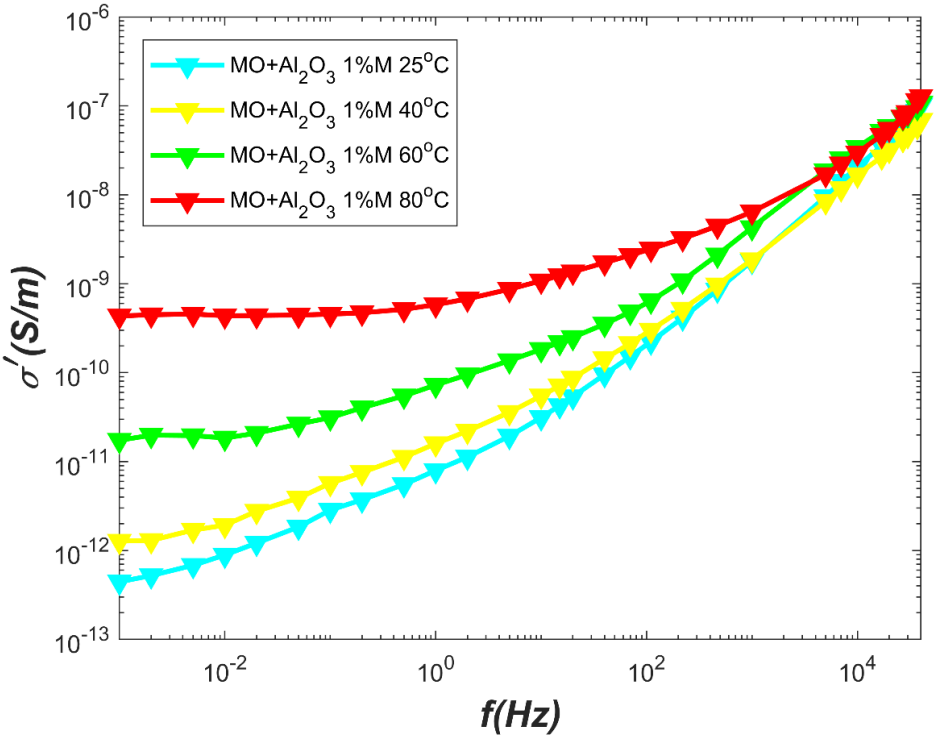

Fig. 5.60. Variation of the AC conductivity of mineral oil-based Alumina NOPS for different temperatures at 140V (rms).

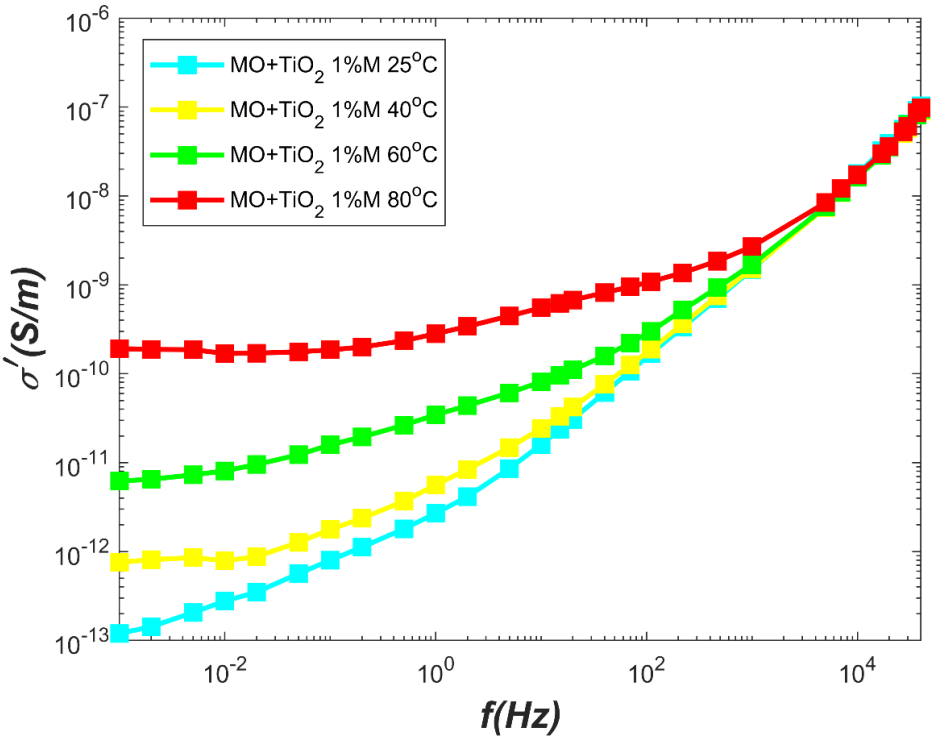

Fig. 5.61. Variation of the AC conductivity of mineral oil-based Titania NOPS for different temperatures at 140V (rms).

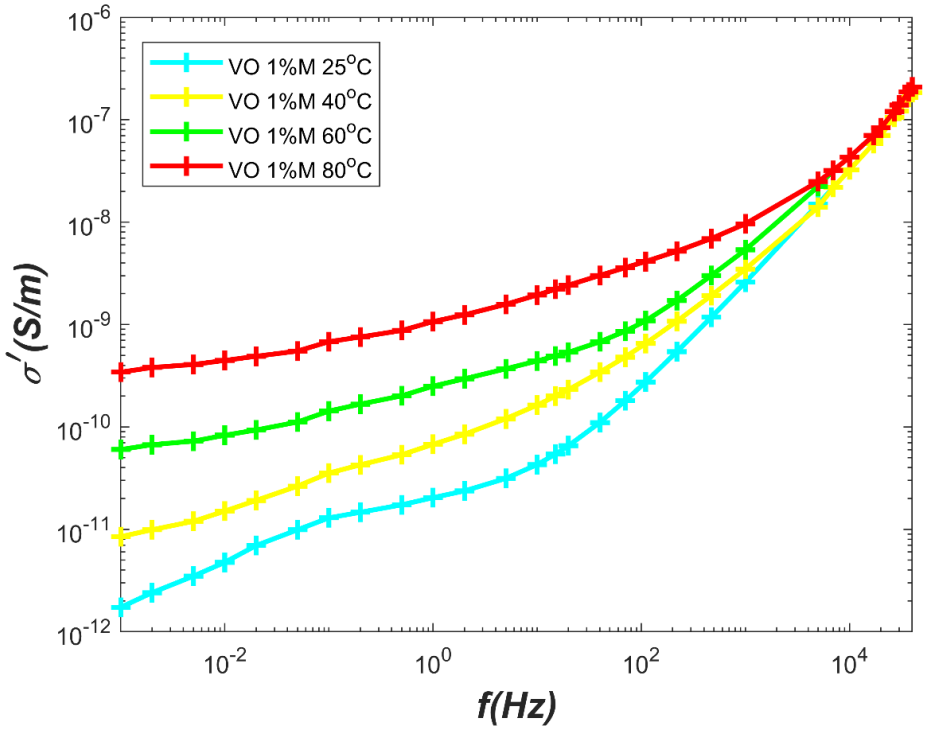

Fig. 5.62. Variation of the AC conductivity of the pure vegetable OPS for different temperatures at 140V (rms).

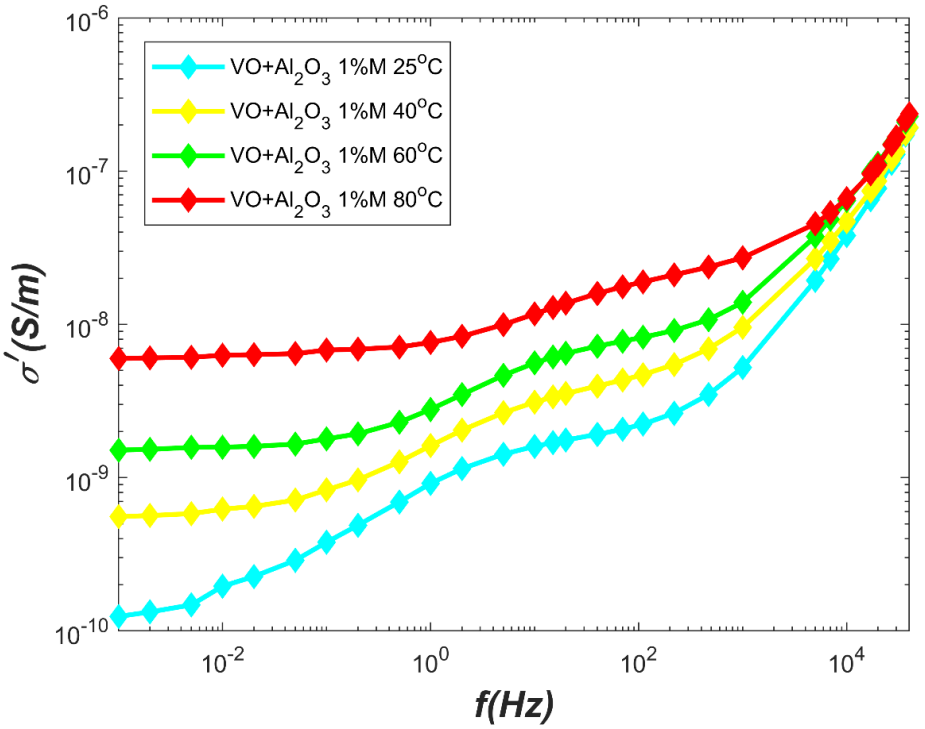

Fig. 5.63. Variation of the AC conductivity of vegetable oil-based Alumina NOPS paper sample for different temperatures at 140V (rms).

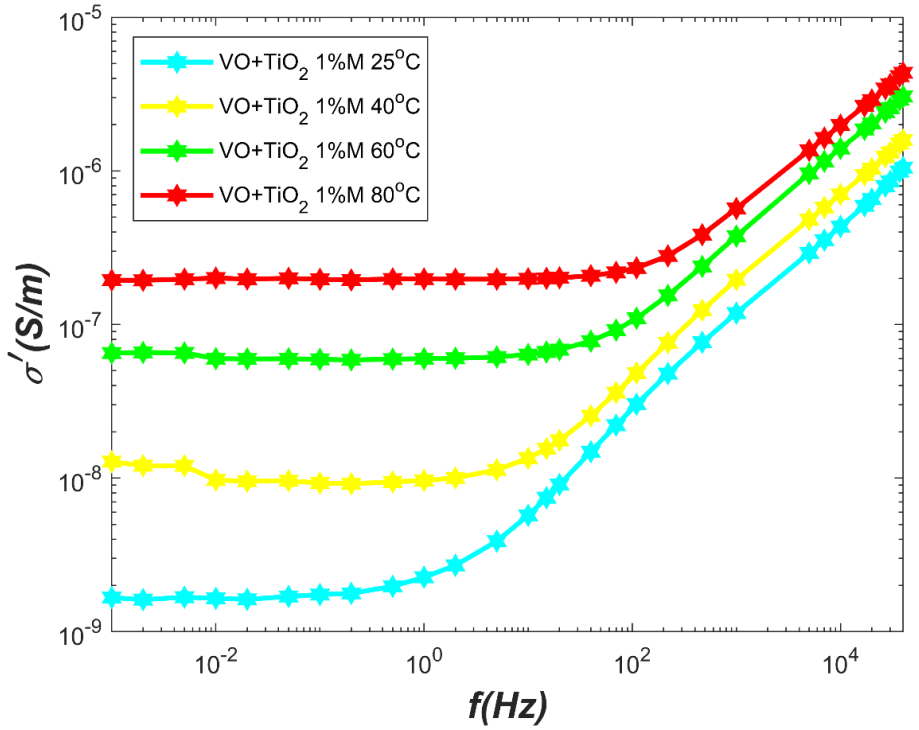

Fig. 5.64. Variation of the AC conductivity of vegetable oil-based Titania NOPS OPS for different temperatures at 140V (rms).

5.8.2 COMPARATIVE ANALYSIS FOR THE AC CONDUCTIVITY FOR DIFFERENT NOPS(S) WITH THEIR BASE OPS(S) AT DIFFERENT TEMPERATURES

In this subsection, a comparative study of the AC conductivity has been carried out between pure OPS and its NOPS(s) at different temperatures. In Fig. 5.65, 5.66 and 5.67, the value of the AC conductivity of pure mineral OPS, mineral oil-based Alumina and Titania NOPS(s) have been shown at 25°C, 50°C and 80°C, respectively.

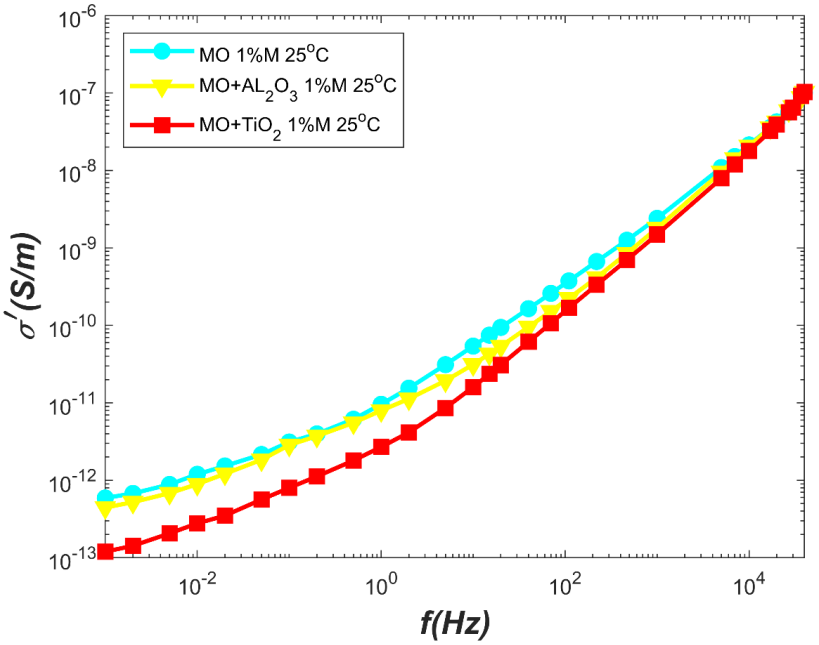

Fig. 5.65. Comparison of the AC conductivity of the pure mineral OPS with its NOPS(s) at 25°C [140V (rms)].

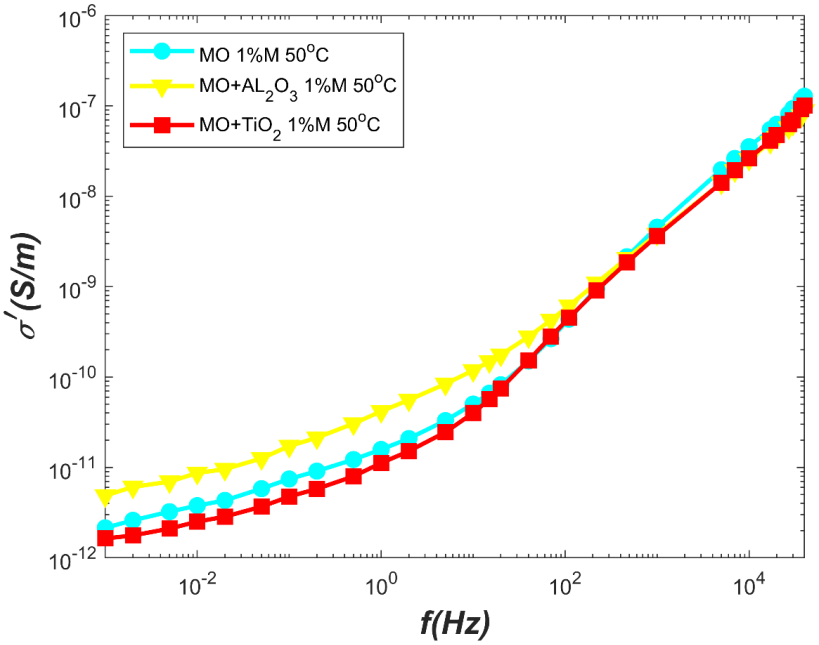

Fig. 5.66. Comparison of the AC conductivity of the pure mineral OPS with its NOPS(s) at 50°C [140V (rms)].

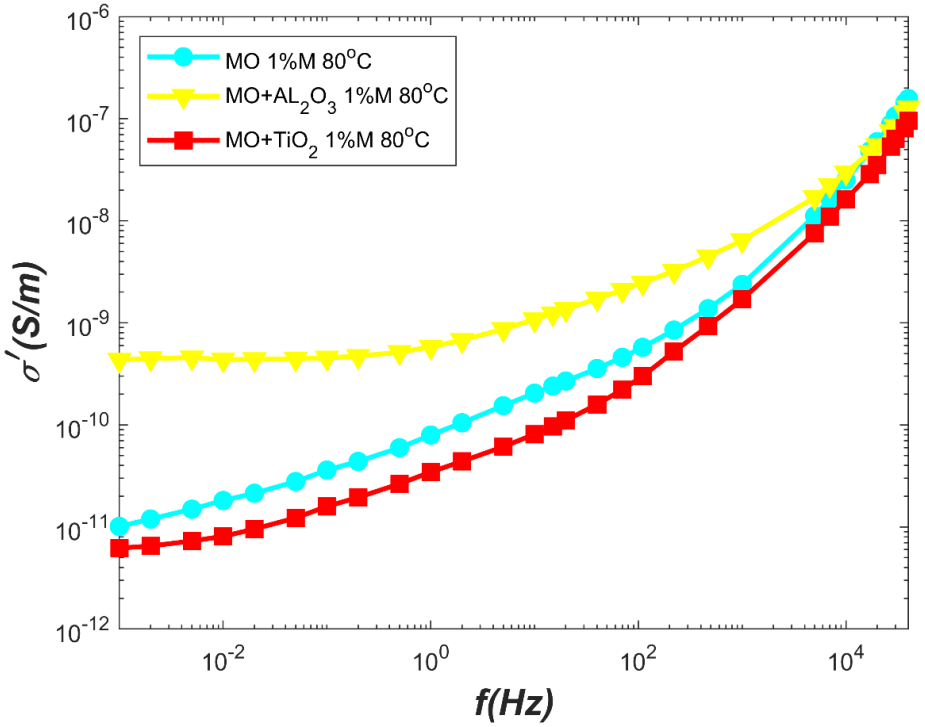

Fig. 5.67. Comparison of the AC conductivity of the pure mineral OPS with its NOPS(s) at 80°C [140V (rms)].

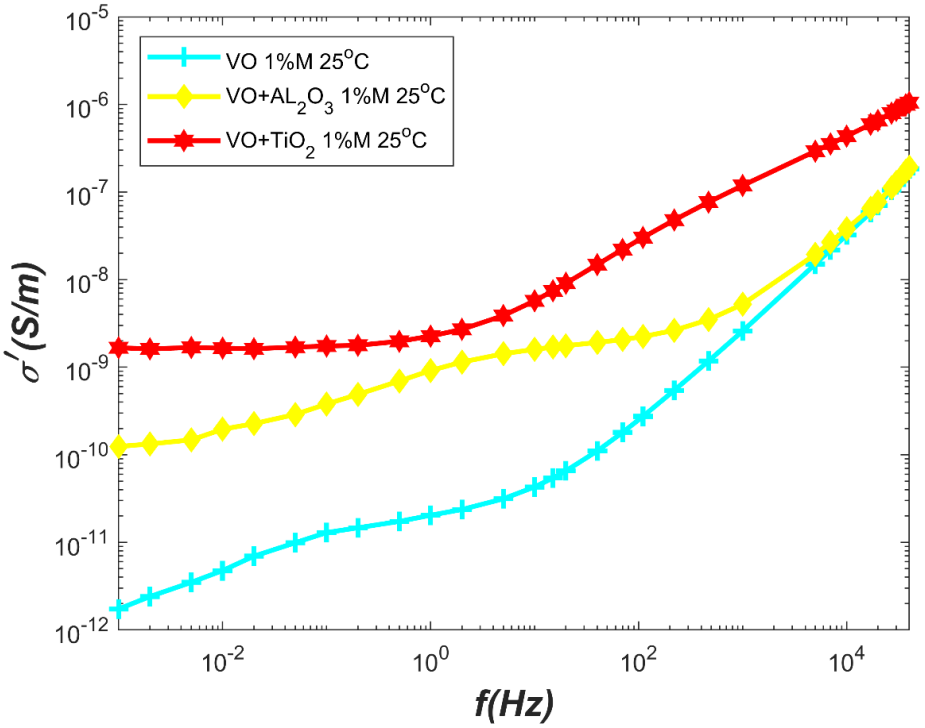

Fig. 5.68. Comparison of the AC conductivity of the pure vegetable OPS with its NOPS(s) at 25°C [140V (rms)].

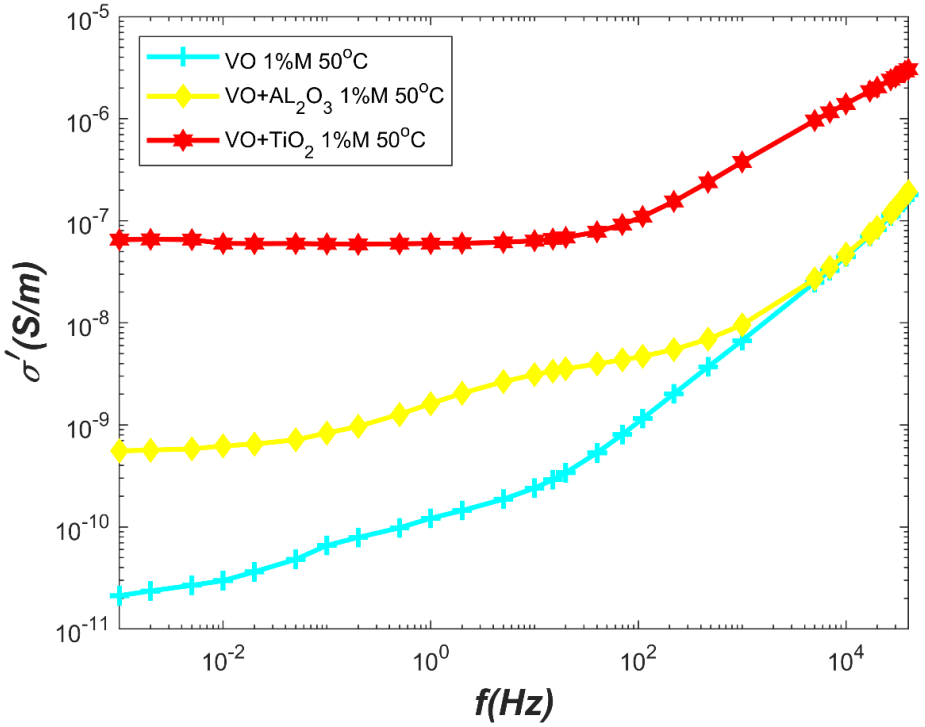

Fig. 5.69. Comparison of the AC conductivity of the pure vegetable OPS with its NOPS(s) at 50°C [140V (rms)].

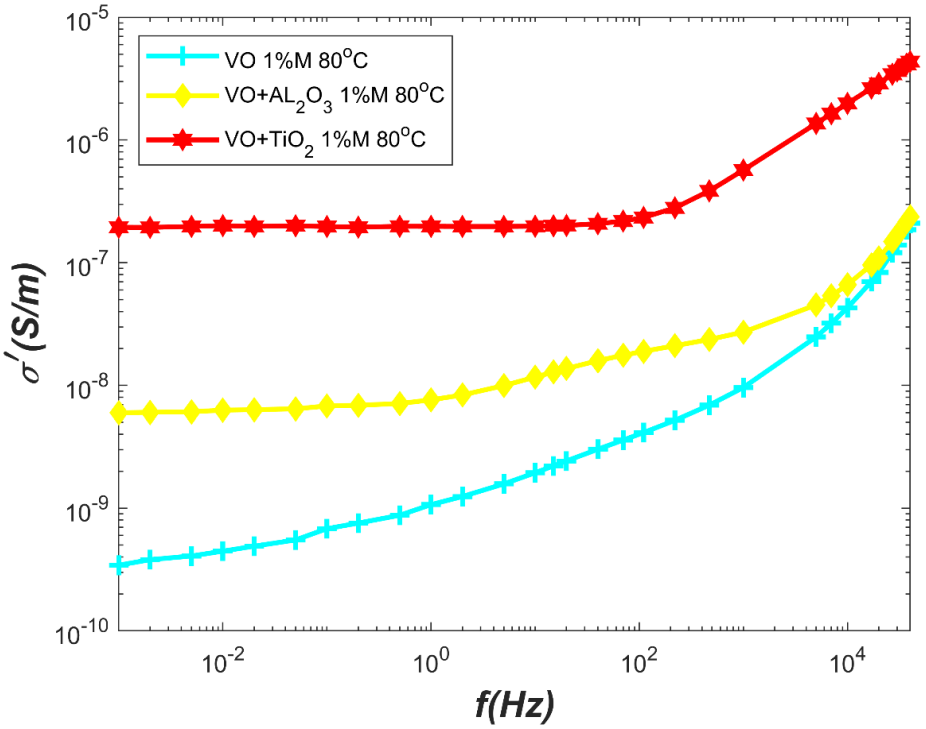

Fig. 5.70. Comparison of the AC conductivity of the pure vegetable OPS with its NOPS(s) at 80°C [140V (rms)].

5.8.3 OVERALL COMPARATIVE ANALYSIS FOR THE AC CONDUCTIVITY FOR MINERAL OIL-BASED NOPS(S) WITH VEGETABLE OIL-BASED NOPS(S) AT DIFFERENT TEMPERATURES

In this subsection, a comparative study of the AC conductivity has been carried out between mineral oil-based NOPS(s) and vegetable oil-based NOPS(s) at different temperatures. In Fig. 5.71, 5.72 and 5.73, the value of the AC conductivity of the pure mineral OPS, pure vegetable OPS, mineral oil-based Alumina and Titania NOPS(s), vegetable oil-based Alumina and Titania NOPSs have been shown at 25ºC, 50ºC and 80ºC, respectively.

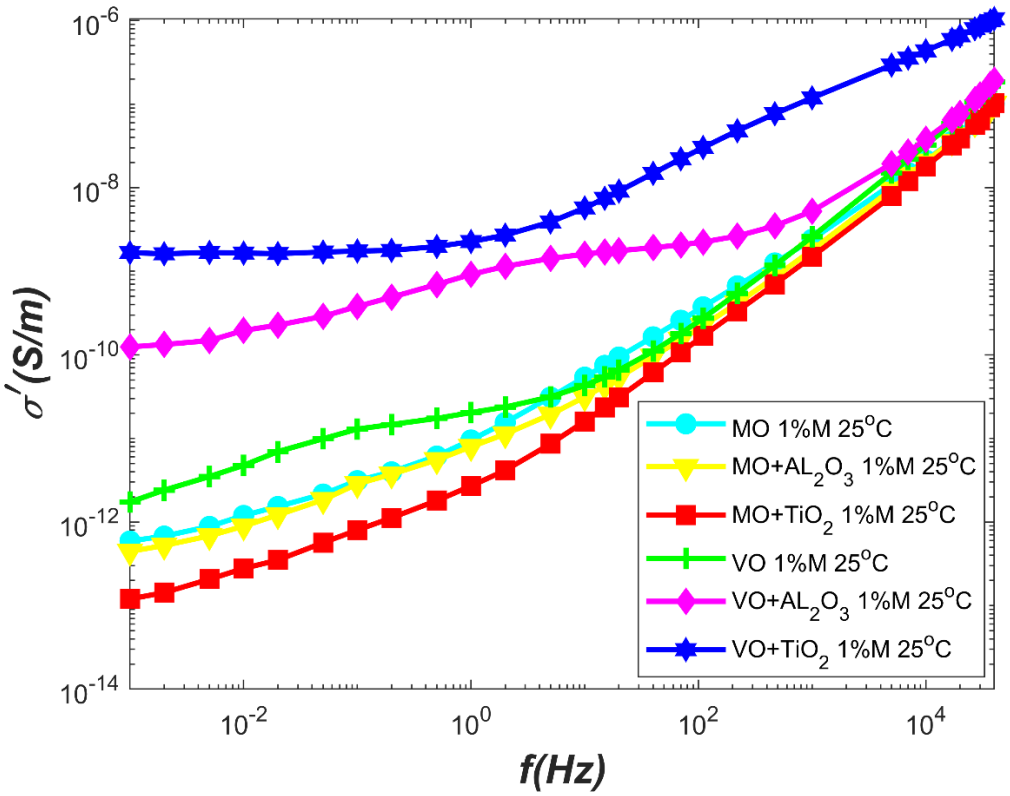

Fig. 5.71. Comparison of the AC conductivity of mineral oil-based NOPS(s) with vegetable oil-based NOPS(s) at 25ºC [140V (rms)].

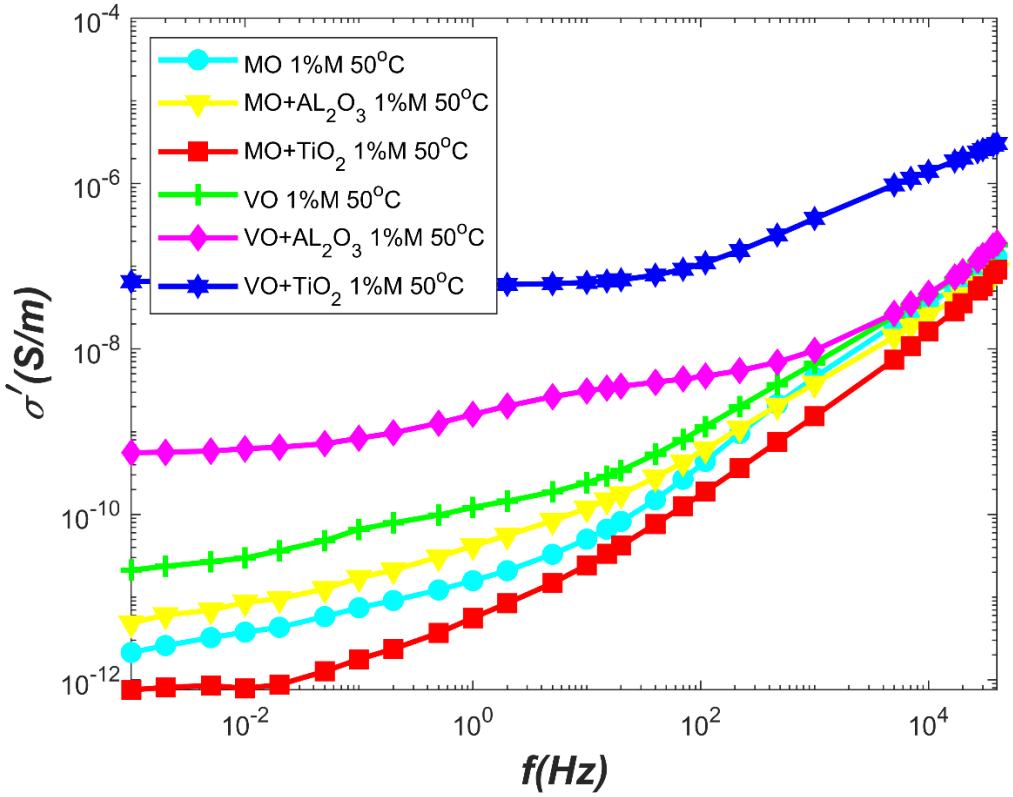

Fig. 5.72. Comparison of the AC conductivity of mineral oil-based NOPS(s) with vegetable oil-based NOPS(s) at 50°C [140V (rms)].

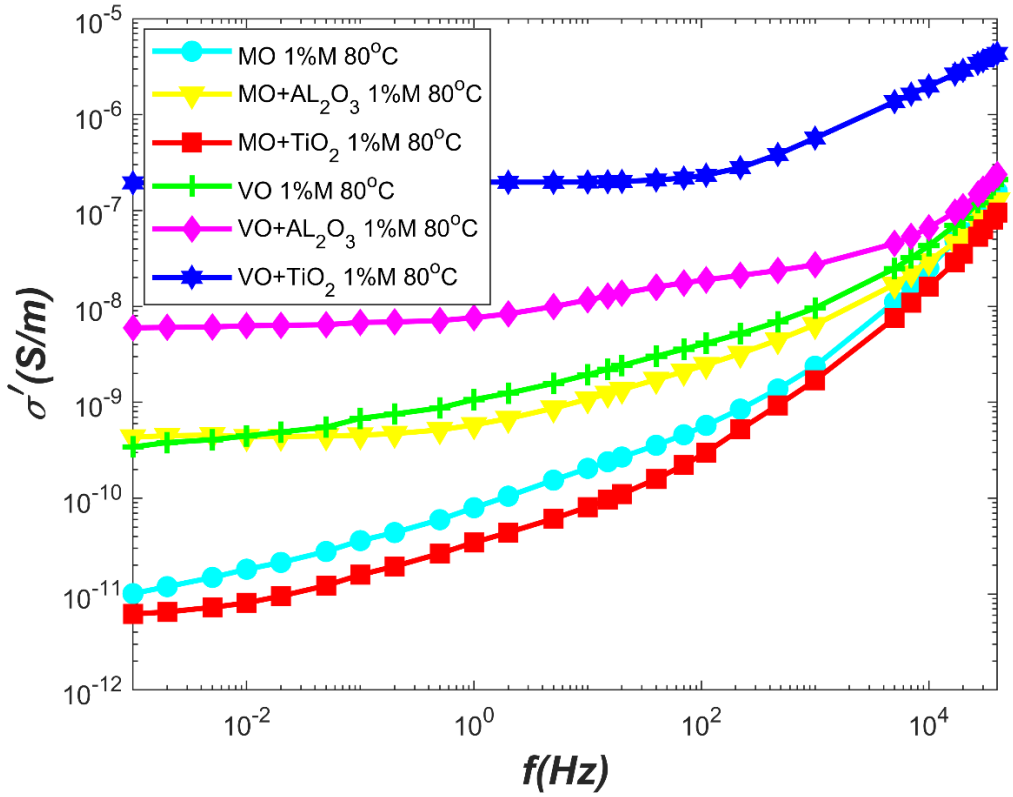

Fig. 5.73. Comparison of the AC conductivity of mineral oil-based NOPS(s) with vegetable oil-based NOPS(s) at 80°C [140V (rms)].

5.9 DISCUSSION

❖ Time Domain:

From Fig. 5.1, it is clear that with the increase in temperature, the polarization current of this sample keeps on increasing. On the other hand, For the Alumina and Titania NOPS(s), overall, as the temperature increases from 25^{o}C to 60^{o}C the polarization current of these samples increases accordingly and the rise is significant when the temperature increases from 60^{o}C to 80^{o}C, as shown in Fig 5.2 & Fig. 5.3. As per Fig. 5.4, it can be observed that the polarization current for pure vegetable (FR3) OPS increases nominally when the temperature goes from 25^{o}C to 60^{o}C. After that, there is a substantial increase in polarization current when the temperature reaches 80^{o}C. Hence, For the pure mineral OPS, the polarization current increased proportionately with the increase in temperature but for mineral oil-based NOPS(s) this current increased substantially at a very high temperature (80^{o}C). From Fig. 5.5, it can be seen charging current of the Alumina NOPS increases proportionately with the increasing temperature. On the other hand, for the Titania NOPS the polarization current increases nominally when the temperature ranges from 25^{o}C to 60^{o}C and there is a considerable increase in the current at 80^{o}C like the pure vegetable (FR3) OPS, as shown in Fig. 5.6.

From Fig. 5.7, it can be observed that the depolarization current of the pure mineral OPS increases proportionally with the temperature rise. But As per Fig. 5.8 though initially the depolarization current increases with temperature, after a certain interval (100 sec) the current decreases with the increase in temperature for mineral oil-based Alumina NOPS. Also, from Fig. 5.9, it can be noticed that initially up to a certain interval (100 sec) the depolarization currents do not follow any pattern with the temperature rise, but after 100 sec the discharging current decreases with the increase in temperature for mineral oil-based Titania NOPS. Hence, For the mineral oil-based NOPS(s) (both Alumina & Titania), after a certain interval, the depolarization current decreased with the increase in temperature. For the other four samples, after a certain interval, this current was found to be increasing with the temperature rise. From Fig. 5.10, it can be seen that the depolarization current increases with the temperature rise for the pure vegetable (FR3) OPS. However, the increase in the current is nominal. Now, as per Fig. 5.11, it can be observed that initially (up to 50 sec) the depolarization current decreases with the increase in temperature for vegetable (FR3) oil-based Alumina NOPS. Afterwards, the current increases with the temperature rise as the pure one. Then, from Fig. 5.12, it can be noticed that with the temperature rise, the depolarization current increases for the vegetable oil-based Titania NOPS.

As per Fig. 5.13, It can be seen that the mineral oil-based Titania NOPS accounts for the highest polarization current and the mineral oil-based Alumina NOPS exhibits a lesser polarization current than the pure mineral OPS at 25^{o}C. From Fig. 5.14, it can be inferred that the addition of nanoparticles in the pure vegetable (FR3) OPS results in the increase in polarization current for both the cases at 25^{o}C. From Fig. 5.15, It can be identified that the mineral oil-based Titania NOPS exhibits a comparatively higher polarization current than the pure mineral OPS at 50^{o}C. Whereas, the mineral oil-based Alumina NOPS exhibits a lesser

polarization current than the pure mineral OPS at 50^{o}C. From Fig. 5.16, it can be observed that both vegetable oil (FR3) based NOPS(s) show higher polarization current compared to pure vegetable oil (FR3) OPS at 50^{o}C. As per Fig. 5.17, It can be identified that the mineral oil-based Titania NOPS accounts for the highest polarization current and the mineral oil-based Alumina NOPS exhibits a lesser polarization current than the pure mineral OPS at 80^{o}C. From Fig. 5.18, it can be inferred that the addition of nanoparticles in the pure vegetable (FR3) OPS results in the increase in polarization current for both cases at 80^{o}C. Hence, the addition of Alumina in the pure mineral OPS decreased the polarization current at low and moderately high temperatures. However, for the pure vegetable OPS, the addition of nanoparticles did not help reduce the polarization current.

As per Fig. 5.19, initially (up to 70s) the depolarization current of the mineral oil-based Titania NOPS exhibits a lesser value than the other two currents however, after that it becomes the highest among all at 25^{o}C. Similarly, after some intervals, the depolarization current of mineral oil-based Alumina NOPS also exhibits a higher value than the pure mineral OPS at 25^{o}C. From Fig. 5.20, the overall vegetable (FR3) oil-based Titania NOPS exhibits the highest depolarization current among all at 25^{o}C. And the depolarization current of the vegetable (FR3) oil-based Alumina NOPS is also higher than the pure vegetable (FR3) OPS at 25^{o}C. From Fig. 2.21, it can be observed that the depolarization current of the mineral oil-based Titania NOPS is the highest among all at 50^{o}C. And overall, the depolarization current of mineral oil-based Alumina NOPS also exhibits a higher value than pure mineral OPS at 50^{o}C. From Fig. 5.22, the vegetable (FR3) oil-based Titania NOPS accounts for the highest depolarization current among all at 50^{o}C. And the depolarization current of the vegetable (FR3) oil-based Alumina NOPS is also slightly higher than the pure vegetable (FR3) OPS at 50^{o}C. As per Fig. 5.23, it can be inferred that the mineral oil-based Almina NOPS exhibits a higher depolarization current than the mineral oil-based Titania NOPS up to 180s, after that, the depolarization current of the mineral oil-based Titania NOPS rises and becomes highest in value among all. Pure mineral OPS accounts for the least depolarization current. From Fig. 5.24, it is clear that the vegetable (FR3) oil-based Titania NOPS reports a considerably higher depolarization current than the other two. On the other hand, the vegetable (FR3) oil-based Alumina NOPS exhibits a slightly higher depolarization current than the pure vegetable (FR3) OPS. Hence, at all three temperatures (25°C, 50°C and 80°C), the addition of nanoparticles in both base OPS(s) (mineral & vegetable oil in our case) increased the depolarization current (after a certain interval). This increase was prominent in the case of Titania nanoparticles.

From Table 5.1, it can be identified that in the case of mineral oil-based NOPS conductivity increases with the increase in voltage. Up to 150V the rise in conductivity is somewhat proportional but there is a high jump in conductivity at 200V. On the other hand, for mineral oil-based Alumina NOPS, from 50 to 100V the conductivity increases considerably, after that the conductivity increases gradually with the voltage rise. Also, for the mineral oil-based Titania NOPS, there is a nominal increase in conductivity from 50 to 100V, and then it increases substantially with the rise in voltage. As seen in Table 5.1, for the pure vegetable (FR3) OPS, there is a considerable increase in DC conductivity from 50 to 100V. After that, the conductivity rises gradually with the applied voltage. And for both vegetable (FR3) oil-based Titania and Alumina NOPS(s), the DC conductivity increases proportionally with the

applied voltage up to 150V. At 200V, there is a substantial increase in the DC conductivity for both the NOPS(s). It can also be identified that among these six OPS(s) overall, the variation of DC conductivity with the applied voltage is on the lower side for the mineral oil-based Alumina NOPS. From Table 5.2, it can be observed that for the pure mineral OPS, there is a gradual increase in the DC conductivity up to 60^{o}C, after that at 80^{o}C it rises considerably. On the other hand, for mineral oil-based, both Alumina and Titania NOPS(s) the DC conductivity increases somewhat uniformly with the temperature. For both vegetable (FR3) oil-based NOPS(s), the variation of the DC conductivity with the temperature is minimal compared to pure vegetable (FR3) OPS. And it can also be identified that among these six oil-paper-based samples overall, the variation of DC conductivity with the temperature is on the lower side for mineral oil-based Titania NOPS(s). Hence, the inclusion of nanoparticles in both base OPS(s) reduced the temperature dependency of the DC conductivity. However, it did not provide any improvement in voltage dependency.

As per Fig. 5.25, from the plot, it can be observed that the negative slope is highest for the pure mineral OPS and least for the mineral oil-based Titania NOPS. And from Fig. 5.26, it can also be identified that the negative slope is highest for the pure vegetable (FR3) OPS and least for vegetable (FR3) oil-based Titania NOPS. From Table 5.3, it can safely be concluded that the addition of nanoparticles in the pure OPS (mineral oil/ FR_3) samples, reduces its activation energy compared to pure ones. The activation energies of pure base OPS(s) were higher compared to their corresponding NOPS(s). Hence, it can be concluded that nanoparticles reduce the life span of the insulation.

As per Fig. 5.27 and Table 5.4, it is clear that the conduction current of mineral oil-based Titania nano OPS exhibits highly non-linear characteristics with the increase in voltage. And the pure mineral OPS although shows non-linearity, but the extent of non-linearity is less than that of the mineral oil-based Titania NOPS. Whereas, The mineral oil-based Alumina NOPS accounts for the least non-linearity among all. From Fig. 5.28 and the listed values in table 5.4, it can be inferred that the conduction current of vegetable (FR3) oil-based Alumina NOPS exhibits the least non-linearity (near to 1) among all. Whereas, the vegetable (FR3) oil-based Titania NOPS shows a higher extent of non-linearity than the pure vegetable (FR3) OPS. As per Table 5.4, it can be established that the addition of Alumina nanoparticles on both mineral and vegetable (FR3) OPS(s) shows a remarkable improvement in the linear behaviour of conduction current, unlike Titania nanoparticles.

❖ Frequency Domain

From Fig. 5.29, the temperature dependence on the pure mineral OPS may be observed. For this sample, the value of the real component of complex relative permittivity increases with the increase in temperature. Similarly, for both the mineral oil-based Alumina and Titania NOPS(s), this value keeps on increasing with the temperature rise, as shown in Fig. 5.30 and 5.31. The mineral oil-based Alumina NOPS accounts for the most and the mineral oil-based Titania NOPS exhibits the least temperature variation among all. It can also be seen that this temperature rise is more prominent at particularly low frequencies for all three samples. From Fig. 5.32, For pure vegetable OPS, the value of the real component of complex relative

permittivity is seen to be increasing with temperature. However, for both the mineral oil-based Alumina and Titania NOPS(s), although this value increases with the temperature rise, but not to a considerable extent at the power frequency level, as shown in Fig. 5.33 and 5.34. This result leads to the fact that the addition of nanoparticles (Titania and Alumina in our case) in the pure vegetable OPS reduces the temperature dependency of the real component of complex relative permittivity (at all frequencies).

From Fig. 5.35, the temperature dependence on the pure mineral OPS can clearly be seen. For this sample, the value of the imaginary component of complex relative permittivity increases with the increase in temperature up to the power frequency level, after that the patterns are quite arbitrary to apprehend the true nature of the sample. For mineral oil-based Alumina NOPS, the substantial increase in the value of the same with the temperature at all frequencies can be observed, in Fig. 5.36. Whereas, for mineral oil-based Titania NOPS, the increase is comparatively predominant at lower frequencies, as shown in Fig. 5.37. From Fig. 5.38, for the pure vegetable OPS, the value of the imaginary component of complex relative permittivity is seen to be increasing with temperature. However, for both the mineral oil-based Alumina and Titania NOPS(s), although this value increases with the temperature rise, but not that much at the power frequency level, as shown in Fig. 5.39 and 5.40. This result reflects that the addition of nanoparticles (Titania and Alumina in our case) in the pure vegetable OPS reduces the temperature dependency of the imaginary component of complex relative permittivity to some extent.

As per Fig. 5.41, for mineral oil-based Alumina NOPS, at low frequencies, the value of the real component of complex relative permittivity is higher than that of mineral oil-based Titania NOPS but at power frequencies and above, the exact opposite pattern can be observed at 25^{o}C. Whereas, at all frequencies, the pure mineral OPS exhibits the highest value of the real component of complex relative permittivity among all at 25^{o}C. From Fig. 5.42 and 5.43, it can be seen that at low frequencies mineral oil-based Alumina NOPS accounts for the highest and at high frequencies, it exhibits the lowest value of the real component of complex permittivity compared to pure mineral OPS and its Titania counterpart at both 50^{o}C and 80^{o}C. Overall, mineral oil-based Titania NOPS possess superior dielectric characteristics at all temperatures. From Fig. 5.44, 5.45 and 5.46, it may be observed that the pure mineral OPS exhibits the least and mineral oil-based Titania NOPS shows the highest value of the real component of complex relative permittivity at all frequencies and all temperatures. For mineral oil-based Titania NOPS, this value is in between the other two samples at all frequencies. Hence, it can be deduced from the above that the addition of nanoparticles (Titania and Alumina in our case) in the pure vegetable OPS does not help improve this dielectric characteristic of the sample.

From Fig. 5.47, it can be seen that for the pure mineral OPS, the value of the imaginary component of complex relative permittivity is greater than that of mineral oil-based Alumina NOPS at all frequencies, 25^{o}C. However, the exact opposite of the above is observed at both 50^{o}C and 80^{o}C, as shown in Fig. 5.48 and 5.49. whereas, this value is least for mineral oil-based Titania NOPS for all three temperatures. However, at very high frequencies, the values are quite arbitrary to apprehend the true nature of the samples. From Fig. 5.50, 5.51 and 5.52, it may be observed that the pure mineral OPS exhibits the least and mineral oil-based Titania

NOPS shows the highest value of the imaginary component of complex relative permittivity at all frequencies and all temperatures. For mineral oil-based Alumina NOPS, this value is in between the other two samples at all frequencies. Hence, it can be deduced from the above that the addition of nanoparticles (Titania and Alumina in our case) in the pure vegetable OPS does not help improve this dielectric characteristic of the sample.

As per Fig. 5.53, 5.54 and 5.55, it may be observed that the pure vegetable OPS and its NOPS(s) (Titania and Alumina in our case) constitute a higher value of the real component of the complex permittivity than that of the pure mineral OPS and its NOPS(s) at all three temperatures (25^{o}C, 50^{o}C and 80^{o}C). At all frequencies, it may also be observed that this value for vegetable oil-based Titania NOPS is the highest and for mineral oil-based Titania NOPS is the lowest among all. As per Fig. 5.56, 5.57 and 5.58, it may be seen that on an average, the pure vegetable OPS and its NOPS(s) (Titania and Alumina in our case) constituted a higher value of the imaginary component of the complex permittivity than that of the pure mineral OPS and its NOPS(s) at all three temperatures (25^{o}C, 50^{o}C and 80^{o}C). At all frequencies, it may also be observed that this value for vegetable oil-based Titania NOPS is the highest and for mineral oil-based Titania NOPS is the lowest among all (at all frequencies).

From Fig. 5.59, it may be observed that the value of the AC conductivity increases with the increase in temperature up to the power frequency level, after that the patterns are quite arbitrary to apprehend the true nature of the sample. For mineral oil-based Alumina NOPS, the substantial increase in the value of the same with the temperature at all frequencies can be observed, in Fig. 5.60. Whereas, for mineral oil-based Titania NOPS, the increase is comparatively predominant at lower frequencies, as shown in Fig. 5.61. From Fig. 5.62, 5.63 and 5.64, the value of the AC conductivity is seen to be increasing with temperature for all three samples. However, for the vegetable oil-based Titania NOPS(s), the AC conductivity increases substantially with the temperature rise, especially at the lower frequencies, as shown in Fig. 5.63 and 5.64.

From Fig. 5.65, it can be seen that for the pure mineral OPS, the value of the AC conductivity is greater than that of mineral oil-based Alumina NOPS at all 25^{o}C (at all frequencies). However, the exact opposite of the above is observed at both 50^{o}C and 80^{o}C, as shown in Fig. 5.66 and 5.67. whereas, this AC conductivity is least for mineral oil-based Titania NOPS for all three temperatures. However, at very high frequencies, the values are quite arbitrary to apprehend the true nature of the samples. From Fig. 5.68, 5.69 and 5.70, it may be observed that the pure mineral OPS exhibits the least and mineral oil-based Titania NOPS shows the highest value of AC conductivity at all frequencies and all temperatures. For mineral oil-based Alumina NOPS, this value is in between the other two samples at all frequencies. Hence, it can be deduced from the above that the addition of nanoparticles (Titania and Alumina in our case) in the pure vegetable OPS does not help improve this dielectric characteristic of the sample.

As per Fig. 5.71, 5.72 and 5.73, it may be seen that on an average, the pure vegetable OPS and its NOPS(s) (Titania and Alumina in our case) pose a higher value of the AC conductivity than that of the pure mineral OPS and its NOPS(s) at all three temperatures (25^{o}C, 50^{o}C and 80^{o}C). At all frequencies, it may also be observed that the AC conductivity for vegetable oil-

based Titania NOPS is the highest and for mineral oil-based Titania NOPS is the lowest among all.

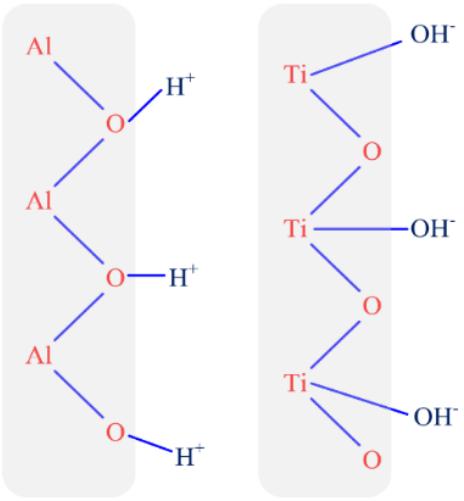

Fig. 5.74. Bond formation with water molecules in nanofluids [22].

Chapter: 5

CONCLUSION AND FUTURE SCOPE

5.1 CONCLUSION

In this thesis work, the dielectric properties of two base OPS(s) and its corresponding four NOPS(s) i.e., mineral oil-based Titania & Alumina NOPS(s) and vegetable (FR3) oil-based Titania & Alumina nanofluids were investigated. After the successful preparation of the nanofluids, all the samples were subjected to different tests in the High-tension Laboratory of Jadavpur University. To investigate the dielectric properties of prepared samples in the time domain, polarization-depolarization current (PDC) measuring equipment, "DIRANA" was employed. From the PDCmeasurements, the DC conductivity of all the samples at four different temperatures (i.e., 25℃, 40℃, 60℃ and 80℃) and voltage levels (i.e., 50V, 100V, 150V and 200V) were figured out. The activation energy of each sample was also calculated. At last, a nonlinearity study of the conduction current had also been done.

Under time-domain spectroscopy, the polarization currents of all the six samples are more or less dependent on the temperature. As the temperature increases, free electrons in the sample also increases which leads to an increase in the polarization current. At all temperatures, the polarization current of the pure vegetable OPS and its NOPS(s) is higher than that of mineral OPS and its NOPS(s) because the vegetable oil is a weaker dielectric material than the mineral oil [30]. Especially, at high temperatures, NOPS(s) exhibit considerably higher polarization currents than that of the base OPS(s). Because as the temperature increases, the trapped electrons in the NOPS acquire the thermal energy and this thermal energy becomes higher than the energy to de-trap and then the electrons get released.

In order to investigate the dielectric properties of the samples in the frequency domain, a frequency domain response measuring device "IDAX" was used. The real and imaginary components of complex relative permittivity were evaluated on a comparative basis using frequency-domain spectroscopy of the samples at four distinct temperature levels, namely 25℃, 40℃, 60℃ and 80^{o}C. At last, the AC conductivities were also evaluated at different frequencies.

Under frequency-domain spectroscopy, for all the samples it can be observed that the value of the real and imaginary components of complex relative permittivity increases as the frequency decreases. The drop in these values with rising frequency may be attributable to the fact that the time period increases as the frequency of the excitation voltage decreases. As a result, the dipoles and free electrons in the dielectric are influenced by a certain polarity in the applied field for a longer period of time. This causes the dipoles to become more aligned with the applied field. Electrons, like dipoles, have enough time to migrate towards the positive electrode. This improves interactions by causing dipoles to align and electrons to migrate towards the anode. The interactions increase frictional loss and the electrical energy storing ability, thus the real and imaginary components of complex relative permittivity, respectively [60].

The values of the imaginary component of complex relative permittivity (for the whole frequency range) for both the pure mineral and vegetable OPS(s) rise with temperature. Setayeshmehr *et al* observed that with the increase in temperature, the activation energy increases within the oil molecules [63]. As a result, the conduction current of dielectric material

rises with temperature. This causes the conduction loss to increase and thus the imaginary component of complex relative permittivity increases.

The value of the real and imaginary components of complex relative permittivity for mineral oil-based Titania NOPS is low (especially at lower frequencies) compared to the pure mineral OPS and mineral oil-based Alumina NOPS at all three temperatures (25^{o}C, 50^{o}C and 80^{o}C). This could be mainly due to the presence of hydroxyl groups on the surfaces of the nanoparticles (found in the water molecules present in the sample). It should be noted that Ti atoms have an affinity for the hydroxyl (OH^{-}) group [62], as shown in Fig. 5.74. As a result, the application of a strong electric field that lasts longer (i.e., at a lower frequency) results in the formation of a bond with the hydroxyl (OH^{-}) group. Sun *et al* showed that the hydroxyl group (on TiO_2 crystal) forms loose bonds with the cellulose chains (in mineral oil), weakening the polarisation capabilities of nanoparticles at lower frequency ranges [61]. The development of weak polarization characteristics of the NOPS results in lower frictional loss and energy storing capability during FDS measurement. Thereby, both the real and imaginary components of complex relative permittivity decrease. Whereas, the value of the imaginary component of complex relative permittivity for mineral oil-based Alumina NOPS is high (especially at lower frequencies) compared to the pure mineral OPS and mineral oil-based Titania NOPS at higher temperatures (50^{o}C and 80^{o}C). Unlike TiO_2, Al_2O_3 absorbs H+ ions from water molecules, forming a bond with its O atom, according to Mansour *et al* [62], as shown in Fig. 5.74. Because of the bonding formed by O—H, this process results in the formation of dipoles. This further results in the strong polarization characteristics of the NOPS. The development of strong polarization characteristics of the NOPS resembles lower frictional loss during FDS measurement and thus the imaginary component of complex relative permittivity increases.

Overall, it can be concluded that mineral oil-based Titania NOPS provided better dielectric characteristics compared to the other five samples and its practical implementation may be possible.

5.2 FUTURE SCOPE

Future works can be directed in a variety of ways. Some of the potential works are listed below.

1. Low-frequency dispersion phenomenon of NOPI needs to be investigated.
2. The complex conductivity of NOPI can be evaluated. From which “Ladder Phenomenon” can be observed.
3. Investigations on the complex dielectric modulus of NOPI can be performed and the “Hump Phenomenon” can be analysed.
4. The relationship between the “Hump phenomenon and Ladder phenomenon” can be established for NOPI.
5. The study of charge mobility and the effect of moisture value in NOPI might provide intriguing insights into its conduction process.

REFERENCES

1. 00 S. Choi, “Enhancing thermal conductivity of fluids with nanoparticles”, in Developments Applications of Non-Newtonian Flows, D. A. Siginer and H. P. Wang, Eds., FED-Vol. 231/MDVol. 66, pp. 99–105, ASME, New York, NY, USA, 1995.
2. Cao, Yang & Irwin, P.C. & Younsi, Karim. (2004), “The Future of Nanodielectrics in the Electrical Power Industry”, Dielectrics and Electrical Insulation, IEEE Transactions on. 11. 797 - 807. 10.1109/TDEI.2004.1349785.
3. I. Fofana, “50 years in the development of insulating liquids”, IEEE Electrical Insulation Magazine, vol. 29, pp. 13-25, 2013.
4. Qi Wang, Muhammad Rafiq, Yuzhen Lv, Chengrong Li, and Kai Yi, “Preparation of Three Types of Transformer Oil-Based Nanofluids and Comparative Study on the Effect of Nanoparticle Concentrations on Insulating Property of Transformer Oil”, Journal of Nanotechnology, vol. 2016, Article ID 5802753, 6 pages, 2016.
5. Yu-zhen Lv *et al*, “Preparation and breakdown strength of TiO_2 fluids based on transformer oil”, IEEE Conference on Electrical Insulation and Dielectric Phenomena (CEIDP), 2010.
6. Y. Du *et al.*, “Effect of semiconductive nanoparticles on insulating performances of transformer oil”, in IEEE Transactions on Dielectrics and Electrical Insulation, vol. 19, no. 3, pp. 770-776, June 2012.
7. Yu-zhen Lv, Le-feng Wang, Xiao-xin Li, Yue-fan Du, Jian-quan Zhou and Cheng-rong Li, “Experimental investigation of breakdown strength of mineral oil-based nanofluids”, 2011 IEEE International Conference on Dielectric Liquids, Trondheim, 2011, pp. 1-3.
8. Y.Z. Lv, Y. Zhou, C.R. Li, Q. Wang, B. Qi, “Recent Progress in Nanofluids Based on Transformer Oil: Preparation and Electrical Insulation Properties”, IEEE Electrical Insulation Magazine.
9. Kocatepe C, Taslak E, Kumru C F, Arıkan O, “An investigation on vegetable oils as potential insulating liquid”, International Journal of Electrical, Computer, Energetic, Electronic and Communication Engineering, 2015, 9(8):794-797.
10. J. Li, Z. Zhang, P. Zou, S. Grzybowski and M. Zahn, “Preparation of a vegetable oil-based nanofluid and investigation of its breakdown and dielectric properties”, in IEEE Electrical Insulation Magazine, vol. 28, no. 5, pp. 43-50, September-October 2012.
11. Muhammad Rafiq, Yuzhen Lv, and Chengrong Li, “A Review on Properties, Opportunities, and Challenges of Transformer Oil-Based Nanofluids”, Journal of Nanomaterials, vol. 2016, Article ID 8371560, 23 pages, 2016.
12. S. Mukherjee and S. Paria, “Preparation and stability of nanofluids-- a review”, IOSR

Journal of Mechanical and Civil Engineering, vol. 9, no. 2, pp. 63-69, 2013.

13. W. S. Zaengl, “Dielectric Spectroscopy in time and frequency domain for HV Power Equipment. I. Theoretical considerations”, IEEE Electrical Insulation Magazine, Vol. 19, No. 5, pp. 5-19, 2003.
14. S. Chakravorti, D. Dey, B. Chatterjee: Recent Trends in the Condition Monitoring of Transformers. Power Systems. Springer, London (2013).
15. T. K. Saha and P. Purkait, “Investigations of temperature effects on the dielectric response measurements of transformer oil paper insulation system”, IEEE Trans. Power Delivery, Vol. 23, pp. 252-260, 2008.
16. H. C. Verma, A. Baral, A. K. Pradhan and S. Chakravorti, “A method to estimate activation energy of power transformer insulation using time domain spectroscopy data”, in IEEE Transactions on Dielectrics and Electrical Insulation, vol. 24, no. 5, pp. 3245-3253, Oct. 2017.
17. Roy, Sukumar & L. K., Sudha & Uma Rao, K. (2014). Evaluation of Activation Energy (Ea) Profiles of Nanostructured Alumina Polycarbonate Composite Insulation Materials. International Journal of Materials, Mechanics and Manufacturing. 2. 96-100. 10.7763/IJMMM.2014.V2.108.
18. Z.T.Yao, T.K.Saha, M. Darveniza “Effects of moisture on the recovery voltage measurement for aged transformer”, In Proceedings of International Conference on Power Engineering, vol 1. pp. 349–353 (1999).
19. M. K. Pradhan, J. H. Yew and T. K. Saha, “Influence of the geometrical parameters of power transformer insulation on the frequency domain spectroscopy measurement”, 2008 IEEE Power and Energy Society General Meeting - Conversion and Delivery of Electrical Energy in the 21st Century, Pittsburgh, PA, 2008, pp. 1-8.
20. M. Chiesa and S. K. Das, “Experimental investigation of the dielectric and cooling performance of colloidal suspensions in insulating media”, Colloids and Surfaces A: Physicochemical and Engineering Aspects, vol. 335, no. 1–3, pp. 88–97, 2009.
21. V. Segal, A. Hjortsberg, A. Rabinovich, D. Nattrass, and K. Raj, “AC (60 Hz) and impulse breakdown strength of a colloidal fluid based on transformer oil and magnetite nanoparticles”, in Proceedings of the Conference Record of the IEEE International Symposium in Electrical Insulation, pp. 619–622, Arlington, Va, USA, June 1998.
22. J. G. Hwang, M. Zahn, F. M. O’Sullivan, L. A. A. Pettersson, O. Hjortstam, and R. S. Liu, “Effects of nanoparticle charging on streamer development in transformer oil-based nanofluids”, Journal of Applied Physics, vol. 107, no. 1, Article ID 014310, 2010.
23. C. H. Lo, T. T. Tsung, L. C. Chen, “Shape-controlled synthesis of Cu-based nanofluid using submerged arc nanoparticle synthesis system (SANSS)”, J Cryst Growth 2005, 277: 636. 10.1016/j.jcrysgro.2005.01.067.
24. Brust, Mathias & Walker, Merryl & Bethell, Donald & Schiffrin, David & Whyman,

Robin. (1994), “Synthesis of Thiol-Derivatized Gold Nanoparticles in a 2-Phase Liquid-Liquid System”, Journal of The Chemical Society, Chemical Communications. 7. 10.1039/c39940000801.

25. Y. Hwang, J-K. Lee, J-K. Lee, Y-M. Jeong, S-i. Cheong, Y-C. Ahn, S.H. Kim, “Production and dispersion stability of nanoparticles in nanofluids”, Powder Technol. 186 (2), pp.145-153, 2008.
26. Y. F. Du, Y. Z. Lv, C. R. Li *et al*., “Effect of water adsorption at nanoparticle-oil interface on charge transport in high humidity transformer oil-based nanofluid”, Colloids and Surfaces A: Physicochemical and Engineering Aspects, vol. 415, pp. 153–158, 2012.
27. Y. F. Du, Y.Z. Lv, J. Q. Zhou, X. X. Li, and C. R. Li, “Breakdown properties of transformer oil-based TiO_2 nanofluid”, in Proceedings of the Annual Report Conference on Electrical Insulation and Dielectric Phenomena (CEIDP ’10), pp. 1–4, West Lafayette, Ind, USA, October 2010.
28. Y. Du, Y. Lv, C. Li *et al*., “Effect of semiconductive nanoparticles on insulating performances of transformer oil”, IEEE Transactions on Dielectrics and Electrical Insulation, vol. 19, no. 3, pp. 770–776, 2012.
29. Z. Zhang, J. Li, P. Zou, and S. Grzybowski, “Electrical properties of nano-modified insulating vegetable oil”, in 2010 Annual Report Conference on Electrical Insulation and Dielectric Phenomena, West Lafayette, IN, pp. 1–4, Oct 2010.
30. Y. X. Zhong, Y. Z. Lv, C. R. Li *et al*., “Insulating properties and charge characteristics of natural ester fluid modified by TiO_2 semiconductive nanoparticles”, IEEE Transactions on Dielectrics and Electrical Insulation, vol. 20, no. 1, pp. 135–140, 2013.
31. T. S. Ramu, B. K. Keshavan, and K. N. Murthy, “Application of a class of nanofluids to improve the load ability of power transformers”, in Proceedings of the IEEE 10th International Conference on the Properties and Applications of Dielectric Materials (ICPADM ’12), pp. 1–6, Bangalore, India, July 2012.
32. P. P. C. Sartoratto, A. V. S. Neto, E. C. D. Lima, A. L. C. Rodrigues de Sa, and P. C. Morais, “Preparation and electrical properties of oil-based magnetic fluids”, Journal of Applied Physics, vol. 97, no. 10, Article ID 10Q917, 2005.
33. J. A. Mergos, M. D. Athanassopoulou, T. G. Argyropoulos, and C. T. Dervos, “Dielectric properties of nano powder dispersions in paraffin oil”, IEEE Transactions on Dielectrics and Electrical Insulation, vol. 19, no. 5, pp. 1502–1507, 2012.
34. S. S. Botha, P. Ndungu, and B. J. Bladergroen, “Physicochemical properties of oil-based nanofluids containing hybrid structures of silver nanoparticles supported on silica”, Industrial and Engineering Chemistry Research, vol. 50, no. 6, pp. 3071–3077, 2011.
35. M. Singh and L. Kundan, “Experimental study on thermal conductivity and viscosity of Al_2O_3-nano transformer oil”, International Journal on Theoretical and Applied Research in Mechanical Engineering (IJTARME), vol. 2, no. 3, pp. 125–130, 2013.

36. H. Jin, Dielectric strength and thermal conductivity of mineral oil based nanofluids [M.S. thesis], Delft University of Technology, Delft, The Netherlands, April 2015.

37. K. Y. Raj, P. Das, A. Kumar, N. Haque, B. Chatterjee and S. Dalai, "Polarization and depolarization current analysis of thermally aged oil impregnated kraft paper," 2017 IEEE Calcutta Conference (CALCON), Kolkata, 2017, pp. 457-460.

38. R. Karthik, T. S. R. Raja, and R. Madavan, "Enhancement of critical characteristics of transformer oil using nanomaterials", Arabian Journal for Science and Engineering, vol. 38, no. 10, pp. 2725–2733, 2013.

39. H. J. Kim, I. C. Bang, and J. Onoe, "Characteristic stability of bare Au-water nanofluids fabricated by pulsed laser ablation in liquids", Optics and Lasers in Engineering, vol. 47, no. 5, pp. 532–538, 2009.

40. X. Wei and L.Wang, "Synthesis and thermal conductivity of microfluidic copper nanofluids", Particuology, vol. 8, no. 3, pp. 262–271, 2010.

41. Y. Fovet, J. Y. Gal, and F. Toumelin-Chemla, "Influence of pH and fluoride concentration on titanium passivating layer: stability of titanium dioxide", Talanta, vol. 53, no. 5, pp. 1053–1063, 2001.

42. A. K. Singh and V. S. Raykar, "Microwave synthesis of silver nanofluids with polyvinylpyrrolidone (PVP) and their transport properties", Colloid and Polymer Science, vol. 286, no. 14-15, pp. 1667–1673, 2008.

43. H. Zhu, D. Han, Z. Meng, D. Wu, C. Zhang, "Preparation and thermal conductivity of CuO nanofluid via a wet chemical method", Nanoscale Research Letters, vol.6, no.1, p.181, 2011.

44. P. Razi, M.A. Akhavan-Behabadi, M. Saeedinia, "Pressure drop and thermal characteristics of CuO–base oil nanofluid laminar flow in flattened tubes under constant heat flux", International Communications in Heat and Mass Transfer, vol.38, pp.964-971, 2011.

45. M. Chandrasekar, S. Suresh, A. Chandra Bose, "Experimental investigations and theoretical determination of thermal conductivity and viscosity of Al_2O_3/water nanofluid", Exp. Therm. Fluid Sci. 34 (2), pp.210-216, 2010.

46. Y. Hwang, J-K. Lee, J-K. Lee, Y-M. Jeong, S-i. Cheong, Y-C. Ahn, S.H. Kim, "Production and dispersion stability of nanoparticles in nanofluids", Powder Technol. 186 (2), pp.145-153, 2008.

47. X.F. Li, D.S. Zhu, X.J. Wang, N. Wang, J.W. Gao, H. Li, "Thermal conductivity enhancement dependent pH and chemical surfactant for Cu-H2O nanofluids", Thermochimica Acta 469 (1-2), pp. 98-103, 2008.

48. W. Yu, H. Xie, "A Review on Nanofluids: Preparation, Stability Mechanisms, and Applications", Journal of Nanomaterials, vol2012, pp.1-17, 2012.

49. L. Chen and H. Xie, "Surfactant-free nanofluids containing double- and single-walled

carbon nanotubes functionalized by a wet mechanochemical reaction", Thermochimica Acta, vol. 497, no. 1-2, pp. 67–71, 2010.

50. Q. Yu, Y. J. Kim, and H. Ma, "Nanofluids with plasma treated diamond nanoparticles", Applied Physics Letters, vol. 92, no. 10, Article ID 103111, 2008.
51. H. Xie, H. Lee, W. Youn, M. Choi, "Nanofluids containing multiwalled carbon nanotubes and their enhanced thermal conductivities", J. Appl. Phys. 94 (8), pp.4967–4971, 2003.
52. X. J. Wang and X. F. Li, "Influence of pH on nanofluids 'viscosity and thermal conductivity", Chinese Physics Letters, vol. 26, no. 5, Article ID 056601, 2009.
53. S. K. Das, S. U. S. Choi, W. Yu, and T. Pradeep, "Nanofluids: Science and Technology", Wiley-Interscience, New York, NY, USA, 2008.
54. P. Krajnik, F. Pusavec, and A. Rashid, "Nanofluids: properties, applications and sustainability aspects in materials processing technologies", in Advances in Sustainable Manufacturing: Proceedings of the 8th Global Conference on Sustainable Manufacturing, pp. 107–113, Springer, Berlin, Germany, 2011.
55. J. W. Sutherland, V. N. Kulur, and N. C. King, "An experimental investigation of air quality in wet and dry turning", CIRP Annals-Manufacturing Technology, vol. 49, no. 1, pp. 61–64, 2000.
56. H. A. Jeng and J. Swanson, "Toxicity of metal oxide nanoparticles in mammalian cells", Journal of Environmental Science and Health, vol. 41, no. 12, pp. 2699–2711, 2006.
57. J. Wang, Y. Liu, F. Jiao *et al.*, "Time-dependent translocation and potential impairment on central nervous system by intranasally instilled TiO_2 nanoparticles", Toxicology, vol. 254, no. 1-2, pp. 82–90, 2008.
58. E. Rial-Gonzalez, S. Copsey, P. Paoli, and E. Schneider, "Priorities for Occupational Safety and Health Research in the EU-25", European Agency for Safety and Health at Work, Strassen, Luxembourg, 2005.
59. I. Fofana, H. Hemmatjou and F. Meghnefi, "Effect of Thermal Transient on the Polarization and Depolarization Current Measurements of Oil-Paper Insulation", IEEE Trans. Dielectr. Electr. Insul., Vol. 18, No. 2, pp. 513-520, 2011.
60. A.K. Pradhan, C. Koley, B. Chatterjee, S. Chakravorti, "Determination of optimized slope of triangular excitation for condition assessment of oil-paper insulation by frequency domain spectroscopy", IEEE Trans. Dielectr. Electr. Insul. 23 (3) (2016) 1303–1312.
61. P. Sun, W. Sima, X. Jiang, D. Zhang, J. He, Q. Chen, "Failure of nano-modified oil impregnated paper under repeated impulse voltage: effects of TiO_2 nanoparticles on space charge characteristics", IEEE Trans. Dielectr. Electr. Insul. vol. 25 (6) (2018) 2103–2111.
62. D. Mansour, A. Elsaeed, M. Lzzularab, "The role of interfacial zone in dielectric

properties of transformer oil-based nanofluids", IEEE Trans. Dielectr. Electr. Insul. 23 (6) (2016) 3364–3372.

63. A. Setayeshmehr, I. Fofana, C. Eichler, A. Akbari, H. Borsiand, E. Gockenbach, "Dielectric spectroscopic measurements on transformer oil-paper insulation under controlled laboratory conditions", IEEE Trans. Dielectr. Electr. Insul. 15 (4) (2008) 1100–1111.

64. IDAX 300 user manual: https://www.arc.ro/userfiles/docs/5.%20Echipamente%20de%20verificare%20PRAM/Testere%20transformatoare%20si%20motoare/Megger/Megger%20IDAX300%20User's%20Manual.pdf

65. DIRANA user manual: https://usermanual.wiki/Document/DIRANAManualBrochureENU.802772574.pdf

END

Dr. Sovan Dalai
Professor
Electrical Engineering Department
Jadavpur University
Kolkata-700032

28.06.2022

28/06/2022

Dr. Biswendu Chatterjee
Professor
Electrical Engineering Department
Jadavpur University
Kolkata-700032

28.06.2022